Università di Genova

Istituto Nazionale di Fisica Nucleare

Scuola di Scienze Matematiche, Fisiche e Naturali
Corso di Dottorato in Fisica e Nanoscienze

Quantum Detectors: the Unruh Effect and Temporal Quantum Correlations

SUPERVISORS: Pierantonio Zanghì
Paolo Solinas

CANDIDATE:
Matteo Cardi

XXXVIII ciclo

Abstract

This thesis investigates quantum detectors as operational probes of relativistic quantum field theory and temporal quantum correlations. On the relativistic side, it addresses the Unruh effect from the perspective of quantum detectors, focusing on the characterization of their response and its relation to thermality.

The first original contribution concerns the analysis of finite-size quantum detectors, whose spatial extension gives rise to nonlocal effects and supports an operational notion of temperature beyond the pointlike approximation. In collaboration with P. Zanghì and P. Solinas, the author demonstrates that the Unruh effect can be recovered for extended detectors in specific regimes and for suitable probe sizes. In these cases, the notion of Unruh temperature can be generalized to account for the detector's spatial delocalization.

A second original result, in collaboration with P. Zanghì and P. Solinas, is the development of a realistic detector model based on a charged particle in relativistic circular motion driven by a magnetic field, revealing an ultrarelativistic excitation plateau with potential experimental relevance.

On the side of temporal correlations, the thesis moves beyond Leggett–Garg inequalities by introducing a quantum non-demolition measurement protocol that allows for the reconstruction of temporal quasi-probabilities. Their negativity is shown to provide a necessary and sufficient witness of macrorealism violation, thereby overcoming the limitations of inequality-based approaches. A central original contribution of this work, developed in collaboration with P. Solinas and D. Melegari, is the demonstration that the proposed protocol achieves the same efficiency as standard Leggett–Garg inequalities and, in certain cases, can even outperform them.

Overall, the work establishes quantum detectors as a unified operational framework for the investigation of the Unruh effect and non-classical temporal statistics.

Contents

Introduction

This thesis explores the use of quantum detectors as operational tools to probe and characterize quantum phenomena. This general idea is developed along two complementary directions. On the one hand, detectors are employed to investigate the emergence and limitations of thermality for non-inertial motion, with particular emphasis on the Unruh effect and its generalizations beyond uniform acceleration. On the other hand, the same operational framework is extended to the study of temporal quantum correlations, where detector-based protocols provide a means to test the boundary between classical and quantum descriptions of time-ordered measurement outcomes.

One of the most far-reaching lessons of relativistic quantum field theory is that notions often treated as "absolute"—vacuum, particles, and even thermal equilibrium—are not intrinsic properties of the field itself. Rather, they acquire meaning only in relation to how the field is accessed along a given motion. The paradigmatic example is the Unruh effect: a localized detector undergoing uniform linear acceleration through the Minkowski vacuum responds as if it were immersed in a thermal bath at a temperature proportional to its proper acceleration. This apparent thermality is not merely a coordinate artifact, but arises naturally within an operational framework in which the populations of ground and excited states are recorded by a system locally coupled to the field along its trajectory.

Within this operational framework, the Unruh–DeWitt detector plays a central conceptual and technical role. It provides a controlled interface between (i) the geometry of observer trajectories in spacetime and (ii) the statistical properties of quantum correlations sampled along those trajectories. In the uniformly accelerated case, thermality can be traced to the analytic structure of field correlation functions and to the Kubo–Martin–Schwinger (KMS) condition, which characterizes equilibrium states in quantum statistical mechanics. At the level of the detector, the same content emerges as a detailed-balance relation between excitation and de-excitation processes. The resulting convergence between an algebraic characterization of equilibrium (KMS) and the dynamical response of a measurable device (transition rates) is a key conceptual bridge that motivates much of the research in this area.

This thesis is situated precisely at the intersection of these ideas, with the aim of testing and refining what, in the Unruh phenomenon, is truly "about acceleration" and what instead depends on more global features of motion and time evolution. Two guiding themes run throughout. The first is that acceleration alone is not sufficient to guarantee a strictly thermal detector response. Uniform linear acceleration is special: it yields exact KMS periodicity for the Wightman function restricted to the appropriate time flow, and hence an exact thermal density matrix. For

more general non-inertial motions, even those with constant proper acceleration, a stationary detector response does not necessarily imply thermality. This prompts a systematic investigation of which conditions are genuinely responsible for equilibrium-like behavior.

A first step in developing these themes is to clarify the privileged role of stationarity. Beyond inertial motion and uniform linear acceleration, the question "when does a detector reach a steady state?" is nontrivial. A landmark result in this direction is the systematic classification of stationary worldlines introduced by John R. Letaw [54]. For such trajectories, the relevant geometric and symmetry properties imply that the generator of time evolution along the observer's proper time can be expressed as a linear combination of generators of the Poincaré group. Operationally, this is precisely what enables the definition of a time-translation symmetry for the detector's interaction picture and, consequently, of transition rates that become time-independent in the long-time regime. In this sense, Letaw's classification identifies the broadest family of motions in Minkowski spacetime for which a steady-state detector response is well defined. Moreover, stationarity ensures a well-defined asymptotic limit—a crucial prerequisite for any statistical analysis of the detector's response in terms of stationary spectra, balance relations, and effective thermodynamic notions.

Once stationarity is established as the correct setting for a steady-state analysis, the natural question becomes: what replaces thermality when exact KMS behavior fails? Addressing this question requires confronting another subtle, but physically essential, aspect: the nature of the measuring device itself. In the idealized Unruh–DeWitt model the detector is pointlike, and the notion of a local temperature emerges cleanly. Realistic probes, however, are extended objects. For an extended system undergoing acceleration, different parts of the probe generally experience different proper accelerations. This is not merely a technical complication; it raises a conceptual difficulty. Quantum states of extended systems are not localized at points, and therefore the act of assigning a single temperature to the probe can become ambiguous. The thesis analyzes concrete models in which a finite-size quantum system (for instance, a confined charged particle whose spin degree of freedom acts as the readout) is used as a "thermometer" for non-inertial effects. In suitable regimes—notably when a single spatial mode dominates the dynamics—the reduced state of the internal degree of freedom can approximate a thermal form with an interpretable effective temperature. Importantly, that temperature can be understood as a nonlocal average induced by the probe's spatial extent and by the structure of the coupling to the field, thereby making explicit the limits of the pointlike idealization.

These considerations become even more compelling when one turns to non-linearly accelerated motions, with uniform circular motion as the most prominent example. Circular trajectories can be stationary and can exhibit constant proper acceleration, yet they generically do not yield a Planckian detector spectrum. The Wightman function sampled along a circular worldline fails to satisfy the KMS condition with respect to the natural time flow of the rotating observer, and the detector response is stationary but not thermal. To meaningfully compare such situations with the standard Unruh effect, the thesis introduces an operational definition of an effective, generally frequency-dependent temperature, derived from a generalized detailed-

balance relation. This "temperature" captures how close the detector's steady-state response is to that of a genuine thermal bath, and it provides a quantitative tool for identifying regimes in which a thermal interpretation is approximately valid and regimes in which it is not.

A central conceptual point emerging from this analysis is the role of the energy associated with the observer's time evolution. For motions generated by combinations of time translations and spatial rotations, the corresponding Hamiltonian in the comoving frame need not be bounded below. This lack of a lower bound obstructs the existence of a bona fide Gibbs state with respect to that generator and, correspondingly, obstructs exact thermality. From this viewpoint, uniform linear acceleration is not representative of "acceleration in general"; it is a particularly well-behaved case in which the relevant generator yields a consistent equilibrium structure. Circular motion and other stationary trajectories thus become a conceptual testing ground for disentangling genuinely local features (e.g. proper acceleration) from global features (e.g. the structure of the time flow and the spectrum of the evolution generator) that control the possibility of equilibrium.

The second theme of this thesis is that quantum detectors, beyond serving as probes of vacuum thermality in non-inertial frames, also provide versatile diagnostic tools for the temporal structure of quantum statistics more broadly. In particular, they can be used to interrogate the boundary between classical and quantum descriptions of time-ordered measurement outcomes. This becomes especially sharp in the context of macrorealism, where one seeks operational criteria distinguishing dynamics compatible with classical trajectories from those exhibiting intrinsically quantum temporal correlations. Macrorealism posits, roughly, that physical observables possess definite values at all times and that it is possible, at least in principle, to measure those values without disturbing the subsequent dynamics. The Leggett–Garg inequalities (LGIs) provide experimentally accessible constraints on combinations of temporal correlation functions that must hold under macrorealistic assumptions. Their violation is therefore a witness of non-classical temporal behavior, playing a role analogous to Bell inequalities for spatial correlations.

However, an important structural limitation is that LGIs constitute a sufficient but not necessary condition for the failure of macrorealism: there exist quantum processes that satisfy all LGIs while still being incompatible with any classical joint probability distribution that is everywhere nonnegative. This motivates the exploration of alternative protocols capable of probing the temporal statistics more directly. The thesis develops a framework based on quantum non-demolition measurements (QNDM), in which an ancillary system coherently accumulates information about an observable at multiple times with controlled invasiveness. Within this framework one can reconstruct a temporal quasi-probability distribution, whose negativity provides a sharp signature of non-classicality. A key conceptual advantage is that, in the operational formulation adopted here, such negativity becomes a necessary and sufficient criterion for the failure of macrorealism, thereby closing the logical gap left by LGI-based tests.

Finally, the thesis connects these conceptual developments to concrete numerical studies and resource considerations. Using simulations implemented in Qiskit, the performance of LGI-based witnesses is compared with that of QNDM-based quasi-

probability reconstruction in realistic scenarios where statistics are estimated from finite samples and thus subject to shot noise. This numerical analysis illustrates how the theoretically stronger criterion based on quasi-probability negativity can remain practically competitive and, in relevant regimes, more robust to noise and finite-sampling effects. In this way, the thesis positions detector-inspired operational methods not only as conceptual probes of foundational physics, but also as potentially useful tools in the characterization and benchmarking of quantum technologies.

Overall, the work presented here advances a unified perspective: quantum detectors are treated as operational devices that translate abstract structural properties—thermality for non-inertial observers, or classicality versus quantumness in time—into measurable response functions, protocols, and statistical criteria. On the Unruh side, this means identifying precisely when thermality is genuine and when it must be replaced by effective, motion-dependent notions that may depend on frequency, global properties of the time flow, and the finite size of the measuring apparatus. On the macrorealism side, it means moving beyond partial correlator constraints toward a more complete reconstruction of temporal statistics, in which quasi-probability negativity becomes the decisive operational signature of non-classical behavior.

Outline of the Thesis

Chapter 1 develops the geometric and field-theoretic framework for stationary motion, reviews the historical development of the Unruh effect, and introduces the KMS characterization of equilibrium for accelerated observers together with the Unruh–DeWitt detector as an operational probe. Chapter 2, based on the original work in collaboration with P. Zanghì and P. Solinas [25], addresses the measurement of Unruh-like thermality with finite-size quantum thermometers, emphasizing the nontrivial role of spatial structure and clarifying the dynamical regimes in which an effective temperature reading emerges for an internal degree of freedom. Chapter 3 investigates stationary but non-thermal motion with uniform circular trajectories as the primary example, introduces generalized detailed balance and frequency-dependent effective temperatures. In Chapter 4 it has been implemented a magnetic circular detector model whose predictions are mapped numerically in the (B, R) laboratory control plane, revealing single-parameter scaling and an ultrarelativistic excitation plateau, together with extensions to alternative particle choices. Chapters 5 and 6 shift the focus to temporal non-classicality: Chapter 5 develops the foundations of Leggett–Garg inequalities and their limitations, formulates macrorealism tests, and introduces the QNDM-based quasi-probability framework; Chapter 6, based on the original work in collaboration with D. Melegari and P. Solinas [60], presents detailed Qiskit-based simulations comparing inequality witnesses and quasi-probability negativity under finite statistics and realistic noise, including resource estimates relevant to near-term implementations.

Chapter 1

Unruh effect and stationary world-lines

In this chapter, the notion of stationary motion in Minkowski spacetime and its connection with the Unruh effect will be investigated in a systematic way. The main goal is to develop a coherent framework that connects the classical description of accelerated trajectories with the quantum field theoretical description of measurements performed by non-inertial observers.

The starting point of the discussion is an historical and conceptual overview of the development of the Unruh effect [84, 36, 30, 29], which places it within the broader context of quantum field theory in non-inertial frames. This perspective motivates the subsequent analysis and highlights the role of stationarity as a key ingredient in the emergence of thermal features.

The first part of the chapter is devoted to the study of stationary worldlines, a class of trajectories characterized by the existence of a timelike Killing vector field along the observer's motion. Uniform linear acceleration appears as a particular example within this broader class, but the framework naturally extends to more general stationary motions, some of which will be examined in later chapters. For stationary trajectories, it is possible to introduce comoving coordinate systems in which the Minkowski metric assumes a stationary form. This geometric property provides the natural setting for discussing equilibrium features from the viewpoint of accelerated observers and for exploring generalizations of the Unruh effect beyond the uniformly accelerated case.

The Unruh effect itself is then analyzed in detail within the framework of a real scalar quantum field in Minkowski spacetime. Following the historical development of the Unruh effect, the discussion focuses on the properties of the quantum state of the field, and in particular on its correlation functions. A central role in this analysis is played by the two-point function of the field and by the Kubo–Martin–Schwinger (KMS) condition [48, 59], which provides a precise and observer-adapted criterion for thermal equilibrium. In the context of Algebraic Quantum Field Theory, the Unruh effect has been extensively analysed. For uniformly accelerated observers, the Minkowski vacuum is shown to satisfy the KMS condition with respect to the appropriate notion of time evolution [14, 15].

After its discovery, several aspects of the Unruh effect have been extensively

investigated. Among the most significant developments are the analysis of the relation between the statistical and gravitational notions of temperature, discussed by Buchholz and Verch [23], and the extension of the Unruh effect to spatially extended quantum systems. The latter was first studied by Bell, Hughes and Leinaas in 1985 [9], and then further examined by Buchholz and Verch in 2015 [22].

Finally, the Unruh–DeWitt detector model is introduced as a conceptual and operational tool for probing the quantum field along prescribed worldlines. This method provides a clear and intuitive framework for translating the otherwise abstract thermal properties inferred from correlation functions into observable transition probabilities. By linking the geometric description of stationary motion with the quantum field theoretical notion of temperature, the detector offers a concrete and physically meaningful interpretation of the Unruh effect, bridging the gap between theoretical predictions and measurable phenomena.

This detector-based perspective will be central in the subsequent analysis, acting as the primary interface between the mathematical formalism of quantum field theory, the geometry of spacetime, and measurements in non-inertial frames.

1.1 Historical development of the Unruh effect

The Unruh effect emerged from a sequence of conceptual advances in quantum field theory that took place in the early 1970s, at the intersection of relativistic kinematics, observer-dependent notions of particles, and the theory of quantum fields in nontrivial coordinate systems. Its discovery was not the result of a single insight, but rather the culmination of several independent developments that gradually revealed the deep connection between acceleration, horizons, and thermality.

The first crucial step was taken by Fulling in 1973 [36], who investigated the quantization of a scalar field in Rindler coordinates, the natural coordinate system adapted to uniformly accelerated observers in Minkowski spacetime. Fulling showed that the vacuum state defined with respect to Rindler time translations—the Rindler vacuum—is inequivalent to the usual Minkowski vacuum. This result provided one of the earliest concrete demonstrations that the notion of particles in quantum field theory is observer dependent, even in flat spacetime, and that different choices of time evolution lead to unitarily inequivalent representations of the canonical commutation relations.

Shortly thereafter, Davies [29] analyzed the response of quantum fields in uniformly accelerated coordinates and found that the transition rates of accelerated systems exhibit a thermal character. Davies' work already contained the essential ingredient of what would later be recognized as the Unruh effect: the appearance of a Planckian distribution [66] governed by the proper acceleration. However, the full physical interpretation of this result was not yet explicit.

The decisive synthesis was provided by Unruh in 1976 [84], who demonstrated that a uniformly accelerated observer moving through the Minkowski vacuum perceives the field as a thermal bath at a temperature

$$T_{\mathrm{U}} = \frac{\hbar a}{2\pi c k_B}.$$

Unruh's analysis unified the earlier observations by relating the thermal spectrum to the presence of an acceleration horizon and to the restriction of the Minkowski vacuum to a causally accessible region of spacetime. This work firmly established that the thermal behaviour is not a dynamical effect of radiation emission, but rather a kinematical consequence of the observer's non-inertial motion.

An important conceptual clarification came from the recognition that the Unruh effect is closely related to Hawking radiation [42]. In both cases, thermality arises from the existence of horizons and from the nontrivial analytic structure of quantum field correlators when restricted to a subset of spacetime. In fact, the Unruh effect can be viewed as the flat-spacetime analogue of Hawking radiation, with the black-hole event horizon replaced by the Rindler horizon associated with uniform acceleration. This analogy played a central role in shaping the modern understanding of quantum fields in curved spacetime.

Further insight was obtained through the introduction of the particle detector model, now commonly known as the Unruh–DeWitt detector [30]. This operational approach models an observer as a localized quantum system coupled to the field along a prescribed trajectory. The detector framework demonstrated unambiguously that the thermal spectrum corresponds to real, measurable transition probabilities, thereby resolving concerns that the Unruh effect might be a mere artifact of coordinate transformations or mode decompositions.

A parallel and complementary line of development emphasized the role of thermal correlation functions and the Kubo–Martin–Schwinger (KMS) condition. It was shown that the Minkowski vacuum, when restricted to the right Rindler wedge, satisfies the KMS condition with respect to Lorentz boosts [14]. This result placed the Unruh effect within the general algebraic framework of quantum statistical mechanics, highlighting that thermality can be characterized purely in terms of the analytic properties of correlation functions, independently of any particle interpretation.

In addition to these foundational developments, a significant contribution was made by Bell, Hughes and Leinaas in 1985 [9], who extended the understanding of the Unruh effect by investigating its manifestation in extended thermometers. They highlighted an ambiguity in the definition of temperature for such systems, where each point along the thermometer would perceive a different temperature due to varying proper accelerations. This topic will be deeply discussed in the next Chapter.

Subsequent work extended and refined these ideas in several directions: the response of detectors undergoing non-uniform acceleration, the role of switching functions and finite-time effects, the behaviour of interacting fields, and the generalization to more complex stationary trajectories. In particular, Letaw's classification of stationary worldlines [54] provided a systematic geometric framework for studying which classes of motion admit a well-defined notion of stationarity and, consequently, a natural extension of the Unruh effect beyond uniform linear acceleration.

In this historical perspective, the Unruh effect appears not as an isolated curiosity, but as a cornerstone of modern quantum field theory, revealing the profound interplay between spacetime geometry, observer motion, and the thermal properties of the vacuum.

1.2 Comoving reference frames and the Frenet–Serret equations

Before discussing the Unruh effect, it is necessary to clarify the geometric structure of accelerated motion in Minkowski spacetime. In general, an observer following a non-inertial trajectory describes physical processes by means of a local comoving reference frame, whose properties encode the kinematical features of the worldline in an invariant way. Among all possible motions, a distinguished role is played by those trajectories for which physical observables evaluated along the worldline exhibit time-translation invariance with respect to the observer's proper time.

A precise characterization of this class of motions was provided by Letaw [54], who introduced the notion of stationary worldlines (for a modern and more formal treatment, see e.g [24]). These are timelike trajectories for which the invariant spacetime interval between two points on the worldline depends only on the proper time separation between them. Equivalently, the Wightman function of a quantum field evaluated along the trajectory is invariant under proper-time translations. As a consequence, particle detectors moving along stationary worldlines exhibit time-independent excitation spectra, allowing for a meaningful spectral interpretation.

The geometric description of stationary worldlines is naturally formulated using the Frenet–Serret formalism generalized to Minkowski spacetime. Given a timelike worldline $x^\mu(\tau)$, one may construct an orthonormal set of four reference vectors comoving with the observer (called a tetrad), whose evolution is governed by three scalar invariants: the curvature, which coincides with the magnitude of the proper acceleration, and two torsion-like invariants that together describe the proper angular velocity of the comoving frame (see Appendix 1.A for a brief introduction). Stationary worldlines are precisely those for which these invariants are constant along the motion. In this sense, stationarity is a purely geometric property, independent of coordinates or of any specific detector model.

Frenet–Serret tetrad. Let $x^\mu(\tau)$ be a timelike worldline parametrized by proper time τ. A convenient local frame is an orthonormal tetrad $\{V_a^\mu(\tau)\}_{a=0,1,2,3}$ smoothly attached to the curve. The unit tangent is

$$V_0^\mu(\tau) = \dot{x}^\mu(\tau), \tag{1.1}$$

and the first spacelike direction is determined by the acceleration,

$$V_1^\mu(\tau) = \frac{\ddot{x}^\mu(\tau)}{\sqrt{\ddot{x}_\alpha(\tau)\,\ddot{x}^\alpha(\tau)}}. \tag{1.2}$$

The remaining vectors V_2^μ and V_3^μ are fixed (up to discrete sign choices) by requiring orthonormality and orientation. A convenient explicit construction, based on Gram–Schmidt orthogonalization of higher derivatives of $x^\mu(\tau)$, is collected in Appendix 1.B.

By construction, the tetrad satisfies

$$V_{a\mu}V_b^\mu = \eta_{ab}, \qquad \eta_{ab} = \mathrm{diag}(-1,1,1,1). \tag{1.3}$$

Frenet–Serret transport. Since $\{V_a^\mu\}$ is a basis along the curve, its derivative closes on the tetrad:

$$\dot{V}_a^\mu = K_a{}^b\, V_b^\mu, \tag{1.4}$$

where $K_{ab} = -K_{ba}$. In Minkowski spacetime one may parameterize $K_a{}^b$ by three scalar functions $\kappa(\tau)$, $\sigma(\tau)$ and $\nu(\tau)$:

$$K_a{}^b = \begin{pmatrix} 0 & -\kappa(\tau) & 0 & 0 \\ \kappa(\tau) & 0 & -\sigma(\tau) & 0 \\ 0 & \sigma(\tau) & 0 & -\nu(\tau) \\ 0 & 0 & \nu(\tau) & 0 \end{pmatrix}. \tag{1.5}$$

Equivalently,

$$\begin{aligned} \dot{V}_0^\mu &= -\kappa\, V_1^\mu, \\ \dot{V}_1^\mu &= \kappa\, V_0^\mu - \sigma\, V_2^\mu, \\ \dot{V}_2^\mu &= \sigma\, V_1^\mu - \nu\, V_3^\mu, \\ \dot{V}_3^\mu &= \nu\, V_2^\mu. \end{aligned} \tag{1.6}$$

Eqs. (1.6) are the so called Frenet–Serret equations [34, 70]. It can be proved that the three functions κ, σ, ν are invariants, and they can be extracted as

$$\kappa(\tau) = V_{0\mu}\, \dot{V}_1^\mu, \qquad \sigma(\tau) = V_{1\mu}\, \dot{V}_2^\mu, \qquad \nu(\tau) = V_{2\mu}\, \dot{V}_3^\mu. \tag{1.7}$$

It has been shown by Letaw [54] that the family of Frenet–Serret tetrads with constant invariants κ, σ, ν defines a class of stationary reference frames, namely frames in which the components of the Minkowski metric expressed in the associated coordinates are independent of the time parameter along the observer's worldline. The simplest case corresponds to inertial motion, for which both the κ and σ vanish. In this case the worldline is a straight timelike line,

$$x^\mu(\tau) = (\tau, 0, 0, 0),$$

with four-velocity $\dot{x}^\mu = dx^\mu/d\tau$ given by

$$\dot{x}^\mu(\tau) = (1, 0, 0, 0)$$

A second class is obtained when κ is constant and nonzero while both σ and ν vanish. In inertial coordinates (T, X, Y, Z), the worldline is a hyperbola in the (T, Z)-plane,

$$x^\mu(\tau) = \left(\frac{1}{\kappa}\sinh(\kappa\tau), 0, 0, \frac{1}{\kappa}\cosh(\kappa\tau)\right).$$

and four-velocity

$$\dot{x}^\mu(\tau) = \left(\cosh(\kappa\tau), 0, 0, \sinh(\kappa\tau)\right).$$

Such a worldline is crucial for our analysis of the Unruh effect as it represents the trajectory of a uniformly accelerated observer. To show this fact, consider the proper acceleration $a^\mu = d^2x^\mu/d\tau^2$. The Minkowski norm $(-a^\mu a_\mu)^{1/2}$ is given by

$$(-a^\mu a_\mu)^{1/2} = |\kappa|(\sinh^2(\kappa\tau) - \cosh^2(\kappa\tau)) = |\kappa|$$

Therefore, the Minkowski norm of the proper acceleration is constant along the trajectory.

There is a stationary motion for $|\kappa| > |\sigma| \neq 0$ and $\nu = 0$: it is called the catenary motion and the trajectory is described by

$$\dot{x}^\mu(\tau) = \rho^{-2}\left(\kappa^2\cosh(\rho\tau) - \sigma^2, \kappa\sigma\cosh(\rho\tau) - \kappa\sigma, 0, \kappa\rho\sinh(\rho\tau)\right)$$

where $\rho^2 = \kappa^2 - \sigma^2$. By application of a finite Poincaré transformation (see [46]) it can be proved that $V_0^\mu = \dot{x}^\mu$ equivalently describes a uniform acceleration in the (T, Z) axis and a linear motion in (T, X):

$$x^\mu(\tau) = \rho^{-2}\left(\frac{1}{\kappa}\sinh(\rho\tau), \rho\sigma\tau, 0, \frac{1}{\kappa}\cosh(\rho\tau)\right).$$

Setting $|\sigma| > |\kappa| \neq 0$ and $\nu = 0$, the resulting V_0^μ is given by

$$\dot{x}^\mu(\tau) = \rho^{-2}\left(\sigma^2 - \kappa^2\cos(\rho\tau), \kappa\rho\sin(\rho\tau), \kappa\sigma - \kappa\sigma\cos(\rho\tau)\right)$$

and, using the same argument as above, it can be proved that V_0^μ equivalently describes a rotation in the (X, Y)-plane, given by

$$x^\mu(\tau) = \left(\frac{\sigma}{\rho}\tau, R\cos(\rho\tau), R\sin(\rho\tau), 0\right) \tag{1.8}$$

where, in this case, $\rho^2 = \sigma^2 - \kappa^2$ represents the constant proper angular velocity and $R = \kappa/\rho^2$ the radius of the orbit.

A particularly important limiting case arises when the proper acceleration and the proper angular velocity have equal magnitude, namely when $\nu = 0$ and $|\sigma| = |\kappa|$. This situation marks the boundary between the circular motion just described and the catenary trajectory. In Letaw's classification [54], it corresponds to a cusped worldline. Choosing the sign conventions so that $\sigma = \kappa > 0$ and setting the integration constants so that $x^\mu(0) = 0$, in Minkowski coordinates it is given by

$$x^\mu(\tau) = \left(\tau + \frac{\kappa^2\tau^3}{6},\ \frac{\kappa\,\tau^2}{2},\ \frac{\kappa^2\tau^3}{6},\ 0\right),$$

whose four-velocity is

$$\dot{x}^\mu(\tau) = \left(1 + \frac{\kappa^2\tau^2}{2},\ \kappa\,\tau,\ \frac{\kappa^2\tau^2}{2},\ 0\right).$$

From the form of their four-velocities it is possible to show that these motions are timelike for all τ:

$$-\dot{x}^\mu(\tau)\dot{x}_\mu(\tau) = \left(1 + \frac{\kappa^4\tau^4}{4} + \kappa^2\tau^2\right) - \kappa^2\tau^2 - \frac{\kappa^4\tau^4}{4} = 1$$

i.e. that $-\dot{x}^\mu(\tau)\dot{x}_\mu(\tau) > 0 \quad \forall\tau$.

More generally, stationary worldlines may involve both nonzero proper acceleration and nonzero angular velocity. In particular, when all the invariants are non-vanishing,

the resulting worldlines describe helical motions with simultaneous linear acceleration and rotation and the trajectory can be written as a superposition of hyperbolic and circular components,

$$x^\mu(\tau) = \left(\frac{\Delta}{RR_+} \sinh(\alpha\tau), \frac{\kappa\sigma}{\Delta RR_-} \cos(\beta\tau), \frac{\kappa\sigma}{\Delta RR_-} \sin(\beta\tau), \frac{\Delta}{RR_+} \cosh(\alpha\tau) \right),$$

where $R_\pm = (\sqrt{a^2+b^2} \pm a)^{1/2}$, $a = \frac{1}{2}(\kappa^2 - \sigma^2 - \nu^2)$, $b = |\kappa\nu|$, $R = \sqrt{R_+^2 + R_-^2}$ and $\Delta = \frac{1}{2}(\kappa^2 + \sigma^2 + \nu^2 + R^2)$.

A remarkable property of stationary worldlines is their equivalence to the integral curves of timelike Killing vector fields in Minkowski spacetime [54]. For each stationary trajectory, one can introduce a comoving coordinate system in which the observer is at rest and the metric coefficients are independent of the time coordinate associated with the integral curves of the Killing vector. Conversely, any timelike Killing vector defines a stationary worldline. This establishes a deep connection between the geometric classification of stationary motions and the existence of stationary coordinate systems in flat spacetime.

The relevance of stationary worldlines for quantum field theory and in particular for the Unruh effect lies in the fact that they provide the natural setting in which the relevant physical quantities become dependent only on the time interval between two space-time events.

1.3 Canonical quantization of a free scalar field

In this section we provide a self-contained construction of the quantum theory of a free, real scalar field in Minkowski spacetime. The goal is to introduce the notions of field operators, creation and annihilation operators, vacuum states, and field correlation functions. These concepts will form the foundation for the analysis of accelerated observers and vacuum fluctuations in the following sections.

Unless otherwise stated, we work in $(3+1)$-dimensional Minkowski spacetime with metric signature $(-,+,+,+)$.

1.3.1 Classical scalar field and Klein–Gordon equation

Let $\phi(x)$ be a real scalar field on Minkowski spacetime. The dynamics of the field is governed by the Klein–Gordon equation [65]

$$(\Box - m^2)\phi(x) = 0, \tag{1.9}$$

where $\Box = \partial_\mu \partial^\mu$ and m is the mass of the field. Equation (1.9) follows from the action

$$S = \frac{1}{2} \int d^4x \left(\partial_\mu \phi \, \partial^\mu \phi - m^2 \phi^2 \right). \tag{1.10}$$

The space of classical solutions of Eq. (1.9) forms a real vector space. Allowing complex-valued solutions is technically convenient and does not introduce any physical ambiguity, as the reality condition on ϕ can be imposed at the end.

1.3.2 Solution space and Klein–Gordon inner product

Given two (possibly complex) solutions f and g of the Klein–Gordon equation, their Klein–Gordon inner product is defined on any Cauchy hypersurface[1] Σ as

$$(f,g)_{\mathrm{KG}} = i\int_{\Sigma} d^3x\,(f^*\partial_T g - (\partial_T f^*)g)\,, \tag{1.11}$$

where $\partial_T = \partial/\partial T$. Current conservation guarantees that this inner product is independent of the choice of Σ.

The Klein–Gordon inner product is not positive definite. Positive-frequency solutions with respect to a given time evolution have positive norm, while negative-frequency solutions have negative norm. This indefinite structure is central to the construction of the quantum theory.

1.3.3 Mode decomposition and positive-frequency solutions

In Minkowski spacetime, inertial observers naturally define time evolution with respect to the global time coordinate T. Positive-frequency solutions are defined as eigenfunctions of the operator $i\partial_T$ with positive eigenvalue.

A complete set of normalized positive-frequency modes is given by plane-wave solutions

$$u_{\mathbf{k}}(x) = \frac{1}{(2\pi)^{3/2}}\frac{1}{\sqrt{2\omega_{\mathbf{k}}}}e^{-i(\omega_{\mathbf{k}}T-\mathbf{k}\cdot\mathbf{X})}, \qquad \omega_{\mathbf{k}} = \sqrt{\mathbf{k}^2+m^2}. \tag{1.12}$$

These modes satisfy the orthonormality relations

$$(u_{\mathbf{k}}, u_{\mathbf{k}'})_{\mathrm{KG}} = \delta^{(3)}(\mathbf{k}-\mathbf{k}'), \tag{1.13}$$

$$(u^*_{\mathbf{k}}, u^*_{\mathbf{k}'})_{\mathrm{KG}} = -\delta^{(3)}(\mathbf{k}-\mathbf{k}'), \tag{1.14}$$

$$(u_{\mathbf{k}}, u^*_{\mathbf{k}'})_{\mathrm{KG}} = 0. \tag{1.15}$$

1.3.4 Canonical quantization and vacuum state

Quantization is achieved by promoting the classical field $\phi(x)$ to an operator-valued distribution $\phi(x)$ and the mode coefficients to operators. The field operator is expanded as

$$\phi(x) = \int d^3k\left(a(\mathbf{k})u_{\mathbf{k}}(x) + a^\dagger(\mathbf{k})u^*_{\mathbf{k}}(x)\right), \tag{1.16}$$

where $a(\mathbf{k})$ and $a^\dagger(\mathbf{k})$ satisfy the canonical commutation relations

$$[a(\mathbf{k}), a^\dagger(\mathbf{k}')] = \delta^{(3)}(\mathbf{k}-\mathbf{k}'), \qquad [a(\mathbf{k}), a(\mathbf{k}')] = 0. \tag{1.17}$$

The Minkowski vacuum $|0_M\rangle$ is defined as the state annihilated by all annihilation operators:

$$a(\mathbf{k})|0_M\rangle = 0 \qquad \forall\,\mathbf{k}. \tag{1.18}$$

[1] A Cauchy hypersurface is a spacelike hypersurface that is intersected exactly once by every inextendible timelike curve, so that suitable initial data specified on it uniquely determine the solution in the entire spacetime.

1.3.5 Field correlation functions

A central role in quantum field theory is played by correlation functions of the field. The correlator function of a scalar field $\phi(x)$ in a state $|\Psi\rangle$ is defined as

$$G_\Psi(x,x') = \langle\Psi|\phi(x)\phi(x')|\Psi\rangle. \tag{1.19}$$

For the Minkowski vacuum, the correlator is called the Wightman function [88] and, if ϕ is scalar and massless, one finds

$$G_0(x,x') = \frac{1}{4\pi^2}\frac{1}{-(T-T'-i\epsilon)^2+|\mathbf{X}-\mathbf{X}'|^2}. \tag{1.20}$$

where $-i\epsilon$ is the prescription used to solve the light cone singularities and to perform the contour integrations.

1.3.6 Thermal two-point function of a massless scalar field

A thermal state at inverse temperature β with respect to inertial time translations is characterized by the thermal Wightman function [17]. For a massless scalar field in four dimensions, evaluated at $x_1 = (T_1, X_1, Y_1, Z_1)$ and $x_2 = (T_2, X_1, Y_1, Z_1)$ (fixed spatial coordinates), the thermal correlator takes the closed form

$$G_\beta(x_1;x_2) = -\frac{\pi}{4}\frac{1}{\beta^2}\frac{1}{\sinh^2\left(\frac{\pi\Delta T}{\hbar\beta}\right)}, \tag{1.21}$$

where $\Delta T = T_2 - T_1$. This expression exhibits a $\sinh^{-2}$ dependence on the time separation, with the inverse temperature β setting the characteristic scale. This standard result, which can be found in standard textbook of quantum field theory (e.g. [65]), is of pivotal importance, as we will see that the very same form of the Wightman function will be found in uniformly accelerated coordinates.

1.3.7 Bogoliubov transformations and observer dependence

The decomposition of the field into positive- and negative-frequency modes depends on the choice of time evolution. Given two complete sets of modes $\{u_i\}$ and $\{v_\lambda\}$, adapted to different notions of time, one has the Bogoliubov transformation

$$v_\lambda = \sum_i \left(\alpha_{\lambda i}u_i + \beta_{\lambda i}u_i^*\right). \tag{1.22}$$

At the operator level, this induces the transformation

$$b_\lambda = \sum_i \left(\alpha^*_{\lambda i}a_i - \beta^*_{\lambda i}a_i^\dagger\right). \tag{1.23}$$

If $\beta_{\lambda i} \neq 0$, the vacuum states associated with the two mode decompositions are inequivalent.

Such transformations play a central role in recovering the Unruh effect. In particular, the Unruh effect can be recovered by studying the Bogoliubov transformation between Minkowski modes and modes adapted to uniformly accelerated motion, as explicitly shown in Appendix 1.C.

1.4 The Unruh Effect

Having established the geometric framework for stationary motion and the quantum field theoretical framework required to define operator-valued fields and their correlation functions, we now arrive at the core result of this chapter: the Unruh effect. In its most direct formulation, the Unruh effect concerns the structure of vacuum fluctuations when they are evaluated along a uniformly accelerated worldline.

The Unruh effect states that a uniformly accelerated observer in the Minkowski vacuum perceives a thermal bath of excitations at the temperature

$$T_{\mathrm{U}} = \frac{\hbar a}{2\pi c k_B}, \tag{1.24}$$

where a is the magnitude of the proper acceleration. In natural units ($\hbar = c = k_B = 1$), this simplifies to $T_{\mathrm{U}} = a/(2\pi)$.

In the present approach, the emergence of this temperature can be understood without introducing the more general thermal equilibrium condition, which will be introduced in the next section. The essential ingredients are:

- the geometric description of uniform acceleration as a stationary worldline (hence admitting a preferred notion of proper-time translation along the trajectory);
- the vacuum two-point function of the field computed along the trajectory.

Intuitively, the key observation is that the Minkowski vacuum Wightman function, when restricted to a uniformly accelerated trajectory and expressed in terms of the observer's proper time, takes a form involving $\sinh^{-2}$ of the proper-time separation. This structure is precisely the one that characterizes a thermal correlator at inverse temperature $\beta_{\mathrm{U}} = 2\pi/a$ given in Eq. (1.21). In what follows we introduce a natural reference frame for a hyperbolic trajectory and explicitly show this equivalence between the thermal correlator and the vacuum correlator in uniformly accelerated coordinates.

1.4.1 Uniform Acceleration as a Stationary Worldline

For a better physical intuition, from now on we use the SI units for our discussion. The uniformly accelerated trajectory discussed in Section 2 represents the simplest non-trivial example of a stationary worldline, in the sense of Letaw [54]. For this motion, the Frenet-Serret invariants given in Eqs. (1.7) are

$$\kappa = \frac{a}{c^2} = \text{constant}, \quad \tau = 0, \quad \nu = 0, \tag{1.25}$$

where a is the constant proper acceleration. The worldline is given by

$$x^\mu(\tau) = \left(\frac{c^2}{a} \sinh\left(\frac{a\tau}{c}\right),\, 0,\, 0,\, \frac{c^2}{a} \cosh\left(\frac{a\tau}{c}\right) \right), \tag{1.26}$$

which describes hyperbolic motion in the (cT, Z)-plane.

The geometric structure underlying the Unruh effect finds its natural expression in the Rindler coordinate system, which provides the comoving reference frame for uniformly accelerated observers. As established in Section 1.2, for stationary worldlines like uniform acceleration, there exists a coordinate system where the Minkowski metric appears stationary.

For a system undergoing constant proper acceleration while maintaining Born rigidity (experiencing no internal stresses or deformations), the appropriate coordinate system is provided by the Kottler-Møller (KM) coordinates [47, 61]. Starting from inertial coordinates (cT, X, Y, Z) in Minkowski spacetime and assuming motion along the Z direction, the transformation to KM coordinates (ct, x, y, z) is given by [61, 47]:

$$\begin{aligned} cT &= \frac{c^2}{a}\left(1+\frac{az}{c^2}\right)\sinh\left(\frac{at}{c}\right) \\ Z &= \frac{c^2}{a}\left(1+\frac{az}{c^2}\right)\cosh\left(\frac{at}{c}\right) - \frac{c^2}{a} \\ X &= x, \quad Y = y \end{aligned} \tag{1.27}$$

In these coordinates, the Minkowski metric takes the form

$$-c^2dT^2 + dX^2 + dY^2 + dZ^2 = -c^2N(z)^2dt^2 + dx^2 + dy^2 + dz^2, \tag{1.28}$$

where the lapse function

$$N(z) = 1 + \frac{az}{c^2} \tag{1.29}$$

encodes the gravitational-like time dilation effects experienced in the accelerated frame [67]. Note that in this form the Minkowski metric does not depend on the time coordinate t, in accord with the discussion of Section 1.2.

The Kottler-Møller coordinates cover only the right Rindler wedge $Z > |cT|$, with the boundary $z = -c^2/a$ ($N = 0$) representing the acceleration horizon for the uniformly accelerated observer. This horizon structure plays a crucial role in the thermal nature of the Unruh effect.

An important feature of this coordinate system is that it provides a natural description for extended rigid bodies in acceleration. The proper acceleration varies with position as

$$a(z) = \frac{a}{N(z)}, \tag{1.30}$$

with respect to the reference acceleration, while the proper time along each hyperbola is

$$\tau(z) = N(z)t. \tag{1.31}$$

This ensures that $a(z)\tau(z) = at$ holds for all trajectories, maintaining the Born rigidity condition, which states that different parts of an extended body maintain constant proper distance.

From a geometric perspective, the KM coordinates can be understood as generating a sequence of instantaneous inertial frames. At each proper time t, the

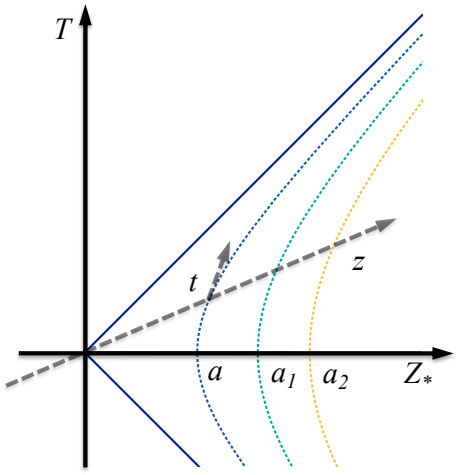

Figure 1.1: Rindler coordinate system in the (cT, Z)-plane. The hyperbolas represent worldlines of points at fixed spatial coordinate z in the KM frame, with different proper accelerations a (corresponding to $z = 0$), a_L and a_R. The dashed lines indicate the acceleration horizons at $Z + c^2/a = \pm cT$.

transformation from the comoving frame to the laboratory frame is given by a Lorentz boost with rapidity at/c:

$$\Lambda(t) = \begin{pmatrix} \cosh(at/c) & \sinh(at/c) \\ \sinh(at/c) & \cosh(at/c) \end{pmatrix}. \tag{1.32}$$

The coordinate transformation (1.27) can then be expressed as:

$$\begin{pmatrix} cT \\ Z \end{pmatrix} = \begin{pmatrix} cT(t) \\ Z(t) \end{pmatrix} + \Lambda(t) \begin{pmatrix} 0 \\ z \end{pmatrix}, \tag{1.33}$$

showing the underlying Lorentz structure of the accelerated frame. Hence, the KM coordinates can be interpreted as describing events in a sequence of inertial frames $\mathcal{F}(t)$, such that the relation between the coordinates of the same event in two infinitesimally close inertial frames $\mathcal{F}(t)$ and $\mathcal{F}(t + dt)$ are:

$$\begin{aligned} cT_{t+dt} &= cT_t - (a\,dt/c)Z_t - cdt \\ Z_{t+dt} &= Z_t - (a\,dt)T_t\,. \end{aligned} \tag{1.34}$$

In other words, two infinitesimally close members of the inertial frames set $\mathcal{F}(t)$ and $\mathcal{F}(t+dt)$ can be transformed into each other through a combination of an infinitesimal time translation and an infinitesimal boost in the Z_t-direction with infinitesimal rapidity $(a/c)dt$.

This interpretation will prove particularly valuable when discussing extended quantum systems, as it provides a clear physical picture of how the comoving frame evolves through successive infinitesimal boosts and time translations.

1.4.2 Thermal Response from Accelerated Trajectories

The thermal nature of the Minkowski vacuum as perceived by a uniformly accelerated observer can be demonstrated directly through the analysis of field correlation

functions in the KM coordinate system.

Consider a free massless scalar field $\phi(x)$ in Minkowski spacetime. In the KM coordinates (ct, x, y, z) defined by equations (1.27), the field operator can be expressed as $\phi(t, z)$ along a trajectory at fixed spatial coordinate z.

In KM coordinates, we consider a trajectory at fixed spatial position $(T(t, z_0)$, X_0, Y_0, $Z(t, z_0))$, which describes a single uniformly accelerated worldline.

$$G_0(t, t'; z_0) = \langle 0_M | \phi(t, z_0)\phi(t', z_0) | 0_M \rangle, \tag{1.35}$$

where $|0_M\rangle$ denotes the Minkowski vacuum state.

For a massless scalar field in 4-dimensional Minkowski spacetime, the correlator function in inertial coordinates is given by Eq. (1.20). Using the coordinate transformations (1.27), it is possible to express the inertial coordinates in terms of KM coordinates. For two events at the same spatial coordinate z_0 but different coordinate times t and t':

$$cT = \left(z_0 + \frac{c^2}{a}\right) \sinh\left(\frac{at}{c}\right), \qquad Z = \left(z_0 + \frac{c^2}{a}\right) \cosh\left(\frac{at}{c}\right) - \frac{c^2}{a}, \tag{1.36}$$

$$cT' = \left(z_0 + \frac{c^2}{a}\right) \sinh\left(\frac{at'}{c}\right), \qquad Z' = \left(z_0 + \frac{c^2}{a}\right) \cosh\left(\frac{at'}{c}\right) - \frac{c^2}{a}. \tag{1.37}$$

Computing the two intervals:

$$\Delta T = T - T' = \frac{1}{c}\left(z_0 + \frac{c^2}{a}\right)\left[\sinh\left(\frac{at}{c}\right) - \sinh\left(\frac{at'}{c}\right)\right], \tag{1.38}$$

$$\Delta Z = Z - Z' = \left(z_0 + \frac{c^2}{a}\right)\left[\cosh\left(\frac{at}{c}\right) - \cosh\left(\frac{at'}{c}\right)\right]. \tag{1.39}$$

A direct calculation shows that

$$-(c\Delta T)^2 + (\Delta Z)^2 = 4\left(z_0 + \frac{c^2}{a}\right)^2 \sinh^2\left(\frac{a(t-t')}{2c}\right). \tag{1.40}$$

Therefore, from Eq. (1.20), the Wightman function along the trajectory at fixed z_0 becomes

$$G_0(t - t'; z_0) = -\frac{1}{16\pi^2 c\hbar} \frac{1}{\left(z_0 + \frac{c^2}{a}\right)^2 \sinh^2\left(\frac{a(t-t'-i\epsilon)}{2c}\right)}. \tag{1.41}$$

Note that Eq. (1.41) is exactly of the form of Eq. (1.21), which describes the correlator of the field $\phi(x)$ with respect to the thermal state ω. Therefore, imposing in Eq. (1.41) the relation $a/(2c) = \pi/(\hbar\beta)$, we can interpret the vacuum state, as seen by an accelerated observer, to be a thermal state at temperature $T = a\hbar/(2\pi c k_B)$.

1.4.3 Proper Time and the KMS Condition

The physical interpretation becomes clearer when the correlation function is expressed in terms of proper time along the trajectory. From equation (1.31), the proper time at distance z_0 from the reference hyperbola is

$$\tau(z_0) = N(z_0)t = \left(1 + \frac{az_0}{c^2}\right) t. \tag{1.42}$$

In terms of proper time differences $s = \tau - \tau' = N(z_0)(t - t')$, the correlator function (1.41) becomes

$$G_0(s; z_0) = -\frac{1}{16\pi^2\hbar c}\frac{a^2/N(z_0)^2}{\sinh^2\left(\frac{a(s-i\epsilon)}{2cN(z_0)}\right)}. \tag{1.43}$$

Using the relation for proper acceleration at position z_0 from equation (1.30):

$$a(z_0) = \frac{a}{N(z_0)}, \tag{1.44}$$

the final form becomes

$$G_0(s; z_0) = -\frac{1}{16\pi^2\hbar c}\frac{a(z_0)^2}{\sinh^2\left(\frac{a(z_0)(s-i\epsilon)}{2c}\right)}. \tag{1.45}$$

This establishes that the correlator is described by a local temperature

$$T(z_0) = \frac{\hbar}{2\pi c k_B} a(z_0) \tag{1.46}$$

which is the redshifted Unruh temperature. Therefore, an observer at fixed z_0 perceives the Minkowski vacuum as a thermal state with temperature set by the local proper acceleration.

1.4.4 Physical Interpretation

The analysis highlights several interconnected physical aspects of the Unruh effect for uniformly accelerated observers. A first important feature is the intrinsically local character of the temperature perceived along the family of hyperbolic trajectories. Observers located at different positions within the Kottler–Møller frame experience different proper accelerations and therefore perceive different Unruh temperatures. This position dependence reflects the fact that uniform acceleration cannot be extended globally to an entire rigid frame without introducing variations in the local acceleration.

A central role in this construction is played by the lapse function $N(z) = 1 + \frac{az}{c^2}$, in which the geometric properties of the accelerated frame resides. On the one hand, it determines the relation between coordinate time and proper time along each trajectory. On the other hand, it governs the spatial variation of the proper acceleration through $a(z) = a/N(z)$, and therefore directly controls the local Unruh temperature. In this way, the lapse function links the geometric description of the comoving frame to the thermodynamic properties perceived by accelerated observers, providing a unified interpretation of time dilation, acceleration, and temperature within the same geometric framework.

It is important to emphasize that the Unruh temperature, as defined in this context, is a local property of the coordinate system, and it is not related to any real physical system. The fact that each hyperbolic trajectory defines a unique temperature cannot be generalized, a priori, to a property of an extended system performing a uniformly accelerated trajectory. This discussion is quite delicate and it will be the subject of Chapter 2.

1.5 The Kubo–Martin–Schwinger condition

In this Section, we introduce a key concept in the analysis of thermal states in general space-times. In space-times admitting a timelike Killing vector field V^a, the notion of time evolution for a stationary observer is well defined, and so is the corresponding notion of energy [86]. In such settings, thermal states in quantum field theory can be characterized in a general and covariant way by the Kubo–Martin–Schwinger (KMS) condition [48, 59].

Consider a quantized scalar field $\phi(x)$ on a stationary space-time, and let $\langle\cdot\rangle_\omega$ denote expectation values with respect to a given state ω. The key idea behind the KMS condition is to formulate thermal equilibrium directly in terms of correlation functions, without relying on a specific representation such as a density matrix. In a system at temperature $k_B T = 1/\beta$ (from now on, T will be used to identify the temperature), two-point correlators must satisfy a specific analyticity property and an imaginary-time periodicity reflecting the structure of finite-temperature field theory.

Let t be the time coordinate associated with the flow generated by V^a. For two local observables $A(t)$ and $B(0)$ we define two correlator functions:

$$\begin{aligned} G_{AB}(t) &= \langle A(t)B(0)\rangle_\omega \\ F_{AB}(t) &= \langle B(0)A(t)\rangle_\omega. \end{aligned} \tag{1.47}$$

If $F_{AB}(t)$ admits an analytic continuation to complex times with imaginary part in the interval $0 < \mathrm{Im}\, t < \beta$, and if the state ω satisfies the KMS condition

$$G_{AB}(t) = F_{AB}(t + i\beta), \tag{1.48}$$

then the state is in thermal equilibrium. It implies that thermal correlators are periodic in Euclidean time with period β, thereby reproducing the familiar correspondence between finite-temperature quantum field theory and Euclidean field theory formulated on a cylinder of circumference β.

In what follows, it is shown how (i) a Gibbs state satisfies the KMS condition, (ii) in finite-dimensional systems the KMS condition characterizes equilibrium states, and (iii) the Minkowski vacuum, when restricted to the right Rindler wedge, is verified to satisfy the KMS condition for Lorentz boosts, leading to the Unruh temperature.

1.5.1 Gibbs state implies KMS

Let H be the Hamiltonian generating time translations $A(t) = e^{iHt} A e^{-iHt}$ of any bounded operator A on a Hilbert space $\mathcal{H}$. Consider the Gibbs state at inverse temperature $\beta > 0$,

$$\rho_\beta = \frac{e^{-\beta H}}{Z}, \qquad Z = \mathrm{Tr}(e^{-\beta H}).$$

For any two bounded operators A, B, the functions in Eq. (1.47) are given by

$$\begin{aligned} G_{AB}(t) &= \mathrm{Tr}\big(\rho_\beta\, A(t)\, B\big) \\ F_{AB}(t) &= \mathrm{Tr}\left(\rho_\beta\, BA(t)\right). \end{aligned}$$

It can be proved (see e.g. [20, 39]) that $F_{AB}(t)$ admits an analytic continuation to the strip $0 < \mathrm{Im}\, t < \beta$ (under standard assumptions on domains). Using the Heisenberg evolution and the cyclicity of the trace[2],

$$\begin{aligned} F_{AB}(t+i\beta) &= \mathrm{Tr}\Big(\rho_\beta\, B\, A(t+i\beta)\Big) \\ &= \frac{1}{Z}\mathrm{Tr}\Big(e^{-\beta H} B\, e^{iH(t+i\beta)/\hbar} A e^{-iH(t+i\beta)/\hbar}\Big) \\ &= \frac{1}{Z}\mathrm{Tr}\Big(e^{iHt/\hbar} e^{-H\beta} A e^{-iHt/\hbar} e^{H\beta} e^{-\beta H} B\Big) \\ &= \frac{1}{Z}\mathrm{Tr}\Big(e^{-\beta H} e^{iHt/\hbar} A e^{-iHt/\hbar} B\Big) \\ &= \mathrm{Tr}\Big(\rho_\beta\, A(t) B\Big) \\ &= G_{AB}(t), \end{aligned}$$

where, in the third equality, the cyclicity of the trace has been used to move $e^{-\beta H} B$ past $e^{-iH(t+i\beta)/\hbar}$, and in the fourth equality we used the commutativity between $e^{-\beta H}$ and $e^{iHt/\hbar}$. This is exactly the KMS condition (1.48). The analyticity in the strip $0 < \mathrm{Im}\, t < \beta$ follows in many physically relevant cases from the existence of bounds on the Hamiltonian spectrum.

1.5.2 The converse and the accelerated case

In infinite-dimensional quantum field theory, the converse implication "KMS $\Rightarrow$ Gibbs" is generally not valid in a naive sense, as the operator $e^{-\beta H}$ may fail to be trace class and a density matrix representation may not exist.

However, for finite-dimensional quantum systems—or more generally whenever $e^{-\beta H}$ is trace class—the KMS condition with respect to the dynamics generated by H is equivalent to the Gibbs form. In this case, if a state ω satisfies Eq. (1.48) for all observables A, B, together with the required analyticity properties, one can reconstruct the thermal density matrix ρ_β and show that $\omega(A) = \mathrm{Tr}(\rho_\beta A)$ [39].

In the infinite-dimensional setting, the appropriate general framework is provided by Tomita–Takesaki modular theory: a faithful normal KMS state uniquely determines a modular automorphism group, and the notion of a Gibbs state is replaced by the modular operator formalism [81].

Having clarified the general status of the KMS condition, we now show how it arises concretely in the case of uniformly accelerated motion. The origin of the thermal behavior of the Wightman function (1.20) in the accelerated reference frame can be traced back to the analytic structure of the field correlation function given in Eq. (1.45). In particular, its dependence on the hyperbolic sine leads to a characteristic periodicity under imaginary shifts of the proper time. To make this explicit, consider the effect of the complex shift $s \mapsto s + i\beta$ on the argument of the

[2]The cyclicity of the trace states that, for three operators A, B, C, then $\mathrm{Tr}(A\,B\,C) = \mathrm{Tr}(B\,C\,A) = \mathrm{Tr}(C\,A\,B)$.

hyperbolic sine:

$$\sinh^2\left(\frac{a(z_0)s}{2c}\right) \mapsto \sinh^2\left(\frac{a(z_0)(s+i\beta)}{2c}\right) \tag{1.49}$$
$$= \left(\sinh\left(\frac{a(z_0)s}{2c}\right)\cos\left(\frac{a(z_0)\beta}{2c}\right) + i\cosh\left(\frac{a(z_0)s}{2c}\right)\sin\left(\frac{a(z_0)\beta}{2c}\right)\right)^2.$$

This expression is periodic in imaginary time with period given by

$$\frac{a(z_0)\beta}{2c} = \pi k, \quad k \in \mathbb{Z},$$

and therefore $\beta = 2\pi c/a(z_0)$. Thus, as the Wightman function in the accelerated case is given by Eq. (1.45), for $A = B = \phi$, $G_{\phi\phi}(t) = G_0(t; z_0)$, and $F_{\phi\phi}(t) = G_0(t; z_0)$. Using Eq. (1.49) and $\beta = 2\pi c/a(z_0)$:

$$G_{\phi\phi}(t) := G_0(t; z_0) = -\frac{1}{16\pi^2\hbar c}\frac{a(z_0)^2}{\sinh^2\left(\frac{a(z_0)t}{2c}\right)}$$
$$= -\frac{1}{16\pi^2\hbar c}\frac{a(z_0)^2}{\sinh^2\left(\frac{a(z_0)(t+i\beta)}{2c}\right)} = G_0(t+i\beta; z_0) := F_{\phi\phi}(t+i\beta),$$

and the KMS condition (1.48) is satisfied.

1.6 The Unruh–DeWitt Detector Model

While the analysis of field correlations provides the structural origin of the Unruh effect, the Unruh–DeWitt (UDW) detector model gives it a concrete and physical meaning. The detector is a localized quantum system that couples linearly and locally to the field along its worldline. In the weak-coupling regime, its transition rates are governed by the two-point function of the field computed along the trajectory. In particular, when the correlation functions satisfy a KMS condition with respect to the detector time evolution, the detector necessarily obeys a detailed balance relation, exactly as for an ordinary thermometer immersed in a thermal reservoir. This is the sense in which the Unruh effect becomes a statement about thermalization and measurable transition statistics, rather than about coordinate-dependent mode decompositions.

1.6.1 Motivation and physical intuition in the detailed-balance perspective

In the canonical approach to the Unruh effect, it is seen as a mathematical statement about the change from inertial to uniformly accelerated coordinates. The UDW model bridges the gap between an abstract property of the Wightman function and a real and measurable effect in quantum field theory defining the "detection" in terms of transitions of a finite-dimensional quantum system coupled locally to the field.

The detector formalism is designed to match the logic of thermalization in open quantum systems. In weak coupling, transition probabilities become proportional to a response function that is the Fourier transform (in the detector time) of a suitable field correlator. If these correlators are KMS, then the detector satisfies detailed balance and equilibrates to a Gibbs distribution. We present the relation between the quantum field and the detector summarizing the Bell–Hughes–Leinaas (BHL) analysis [9], which makes this connection completely explicit: the Unruh effect is equivalently the statement that the Minkowski vacuum, restricted to uniformly accelerated time evolution, has the KMS property, and therefore acts as a thermal reservoir for any weakly coupled detector.

1.6.2 Mathematical formulation: detector–field interaction and transition probability

Consider a quantum system with free Hamiltonian H_{T} and energy eigenstates $\{|i\rangle\}$,

$$H_{\mathrm{T}}|i\rangle = E_i|i\rangle, \tag{1.50}$$

moving along a prescribed worldline $x^\mu(\tau)$ parametrized by the proper time τ. We will refer to this quantum system as the detector (the label T is chosen as the detector in our analysis plays the role of a thermometer). The detector couples locally to a real scalar field $\phi(x)$ through the interaction Hamiltonian

$$H_{\mathrm{int}}(\tau) = \lambda\,\chi(\tau)\,m(\tau)\,\phi\big(x(\tau)\big), \tag{1.51}$$

where λ is a small coupling constant, $\chi(\tau)$ is the switching function, i.e. the function that establishes the duration of the interaction with respect to τ, and $m(\tau)$ is the detector monopole operator in the interaction picture,

$$m(\tau) = e^{\frac{i}{\hbar}H_{\mathrm{T}}\tau}\,m(0)\,e^{-\frac{i}{\hbar}H_{\mathrm{T}}\tau}. \tag{1.52}$$

The relevant matrix elements are $m_{fi} \equiv \langle f|m(0)|i\rangle$.

Let the initial state be $|i\rangle \otimes |\psi\rangle$ with the field in $|\psi\rangle$ (later specialized to $|0_M\rangle$). At leading nontrivial order in perturbation theory , and summing over final field states ([21]), the transition probability for $i \to f$ can be written in the form

$$P_{f\leftarrow i} = \lambda^2\,|m_{fi}|^2\,\mathcal{G}(\Omega_{fi}), \qquad \Omega_{fi} \equiv E_f - E_i, \tag{1.53}$$

where the response function is

$$\mathcal{G}(\Omega) = \int_{-\infty}^{+\infty} d\tau \int_{-\infty}^{+\infty} d\tau'\;\chi(\tau)\chi(\tau')\,e^{-\frac{i}{\hbar}\Omega(\tau-\tau')}\,G_0(\tau,\tau'). \tag{1.54}$$

From now on, we assume the interaction time to be long enough to set the switching function to be $\chi(\tau) = 1\,\forall\tau$ [21]. As mentioned before, for stationary trajectories, the correlator depends only on $s = \tau - \tau'$, and it is natural to define the transition rate per unit proper time,

$$\Gamma_{f\leftarrow i} \equiv \mathcal{G}(\Omega) = \int_{-\infty}^{+\infty} ds\;e^{-\frac{i}{\hbar}\Omega s}\,G_0(s). \tag{1.55}$$

This is the general form of the transition rates for stationary trajectories.

1.6.3 The Unruh–DeWitt detector for uniform acceleration and detailed balance

We now specialize to the case in which the field is prepared in the Minkowski vacuum, ($|\psi\rangle = |0_M\rangle$), and the detector is modeled as a two-level quantum system (Unruh–DeWitt detector) undergoing uniform acceleration along the Z-axis.

The internal Hilbert space of the detector is spanned by two energy eigenstates, ($|0\rangle$) and ($|1\rangle$), with energies (E_0) and (E_1), respectively. The interaction between the detector and the scalar field is governed by the monopole operator ($m(\tau)$), which is assumed to be Hermitian. In the energy eigenbasis, this implies that its matrix elements satisfy $m_{10}(0) = m_{01}^*(0)$. In addition, we assume that the diagonal matrix elements vanish, ($m_{00}(0) = m_{11}(0) = 0$), so that the interaction induces only transitions between the two levels. In Minkowski coordinates (cT, Z), a uniformly accelerated trajectory with constant proper acceleration a is given by Eq. (1.26). For a stationary worldline, $G_0(\tau, \tau') = G_0(s)$, and the rate is given by (1.55). The Wightman function along a uniformly accelerated trajectory in the Minkowski vacuum takes the standard form

$$G_0(s) = -\frac{\hbar}{16\pi^2 c^2} \frac{a^2}{\sinh^2\left(\dfrac{a(s - i\epsilon)}{2c}\right)}. \tag{1.56}$$

Inserting (1.56) into (1.55) gives

$$\mathcal{G}(\Omega) = -\frac{\hbar a^2}{16\pi^2 c^2} \int_{-\infty}^{+\infty} ds \, \frac{e^{-\frac{i}{\hbar}\Omega s}}{\sinh^2\left(\dfrac{a(s - i\epsilon)}{2c}\right)}. \tag{1.57}$$

The integrand has second-order poles at

$$\sinh\left(\frac{as}{2c}\right) = 0 \quad \Longrightarrow \quad s = i\,\frac{2\pi c}{a}\,n, \qquad n \in \mathbb{Z}. \tag{1.58}$$

A standard contour evaluation (see [13] for the explicit calculation) yields the Planckian distribution [66]

$$\mathcal{G}(\Omega) = \frac{1}{2\pi\hbar} \frac{\Omega}{e^{\frac{2\pi c}{a\hbar}\Omega} - 1}. \tag{1.59}$$

Consequently, the excitation rate $\Gamma_\uparrow$ of the UDW detector from the ground to the excited state $|0\rangle \to |1\rangle$ satisfies

$$\Gamma_\uparrow = \frac{1}{2\pi\hbar} \frac{\Omega}{e^{\frac{2\pi c}{a\hbar}\Omega} - 1}, \qquad \Omega \equiv E_1 - E_0 > 0. \tag{1.60}$$

The de-excitation rate is obtained by replacing $\Omega \mapsto -\Omega$ in (1.55),

$$\Gamma_\downarrow = \frac{1}{2\pi\hbar} \frac{-\Omega}{e^{-\frac{2\pi c}{a\hbar}\Omega} - 1}. \tag{1.61}$$

It is easy to check that the detector obeys the detailed balance relation $\frac{\Gamma_\uparrow}{\Gamma_\downarrow} = e^{-\beta_U \Omega}$. for some β_U, as

$$\frac{\Gamma_\uparrow}{\Gamma_\downarrow} = \frac{1}{2\pi\hbar} \frac{\Omega}{e^{\frac{2\pi c}{a\hbar}\Omega} - 1} \cdot 2\pi\hbar \frac{e^{-\frac{2\pi c}{a\hbar}\Omega} - 1}{-\Omega} = e^{-\frac{2\pi c}{a\hbar}\Omega} \tag{1.62}$$

Therefore, the detector reaches a thermal equilibrium at the Unruh temperature

$$T_U = \frac{\hbar a}{2\pi c k_B}. \tag{1.63}$$

1.6.4 Bell–Hughes–Leinaas: derivation of the accelerated KMS condition and detailed balance

The derivation above shows the Planckian distribution by explicit evaluation of the Fourier transform of the accelerated Wightman function. We now prove that Minkowski vacuum is KMS state with respect to uniformly accelerated time evolution. This accelerated KMS property can be established rigorously using analyticity of vacuum correlators and microcausality across Rindler wedges. Bell, Hughes and Leinaas [9] provided a particularly transparent proof, and we now reproduce their argument in detail, emphasizing how uniform acceleration induces the corresponding KMS structure.

The purpose of this discussion is twofolded: on one hand, to show that the thermalization of a quantum field implies the thermalization of a small system weakly coupled it; on the other hand, to demonstrate how an analogous KMS structure naturally emerges when the system undergoes uniform acceleration at the level of the quantum field and the vacuum state.

(i) KMS condition and detailed balance in an inertial thermal reservoir. We begin by introducing a thermometer weakly coupled to the reservoir through an interaction Hamiltonian of the form

$$H_{int}(t) = m(t)\,\phi(t), \tag{1.64}$$

where $\phi(t)$ and $m(t)$ denote the reservoir and thermometer Heisenberg operators, respectively. For simplicity, we assume both systems to be scalar, although the argument straightforwardly generalizes to higher-rank operators. Let $|i\rangle$ be the energy eigenstates of the free thermometer Hamiltonian $H_{\rm T}$,

$$H^{(\rm T)}|i\rangle = E_i|i\rangle. \tag{1.65}$$

At lowest nontrivial order in perturbation theory, and after transient effects have decayed, the transition rate per unit time from an initial state i to a final state f can be written as

$$\Gamma_{f\leftarrow i} = \int_{-\infty}^{+\infty} dt\; e^{\frac{i}{\hbar}(E_f - E_i)t} \left\langle \phi^\dagger(0)\,\phi(t) \right\rangle \langle i|m^\dagger(0)|f\rangle \,\langle f|m(0)|i\rangle, \tag{1.66}$$

where the thermal average over the reservoir degrees of freedom is implicit. The reverse rate $\Gamma_{i\leftarrow f}$ is obtained by exchanging $i \leftrightarrow f$ and exploiting the hermiticity properties of the interaction Hamiltonian.

To relate the two rates, one performs the shift $t \mapsto t - i\hbar\beta$ in the integral representation of $\Gamma_{i\leftarrow f}$, and using the KMS condition to replace the shifted correlator with the unshifted correlator in reversed operator order. This procedure yields the detailed balance relation

$$\Gamma_{i\leftarrow f} = e^{\beta(E_f - E_i)}\,\Gamma_{f\leftarrow i}. \tag{1.67}$$

As a consequence, in the weak-coupling regime the thermometer equilibrates with stationary occupation probabilities $p_i \propto e^{-\beta E_i}$, namely at the same temperature as the reservoir.

(ii) Uniform acceleration as dynamics generated by a boosted Hamiltonian. From Eq. (1.34), it can be seen that uniform acceleration is generated by a combination of the time translation and boost operator: Consider a family of instantaneous inertial frames $\mathcal{F}(t)$ adapted to uniformly accelerated motion along the Z-axis. Infinitesimally neighboring frames differ by a combination of an infinitesimal time translation and an infinitesimal Lorentz boost, as shown in Eq. (1.34).

Let H denote the generator of Minkowski time translations, and let K_z be the generator of boosts along the Z-direction, so that a boost of rapidity η is represented by $e^{-\frac{i}{\hbar}\eta K_z}$. For motion with constant proper acceleration a, the natural generator of evolution along the accelerated time parameter t is the boosted Hamiltonian

$$\exp\left(-\frac{i}{\hbar}H_a t\right) \equiv \exp\left(-\frac{i}{\hbar}\left(H + \frac{a}{c}\,K_z\right)t\right). \tag{1.68}$$

The total boosted Hamiltonian describing the combined system of thermometer, reservoir, and interaction can be decomposed as

$$H_a = H_a^{(\mathrm{T})} + H_a^{(\mathrm{R})} + H_{int}, \tag{1.69}$$

and we work in the interaction picture with respect to $H_a^{(\mathrm{T})} + H_a^{(\mathrm{R})}$. Under the same weak-coupling assumptions as in the inertial case, the transition rates of the thermometer again take the form (1.66). The crucial difference is that the reservoir correlation functions are now evaluated as vacuum expectation values in the Minkowski vacuum $|0\rangle$,

$$\langle\cdots\rangle_0 \equiv \langle 0|\cdots|0\rangle, \tag{1.70}$$

with time evolution generated by $H_a^{(\mathrm{R})}$. Therefore, in order to recover detailed balance at some inverse temperature β, it suffices to establish an accelerated KMS condition of the form

$$\langle\phi(t - i\hbar\beta)\,\Phi(0)\rangle_0 = \langle\Phi(0)\,\phi(t)\rangle_0, \tag{1.71}$$

for the scalar reservoir operator ϕ evolved with respect to $H_a^{(\mathrm{R})}$.

(iii) The accelerated KMS condition: analytic continuation and wedge locality. The validity of the accelerated KMS condition (1.71) for a Rindler trajectory can be established by combining the analyticity properties of vacuum correlation functions with microcausality across Rindler wedges [9].

We consider the vacuum two-point function

$$F(T;Z,Z') \equiv \langle \phi(T,Z)\,\phi(0,Z')\rangle_0. \tag{1.72}$$

This correlator admits an expansion in terms of energy and momentum eigenstates,

$$\begin{aligned}\langle \phi_{\rm lab}(T,Z)\phi_{\rm lab}(0,Z')\rangle_0 &= \int dE\,dP\ \langle 0|U(T,Z)\phi_{\rm lab}(0,0)U^\dagger(T,Z)|E_nP_n\rangle\times\\ &\times\langle E_nP_n|U(0,Z')\phi_{\rm lab}(0,0)U^\dagger(0,Z')|0\rangle\\ &= \int dE\,dP\ \langle 0|e^{-iP_\mu X^\mu}\phi_{\rm lab}(0,0)e^{iP_\mu X^\mu}|E_nP_n\rangle\times\\ &\times\langle E_nP_n|e^{-iP_\mu (X^\mu)'}\phi_{\rm lab}(0,0)e^{iP_\mu (X^\mu)'}|0\rangle\\ &= \int dE\,dP\ \sigma(E,P)\,e^{-iE_n(cT)+iP_nZ-iP_nZ'},\end{aligned}$$

where

$$\begin{aligned}\sigma(E,P) &= \sum_n \langle 0|\phi_{\rm lab}(0,0)|E_nP_n\rangle\langle E_nP_n|\phi_{\rm lab}(0,0)|0\rangle\delta(E_n-E)\delta(P_n-P)\\ U(T,Z) &= \exp\left(-iP_\mu X^\mu\right)\end{aligned}$$

Here we have used the relations

$$\begin{aligned}e^{-iP_\mu (X^\mu)'}|0\rangle &= 0,\\ e^{iP_\mu X^\mu}|E_nP_n\rangle &= e^{-i(H(cT)-PZ)}|E_nP_n\rangle = e^{-iE_n(cT)+iP_nZ}|E_nP_n\rangle.\end{aligned}$$

For the subsequent analysis it is convenient to introduce light-cone coordinates,

$$u \equiv cT + Z + \frac{c^2}{a}, \qquad v \equiv cT - Z - \frac{c^2}{a}. \tag{1.73}$$

In the right Rindler wedge, the uniformly accelerated coordinates (t,z) satisfy

$$u = \left(z+\frac{c^2}{a}\right)e^{\frac{at}{c}}, \qquad v = -\left(z+\frac{c^2}{a}\right)e^{-\frac{at}{c}}, \tag{1.74}$$

so that for fixed z one has $u>0$ and $v<0$.

We now extend the correlator to complex values of T by performing the shift $T \mapsto T - i\lambda$, with $\lambda > 0$. In light-cone coordinates this induces the transformation

$$u \mapsto u_\lambda = u\,e^{-i\frac{a}{c}\lambda}, \qquad v \mapsto v_\lambda = v\,e^{i\frac{a}{c}\lambda}. \tag{1.75}$$

The exponent of the exponential appearing in the integral representation of the correlator then becomes

$$\begin{aligned}-iE(u_\lambda+v_\lambda)/2 + iP(u_\lambda - v_\lambda - u' - v')/2 = &-i(E-P)ue^{-i\frac{a}{c}\lambda}/2\\ &-i(E+P)ve^{i\frac{a}{c}\lambda}/2 - iP(u'+v')/2,\end{aligned}$$

whose modulus reads

$$\exp\left[-\frac{(E-P)u}{2}\sin\Big(\frac{a}{c}\lambda\Big)+\frac{(E+P)v}{2}\sin\Big(\frac{a}{c}\lambda\Big)\right]. \tag{1.76}$$

In the right Rindler wedge one has $E \pm P \geq 0$, $u > 0$, and $v < 0$, so convergence of the integral requires $\sin(\frac{a}{c}\lambda) \geq 0$. At $\lambda = \pi c/a$, the point (u, v) is mapped to $(-u, -v)$, which lies in the opposite Rindler wedge. When (u', v') corresponds to a point in the original right wedge, the separation between $(-u, -v)$ and (u', v') is spacelike. Therefore, using the fact that two field operators evaluated at spacelike separated events commute (usually referred to as microcausality), the correlator can be written as

$$\langle\phi(-u,-v)\phi(u',v')\rangle_0 = \langle\phi(u',v')\phi(-u,-v)\rangle_0. \tag{1.77}$$

Proceeding through a second analytic continuation and returning to the boundary of the analyticity domain, one finally obtains

$$\langle\phi(t-i\hbar\beta_U)\,\phi(0)\rangle_0 = \langle\phi(0)\,\phi(t)\rangle_0, \qquad \beta_U = \frac{2\pi c}{a\hbar}. \tag{1.78}$$

Equivalently, the associated temperature is

$$T_U = \frac{\hbar a}{2\pi k_B c}. \tag{1.79}$$

(iv) Detailed balance at the Unruh temperature. Combining the accelerated KMS condition (1.78) with the general argument developed in part (i), one finds that the transition rates of any weakly coupled thermometer evolving with respect to the accelerated time parameter satisfy the Unruh detailed balance relation

$$\Gamma_{i\leftarrow f} = e^{\beta_U(E_f-E_i)}\,\Gamma_{f\leftarrow i}. \tag{1.80}$$

The corresponding stationary populations are therefore Gibbsian with inverse temperature β_U. This result establishes, in the operational sense defined by weak-coupling thermalization, that the Minkowski vacuum behaves as a thermal reservoir at temperature T_U for uniformly accelerated observers [9].

1.6.5 Physical Interpretation and Significance

The analysis based on the Unruh–DeWitt detector leads to a clear and physically compelling conclusion: the thermal response predicted for accelerated observers can be measured in a real particle experiment rather than been only an artifact arising from coordinate choices. The detector undergoes real quantum transitions between its internal energy levels as a consequence of its interaction with the quantum field. Such transitions are absent for an inertial detector traversing the Minkowski vacuum, whereas they do occur for a uniformly accelerated detector, whose excitation spectrum is indistinguishable from that of a detector immersed in a thermal bath. In this sense, the Unruh effect acquires a direct operational meaning: different observers interacting locally with the same quantum state of the field may record

different physical outcomes, and this observer dependence reflects an intrinsic feature of relativistic quantum field theory.

The structure of the detector response further substantiates this interpretation. The response function displays the characteristic Planckian form associated with thermal equilibrium, with a spectrum proportional to $\Omega/(e^{\Omega/T} - 1)$ for a positive energy gap Ω. The temperature entering this distribution is precisely

$$T = \frac{\hbar a(z)}{2\pi c k_B},$$

which coincides with the Unruh temperature previously derived from the Kubo–Martin–Schwinger condition. The agreement between these two independent approaches—one rooted in the analytic properties of correlation functions, the other in the dynamical behavior of a localized quantum system—provides strong evidence that the thermal character of the response is neither formal nor accidental, but instead a robust and physically meaningful prediction.

From a broader perspective, the detector model also clarifies the physical and experimental significance of the Unruh effect. Although a direct laboratory observation remains extremely challenging—owing to the enormous accelerations required to generate an appreciable temperature—the Unruh–DeWitt detector captures essential features of realistic detection processes, such as the interaction of atoms with quantum fields. It shows that, at least in principle, the effect is accessible to physical measurement and resolves longstanding conceptual questions concerning the reality of particles in different reference frames. Moreover, the same conceptual framework provides a valuable template for understanding closely related phenomena in curved spacetime, most notably Hawking radiation.

1.A Tetrad formalism in Minkowski spacetime

In this appendix we briefly review the tetrad (or vierbein) formalism in flat spacetime, restricting attention to those aspects that are directly relevant for the description of non-inertial observers and comoving reference frames. The purpose is not to develop the full Cartan formalism, but to provide a geometric and observer-oriented framework suitable for accelerated motion and stationary worldlines.

1.A.1 Local frames and tetrads

Let $(\mathbb{R}^{1,3}, \eta_{\mu\nu})$ be Minkowski spacetime. A tetrad is a set of four linearly independent vector fields

$$\{e_a{}^{\mu}(x)\}, \qquad a = 0, 1, 2, 3,$$

satisfying the orthonormality condition

$$\eta_{\mu\nu}\, e_a{}^{\mu} e_b{}^{\nu} = \eta_{ab}, \qquad \eta_{ab} = \mathrm{diag}(-1, 1, 1, 1). \tag{1.81}$$

The tetrad provides, at each spacetime point, a local Lorentz frame in which tensor components are referred to an orthonormal basis rather than to a coordinate basis.

Given a vector V^{μ}, its components in the tetrad frame are

$$V^a = e^a{}_{\mu} V^{\mu}, \tag{1.82}$$

where $e^a{}_{\mu}$ denotes the inverse tetrad, defined by $e^a{}_{\mu} e_b{}^{\mu} = \delta^a_b$.

1.A.2 Tetrads adapted to an observer

For a timelike observer with worldline $x^{\mu}(s)$ parametrized by proper time s, a natural choice is an observer-adapted tetrad

$$\{V_a{}^{\mu}(s)\},$$

where the timelike leg coincides with the four-velocity,

$$V_0{}^{\mu}(s) = \dot{x}^{\mu}(s). \tag{1.83}$$

The remaining vectors $V_i{}^{\mu}$ $(i = 1, 2, 3)$ span the local rest space of the observer at each instant of proper time.

Such a tetrad defines a comoving reference frame along the worldline and allows one to decompose physical quantities (forces, accelerations, detector responses) into locally measured components.

1.A.3 Transport of a tetrad along a worldline

The evolution of the tetrad along the curve is governed by

$$\dot{V}_a{}^{\mu}(s) = K_a{}^{b}(s)\, V_b{}^{\mu}(s), \tag{1.84}$$

where $K_{ab}(s)$ is antisymmetric,

$$K_{ab} = -K_{ba}. \tag{1.85}$$

Antisymmetry follows directly from the preservation of the orthonormality condition (1.81) under differentiation.

The tensor $K_a{}^b$ encodes the kinematics of the observer: its components correspond to proper acceleration and rotation of the local frame. In flat spacetime, $K_a{}^b$ plays the role of a Lorentz-algebra–valued connection along the worldline.

1.A.4 Fermi–Walker transport as a special case

A particularly important transport law is Fermi–Walker transport, defined by the requirement that the spatial frame does not rotate with respect to local gyroscopes. For a tetrad adapted to the four-velocity V_0^μ, Fermi–Walker transport corresponds to

$$\dot{V}_i{}^\mu = (V_0^\mu a_\nu - a^\mu V_{0\nu}) V_i{}^\nu, \tag{1.86}$$

where $a^\mu = \dot{V}_0^\mu$ is the four-acceleration. Uniformly accelerated motion provides a simple example where the tetrad is Fermi–Walker transported but not parallel transported.

1.A.5 Relation with the Frenet–Serret formalism

When the tetrad is constructed directly from the derivatives of the worldline, as in the Frenet–Serret construction, the matrix $K_a{}^b$ takes a canonical form parametrized by three scalar invariants: curvature κ, torsion τ and hypertorsion ν. In this case the transport equation (1.84) reduces to the Frenet–Serret equations discussed in Section 1.2.

Stationary worldlines are characterized by constant values of these invariants, which implies that $K_a{}^b$ is constant along the motion. This property is crucial for the existence of comoving coordinate systems with time-independent metric coefficients and underlies the appearance of stationary detector spectra and thermal effects for accelerated observers.

1.A.6 Physical role in quantum field theory

In quantum field theory on flat spacetime, observer-adapted tetrads provide a geometric bridge between spacetime symmetries and the notion of local reference frames. They identify the local time direction used to define positive frequency and make explicit how different observers induce different mode decompositions of the same field. In this sense, the tetrad formalism supplies the geometric backbone for the observer dependence of the particle concept discussed in the main text.

1.B Explicit Gram–Schmidt construction of the Frenet–Serret tetrad

In this appendix we collect an explicit construction of the Frenet–Serret tetrad $\{V_a^\mu(s)\}_{a=0,1,2,3}$ along a timelike worldline $x^\mu(s)$ parametrized by proper time. The construction is based on orthogonalization of successive derivatives of $x^\mu(s)$ and is convenient when one wants closed formulas for the tetrad vectors.

First two vectors. The unit tangent is

$$V_0^\mu = \dot{x}^\mu, \qquad V_{0\mu}V_0^\mu = -1. \tag{1.87}$$

Assuming non-vanishing proper acceleration, the unit acceleration direction is

$$V_1^\mu = \frac{\ddot{x}^\mu}{\sqrt{\ddot{x}_\alpha \ddot{x}^\alpha}}, \qquad V_{1\mu}V_1^\mu = +1, \qquad V_{0\mu}V_1^\mu = 0. \tag{1.88}$$

Third vector via Gram–Schmidt. A convenient intermediate vector orthogonal to V_0^μ and V_1^μ can be obtained from $\dddot{x}^\mu$ by subtracting its components along V_0^μ and $\ddot{x}^\mu$. One explicit choice is

$$\widetilde{V}_2^\mu = \frac{(\ddot{x}^\beta \ddot{x}_\beta)\,\dddot{x}^\mu - (\dddot{x}^\alpha \ddot{x}_\alpha)\,\ddot{x}^\mu + (\ddot{x}^\alpha \ddot{x}_\alpha)^2\,\dot{x}^\mu}{\ddot{x}^\beta \ddot{x}_\beta}. \tag{1.89}$$

By construction, $\widetilde{V}_2^\mu$ is orthogonal to V_0^μ and V_1^μ (whenever $\ddot{x}^\mu \neq 0$). The normalized third vector is then

$$V_2^\mu = \frac{\widetilde{V}_2^\mu}{\sqrt{\widetilde{V}_{2\alpha}\widetilde{V}_2^\alpha}}. \tag{1.90}$$

An explicit expression for the norm that follows from (1.89) is

$$\widetilde{V}_{2\alpha}\widetilde{V}_2^\alpha = \frac{(\dddot{x}^\alpha \dddot{x}_\alpha)(\ddot{x}^\beta \ddot{x}_\beta)^2 - (\dddot{x}^\alpha \ddot{x}_\alpha)^2(\ddot{x}^\beta \ddot{x}_\beta) - (\ddot{x}^\beta \ddot{x}_\beta)^4}{(\ddot{x}^\beta \ddot{x}_\beta)^2}, \tag{1.91}$$

so that (1.90) agrees with the fully expanded form used in the main text.

Fourth vector from orientation. Once $V_0^\mu, V_1^\mu, V_2^\mu$ are fixed, the last vector is determined (up to a sign) by requiring orthonormality and consistent orientation:

$$V_3^\mu = \frac{1}{\sqrt{6}}\,\epsilon^{\mu\nu\rho\sigma} V_{\nu 0}\, V_{\rho 1}\, V_{\sigma 2}. \tag{1.92}$$

This guarantees

$$V_{3\mu}V_3^\mu = +1, \qquad V_{3\mu}V_a^\mu = 0 \quad (a = 0, 1, 2). \tag{1.93}$$

Remark on special cases. If $\ddot{x}^\mu = 0$ the construction of V_1^μ is not defined, reflecting that inertial motion does not single out a unique spatial frame. If $\ddot{x}^\mu \neq 0$ but the higher derivatives become linearly dependent, the construction still works but may lead to degenerate cases where some of the Frenet–Serret invariants vanish identically.

1.C Unruh effect from Bogoliubov transformations in $(1+1)$ dimensions

This appendix collects an explicit derivation of the Unruh thermal spectrum through a direct Bogoliubov transformation between Minkowski and Rindler mode decompositions. The goal is to provide a complete computational complement to the main text: all intermediate steps are displayed in detail, since the same manipulations will later reappear in related contexts (mode expansions, Klein–Gordon product normalizations, and Bogoliubov mixing).

Units. For notational convenience, throughout this appendix we work in natural units $\hbar = c = k_B = 1$.

1.C.1 Classical field equation and solution space

We consider a real, massless scalar field ϕ in $(1+1)$-dimensional Minkowski spacetime, restricted to the (T, Z) plane, since the considered hyperbolic trajectory is given along the Z direction. The metric is $\eta_{\mu\nu} = \mathrm{diag}(-1, +1)$ and the field satisfies the Klein–Gordon equation

$$\Box\phi = (-\partial_T^2 + \partial_Z^2)\phi = 0. \tag{1.94}$$

It is convenient to introduce null (light-cone) coordinates

$$u = T - Z, \qquad v = T + Z, \tag{1.95}$$

in terms of which the d'Alembert operator factorizes as

$$\Box = -4\,\partial_u\partial_v. \tag{1.96}$$

Equation (1.94) then implies

$$\partial_u\partial_v\phi = 0, \tag{1.97}$$

whose general solution can be written as

$$\phi(T, Z) = \phi_R(u) + \phi_L(v). \tag{1.98}$$

Thus the classical solution space splits into two independent sectors, describing right-moving and left-moving degrees of freedom. Since the two sectors decouple, it will be sufficient in what follows to focus on the right-moving sector; the left-moving one can be treated analogously and yields the same thermal factor.

1.C.2 Minkowski time evolution and positive-frequency modes

In Minkowski spacetime, inertial observers naturally parametrize time evolution by the coordinate T, whose flow is generated by the timelike Killing vector ∂_T. Positive-frequency modes are therefore defined as solutions that are eigenfunctions of $i\partial_T$ with positive eigenvalue.

Restricting to the right-moving sector, consider solutions depending only on $u = T - Z$. A natural ansatz for a mode of definite Minkowski frequency $\omega > 0$ is

$$u_\omega(T, Z) = C\, e^{-i\omega(T-Z)} = C\, e^{-i\omega u}. \tag{1.99}$$

Indeed,

$$\partial_T u_\omega = -i\omega\, u_\omega, \tag{1.100}$$

so u_ω is a positive-frequency solution with respect to Minkowski time.

The normalization constant C is fixed by imposing orthonormality with respect to the Klein–Gordon product (1.11). Evaluating the product on a constant-T hypersurface, we find

$$\begin{aligned}(u_\omega, u_{\omega'})_{\mathrm{KG}} &= i \int_{-\infty}^{+\infty} dZ \left(u_\omega^* \partial_T u_{\omega'} - (\partial_T u_\omega^*) u_{\omega'} \right) \\ &= (\omega + \omega') \int_{-\infty}^{+\infty} dZ\, u_\omega^* u_{\omega'}.\end{aligned} \tag{1.101}$$

Using

$$u_\omega^* u_{\omega'} = |C|^2 e^{i(\omega-\omega')(T-Z)}, \tag{1.102}$$

the spatial integral yields

$$\int_{-\infty}^{+\infty} dZ\, e^{-i(\omega-\omega')Z} = 2\pi\, \delta(\omega - \omega'). \tag{1.103}$$

Since $(\omega + \omega')\delta(\omega - \omega') = 2\omega\, \delta(\omega - \omega')$, we obtain

$$(u_\omega, u_{\omega'})_{\mathrm{KG}} = 4\pi\omega |C|^2\, \delta(\omega - \omega'). \tag{1.104}$$

Imposing the standard normalization

$$(u_\omega, u_{\omega'})_{\mathrm{KG}} = \delta(\omega - \omega'), \tag{1.105}$$

fixes the constant to be

$$C = \frac{1}{\sqrt{4\pi\omega}}. \tag{1.106}$$

We therefore take the normalized Minkowski positive-frequency right-moving modes to be

$$u_\omega(u) = \frac{1}{\sqrt{4\pi\omega}}\, e^{-i\omega u}. \tag{1.107}$$

1.C.3 Mode expansion and canonical quantization

The set $\{u_\omega, u_\omega^*\}$ forms a complete basis for the right-moving sector of the classical solution space. Accordingly, any real classical solution can be expanded as

$$\phi(u) = \int_0^\infty d\omega \left(a(\omega)\, u_\omega(u) + a^*(\omega)\, u_\omega^*(u)\right). \tag{1.108}$$

Quantization is implemented by promoting the coefficients $a(\omega)$ and $a^*(\omega)$ to operators $a(\omega)$ and $a^\dagger(\omega)$ satisfying the canonical commutation relations

$$[a(\omega), a^\dagger(\omega')] = \delta(\omega - \omega'), \qquad [a(\omega), a(\omega')] = 0. \tag{1.109}$$

The field operator is then defined as

$$\phi(u) = \int_0^\infty d\omega \left(a(\omega)\, u_\omega(u) + a^\dagger(\omega)\, u_\omega^*(u)\right). \tag{1.110}$$

The Minkowski vacuum $|0_M\rangle$ is characterized by

$$a(\omega)\,|0_M\rangle = 0 \qquad \forall\, \omega > 0. \tag{1.111}$$

1.C.4 Covariance and different observer decompositions

The construction above depends on a specific choice of time evolution, which in turn fixes a notion of positive frequency. In Minkowski spacetime, the global timelike Killing field ∂_T selects the positive-frequency subspace spanned by $\{u_\omega\}$, and hence the operators $a(\omega)$, $a^\dagger(\omega)$ and the vacuum $|0_M\rangle$ defined by $a(\omega)|0_M\rangle = 0$ for all ω.

For another congruence of stationary observers, adapted to a different time parameter (equivalently, to a different timelike Killing vector field), the natural positive-frequency subspace may differ. Let $\{v_\lambda\}$ be a complete orthonormal family of solutions, positive-frequency with respect to that alternative time. Then we may also expand the field operator as

$$\phi(x) = \int_0^\infty d\lambda \left(b(\lambda)\, v_\lambda(x) + b^\dagger(\lambda)\, v_\lambda^*(x)\right). \tag{1.112}$$

Bogoliubov transformation at the level of modes. Because $\{u_\omega, u_\omega^*\}$ is a complete basis of Sol, every v_λ admits an expansion

$$v_\lambda = \int_0^\infty d\omega \left[\, \alpha_{\lambda\omega}\, u_\omega + \beta_{\lambda\omega}\, u_\omega^* \,\right]. \tag{1.113}$$

The Bogoliubov coefficients are fixed by the Klein–Gordon product: using $(u_\omega, u_{\omega'})_{KG} = \delta(\omega - \omega')$ and $(u_\omega, u_{\omega'}^*)_{KG} = 0$, one obtains

$$\alpha_{\lambda\omega} = (u_\omega, v_\lambda)_{KG}, \qquad \beta_{\lambda\omega} = -(u_\omega^*, v_\lambda)_{KG}. \tag{1.114}$$

This step is conceptually important: the "mixing" between positive and negative Minkowski frequencies is not a guess, but the unique expansion dictated by completeness and KG orthonormality.

Induced transformation at the level of operators. Insert (1.113) into (1.112) and compare with the Minkowski expansion

$$\phi(x) = \int_0^\infty d\omega \left(a(\omega)\, u_\omega(x) + a^\dagger(\omega)\, u_\omega^*(x)\right). \tag{1.115}$$

Matching coefficients in front of u_ω and u_ω^* yields the operator identity

$$b(\lambda) = \int_0^\infty d\omega \left(\alpha_{\lambda\omega}^*\, a(\omega) - \beta_{\lambda\omega}^*\, a^\dagger(\omega)\right). \tag{1.116}$$

If $\beta_{\lambda\omega} \neq 0$, the two vacua are inequivalent. Indeed, using $a(\omega)|0_M\rangle = 0$,

$$\langle 0_M|b^\dagger(\lambda)b(\lambda)|0_M\rangle = \int_0^\infty d\omega\, |\beta_{\lambda\omega}|^2. \tag{1.117}$$

Up to this point everything is completely general. The Unruh thermality arises because, for uniformly accelerated observers along the Z direction, the alternative notion of time translation is generated by Lorentz boosts in the (T, Z) plane. The mapping between Minkowski null coordinates and the Rindler time is exponential, and this is what turns generic Bogoliubov mixing into a thermal mixing.

1.C.5 Thermal nature of the Minkowski vacuum from the Rindler number operator

We now specialize to Rindler observers and compute explicitly the Bogoliubov coefficients in the simplest setting. We work in the (T, Z) plane and in the massless theory, where the computation can be carried out in closed form. The final thermal factor is universal and matches the standard Unruh temperature once units are restored.

Rindler wedge and Rindler time along Z. Consider the right Rindler wedge in the (T, Z) plane,

$$\mathcal{R} = \{Z > |T|\}. \tag{1.118}$$

In this wedge, introduce Rindler coordinates (τ, ξ) by

$$T = \xi \sinh(a\tau), \qquad Z = \xi \cosh(a\tau), \qquad \xi > 0, \tag{1.119}$$

so that ∂_τ is the boost Killing vector generating Rindler time translations. In terms of Minkowski null coordinates (1.95),

$$u = T - Z = -\xi e^{-a\tau}, \qquad v = T + Z = \xi e^{a\tau}. \tag{1.120}$$

This exponential relation is the origin of the Planck factor.

Choice of Minkowski and Rindler mode bases in the right-moving sector. From Eq. (1.107), the Minkowski positive-frequency right-moving mode of frequency $\omega > 0$ is

$$u_\omega(u) = \frac{1}{\sqrt{4\pi\omega}}\, e^{-i\omega u}, \tag{1.121}$$

which is positive-frequency with respect to Minkowski time T.

A right-wedge positive-frequency Rindler mode of Rindler frequency $\Omega > 0$ may be chosen as

$$v_\Omega(u) = \frac{1}{\sqrt{4\pi\Omega}}\, \theta(-u)\, (-au)^{i\Omega/a}, \tag{1.122}$$

where $\theta(-u)$ enforces support in the right wedge ($u < 0$ in $\mathcal{R}$) and the complex power is defined by

$$(-au)^{i\Omega/a} = \exp\Big(\frac{i\Omega}{a}\ln(-au)\Big), \qquad u < 0. \tag{1.123}$$

Using $u = -\xi e^{-a\tau}$, the dependence on τ is $e^{-i\Omega\tau}$ up to a ξ-dependent phase, so these are positive-frequency with respect to the boost time τ.

Computing the Bogoliubov coefficients as Fourier coefficients in Rindler time. We want to express the Minkowski mode restricted to $\mathcal{R}$ as a superposition of Rindler positive and negative frequencies. Restrict u_ω to $\mathcal{R}$ and rewrite it as a function of τ at fixed ξ:

$$u_\omega\big(u(\tau)\big) = \frac{1}{\sqrt{4\pi\omega}}\exp\big(-i\omega(-\xi e^{-a\tau})\big) = \frac{1}{\sqrt{4\pi\omega}}\exp\big(i\omega\xi e^{-a\tau}\big). \tag{1.124}$$

As a function of τ, this is not monochromatic: it contains both $e^{-i\Omega\tau}$ and $e^{+i\Omega\tau}$ components. Define its Fourier decomposition (in τ) by

$$\exp\big(i\omega\xi e^{-a\tau}\big) = \int_0^\infty d\Omega\, \Big(A_{\Omega\omega}(\xi)\, e^{-i\Omega\tau} + B_{\Omega\omega}(\xi)\, e^{+i\Omega\tau}\Big). \tag{1.125}$$

Up to normalization conventions, $A_{\Omega\omega}$ corresponds to $\alpha_{\Omega;\omega}$ and $B_{\Omega\omega}$ to $\beta_{\Omega;\omega}$.

Compute $A_{\Omega\omega}(\xi)$ by projection:

$$A_{\Omega\omega}(\xi) = \frac{1}{2\pi}\int_{-\infty}^{+\infty} d\tau\, e^{+i\Omega\tau}\exp\big(i\omega\xi e^{-a\tau}\big). \tag{1.126}$$

Perform the change of variable

$$s = \omega\xi e^{-a\tau} \quad\Longrightarrow\quad \tau = -\frac{1}{a}\ln\Big(\frac{s}{\omega\xi}\Big), \qquad d\tau = -\frac{1}{a}\frac{ds}{s}. \tag{1.127}$$

As τ runs from $-\infty$ to $+\infty$, s runs from $+\infty$ to 0, so

$$A_{\Omega\omega}(\xi) = \frac{1}{2\pi a}\,(\omega\xi)^{i\Omega/a}\int_0^\infty ds\, s^{-1-i\Omega/a}\, e^{is}. \tag{1.128}$$

The remaining integral is a standard representation of the Gamma function, defined by analytic continuation. Using

$$\int_0^\infty ds\, s^{z-1}e^{is} = e^{i\pi z/2}\Gamma(z), \qquad (0 < \Re z < 1), \tag{1.129}$$

and extending to $z = -i\Omega/a$ by analyticity, one obtains

$$\int_0^\infty ds\, s^{-1-i\Omega/a}\, e^{is} = e^{-\pi\Omega/(2a)}\, \Gamma\left(-\frac{i\Omega}{a}\right). \tag{1.130}$$

Hence

$$A_{\Omega\omega}(\xi) = \frac{1}{2\pi a}\, (\omega\xi)^{i\Omega/a}\, e^{-\pi\Omega/(2a)}\, \Gamma\left(-\frac{i\Omega}{a}\right). \tag{1.131}$$

Similarly, compute $B_{\Omega\omega}(\xi)$:

$$B_{\Omega\omega}(\xi) = \frac{1}{2\pi} \int_{-\infty}^{+\infty} d\tau\, e^{-i\Omega\tau} \exp\bigl(i\omega\xi e^{-a\tau}\bigr). \tag{1.132}$$

Repeating the same change of variable gives

$$B_{\Omega\omega}(\xi) = \frac{1}{2\pi a}\, (\omega\xi)^{-i\Omega/a} \int_0^\infty ds\, s^{-1+i\Omega/a}\, e^{is}. \tag{1.133}$$

Now $z = +i\Omega/a$ in (1.129), giving

$$\int_0^\infty ds\, s^{-1+i\Omega/a}\, e^{is} = e^{+\pi\Omega/(2a)}\, \Gamma\left(\frac{i\Omega}{a}\right), \tag{1.134}$$

and therefore

$$B_{\Omega\omega}(\xi) = \frac{1}{2\pi a}\, (\omega\xi)^{-i\Omega/a}\, e^{+\pi\Omega/(2a)}\, \Gamma\left(\frac{i\Omega}{a}\right). \tag{1.135}$$

At this stage the "thermal" structure is explicit: the coefficients multiplying positive- and negative-frequency Rindler harmonics differ by $e^{\pm\pi\Omega/(2a)}$. When translated into KG-normalized Bogoliubov coefficients $\alpha_{\Omega;\omega}$ and $\beta_{\Omega;\omega}$, one obtains the standard closed forms, with the characteristic ratio

$$\frac{|\beta_{\Omega;\omega}|^2}{|\alpha_{\Omega;\omega}|^2} = e^{-2\pi\Omega/a}, \tag{1.136}$$

which is therefore not an assumption: it follows directly from the exponential mapping $u = -\xi e^{-a\tau}$ and the analytic continuation encoded in (1.129).

From the thermal ratio to the Planck spectrum. Taking the modulus square of the Bogoliubov coefficient and using the identity

$$\left|\Gamma\left(\frac{i\Omega}{a}\right)\right|^2 = \frac{\pi a}{\Omega \sinh(\pi\Omega/a)}, \tag{1.137}$$

one finds the Planck factor

$$|\beta_{\Omega;\omega}|^2 = \frac{1}{2\pi a\, \omega}\, \frac{1}{e^{2\pi\Omega/a} - 1}. \tag{1.138}$$

Finally, using the Bogoliubov operator relation (1.116) and $a(\omega)|0_M\rangle = 0$, the expectation value of the Rindler number operator becomes

$$\langle 0_M|N_\Omega|0_M\rangle = \int_0^\infty d\omega\, |\beta_{\Omega;\omega}|^2 = \frac{1}{e^{2\pi\Omega/a} - 1} \int_0^\infty \frac{d\omega}{2\pi a\, \omega}. \tag{1.139}$$

As usual, the remaining integral is a continuum normalization factor, which can be handled by working with wave packets or by adopting a box normalization. Extracting this common density-of-states contribution, one obtains the occupation number per Rindler mode,

$$\langle 0_M|N_\Omega|0_M\rangle = \frac{1}{e^{2\pi\Omega/a}-1}. \tag{1.140}$$

This is the Bose–Einstein distribution with inverse temperature $\beta_U = 2\pi/a$ in the natural units used in this appendix. Restoring physical units gives $\beta_U = 2\pi c/(a\hbar)$ and $T_U = \hbar a/(2\pi c k_B)$.

Chapter 2

On the measurement of the Unruh effect through extended quantum thermometers

2.1 The Unruh Effect in Extended Quantum Thermometers

In the previous chapter we established, in a fully microscopic and rigorous manner, that the Minkowski vacuum satisfies a Kubo–Martin–Schwinger (KMS) condition with respect to uniformly accelerated time evolution. This result, originally due to Unruh, Fulling and Davies [84, 36, 29], as been enriched by DeWitt [30], who provided a concrete and physical meaning to it: a particle detector, coupled to a quantum field in Minkowski vacuum, behave like a thermal bath with temperature given by the Unruh temperature.

While this conclusion is well understood for point-like detectors and localized systems, its extension to spatially extended quantum systems raises conceptual and physical questions that are far from trivial. In particular, when the thermometer itself possesses a finite spatial extent, different parts of the system experience different proper accelerations, and hence are naturally associated with different local Unruh temperatures. This leads to an apparent ambiguity in the notion of temperature, which cannot be interpreted as a simple spatial inhomogeneity in the usual thermodynamic sense.

This issue was first clearly identified and analyzed by Bell, Hughes and Leinaas [9], and has since been revisited from different perspectives [22, 53, 46]. More recently, renewed interest in possible experimental realizations of the Unruh effect, driven by advances in quantum technologies and precision measurements in storage rings [4, 5, 3, 2], has further emphasized the need for a refined theoretical framework capable of addressing the measurement process itself.

The purpose of this chapter is to provide such a framework. Building directly on the results of Chapter 1, we revisit the description of uniformly accelerated quantum systems and develop a fully relativistic microscopic model of an extended quantum thermometer. The key idea is to describe acceleration not by introducing quantum

field theory in non-inertial coordinates, but by formulating the dynamics entirely within standard relativistic quantum theory in inertial frames, using the generators of time translations and Lorentz boosts.

Within this approach, the Unruh effect manifests itself through the properties of the boosted Hamiltonian, which governs the time evolution of the system in the accelerated frame. The thermal character of the vacuum, established in Chapter 1 via the accelerated KMS condition, then implies detailed balance and thermalization for weakly coupled subsystems. In the present chapter, this general structure will be taken as given and used as a foundation to analyze extended thermometers and their effective temperature readings.

2.1.1 Quantum Dynamics in an Accelerated Frame

We now turn to the quantum description of an extended relativistic system undergoing uniform acceleration. As stressed above, no reformulation of quantum field theory in accelerated coordinates is required. The dynamics can be entirely described in terms of operators acting on the Hilbert space of the theory in inertial frames.

Let H denote the generator of time translations in an inertial frame, and let $K \equiv K_z$ be the generator of Lorentz boosts along the Z axis. Consider a family of instantaneous inertial frames $\mathcal{F}(t)$ following to the accelerated motion [9, 82],analogous to the tetrad discussed in Chapter 1. If $\Phi(t)$ denotes the Heisenberg state of the system in the frame $\mathcal{F}(t)$, then the evolution over an infinitesimal time interval dt is given by

$$\Phi(t+dt) = \left[1 - \frac{i}{\hbar}\left(H + \frac{a}{c}K\right) dt\right] \Phi(t). \tag{2.1}$$

This motivates the definition of the boosted Hamiltonian

$$H^a \equiv H + \frac{a}{c}K, \tag{2.2}$$

which acts as the generator of time evolution with respect to the accelerated time parameter t. This operator has already been introduced and discussed in Chapter 1, where its role in the accelerated KMS condition was made explicit.

We now consider a composite system consisting of a quantum thermometer interacting weakly with a quantum field acting as a reservoir. The boosted Hamiltonian (2.2) of the total system can be decomposed as

$$H^a = H^a_{\mathrm{T}} + H^a_{\mathrm{R}} + V, \tag{2.3}$$

where H^a_{T} and H^a_{R} are the boosted Hamiltonians of the thermometer and reservoir, respectively, and V denotes the interaction between the two. In complete analogy with standard open quantum systems, we assume the interaction to be of the generic form

$$V = \sum_m a_m b_m, \tag{2.4}$$

with a_m and b_m operators acting on the thermometer and reservoir Hilbert spaces.

Crucially, uniform acceleration enters the quantum dynamics solely through the replacement of the inertial Hamiltonian by the boosted Hamiltonian H^a. This will be the starting point for all subsequent constructions in this chapter, including the explicit microscopic models introduced below.

2.1.2 KMS Condition, Detailed Balance, and Master Equation

The thermal character of the Minkowski vacuum with respect to accelerated time evolution has already been established in Chapter 1. In particular, following Bell, Hughes and Leinaas, it was shown that vacuum correlation functions of reservoir observables evolved with H^a_{R} satisfy an accelerated KMS condition (1.78) at inverse temperature

$$\beta_a = \frac{2\pi c}{\hbar a}. \tag{2.5}$$

As discussed in detail in Chapter 1, this property implies that, from the perspective of uniformly accelerated dynamics, the reservoir behaves as a thermal system at the Unruh temperature.

For the purposes of the present chapter, we focus on the analysis of the Unruh effect for an extended quantum thermometer weakly coupled to the reservoir. Under standard assumptions—weak coupling, sufficiently large reservoir, and appropriate ultraviolet regularization [82, 16, 87]—the accelerated KMS condition implies detailed balance for transition rates between eigenstates of H^a_{T},

$$W_{mn} = e^{\beta_a(\mathscr{E}_n - \mathscr{E}_m)} W_{nm}, \tag{2.6}$$

where $\mathscr{E}_m$ and $\mathscr{E}_n$ are eigenvalues of the boosted thermometer Hamiltonian H^a_{T}.

Equivalently, the same conclusion can be reached within the master equation formalism for open quantum systems [17]. Working in the interaction picture with respect to $H^a_{\mathrm{T}} + H^a_{\mathrm{R}}$ and applying the Born, Born–Markov and secular approximations [21], one obtains a Pauli master equation for the populations ρ_{mm} of the thermometer,

$$\frac{d\rho_{mm}}{dt} = \sum_{n\neq m} \rho_{nn} W_{mn} - \rho_{mm} \sum_{n\neq m} W_{nm}. \tag{2.7}$$

Due to detailed balance, the stationary solution of this equation is a Gibbs state proportional to $\exp(-\beta_a H^a)$. Here, H^a denotes the boosted Hamiltonian of the thermometer alone. Abusing notations, we have dropped the subscript "T" since we shall exclusively focus only on the thermometer for the remainder of the chapter.

This result provides the operational link between the accelerated KMS property established in Chapter 1 and the thermalization of accelerated quantum systems. In the remainder of this chapter, we will exploit this framework to analyze in detail how an extended quantum thermometer responds to acceleration, and how an effective temperature emerges from suitable observables.

2.1.3 Temperature Ambiguity for an Extended Thermometer

Before delving into the potential measurement of the thermalization process outlined earlier through implementing a realistic thermometer model, we pause and comment on the type of thermalization we are dealing with. As we will elucidate further, drawing from the insights of Ref. [9], we encounter a form of thermalization that defies comparison within both classical theories of extended relativistic systems and the framework of quantum statistical mechanics applied to extended systems in inertial frames.

In the KM coordinates (1.27), let's consider the change of variables:

$$\begin{aligned} \bar{z} &= z - z_0 \\ \bar{t} &= \left(1 + \frac{a}{c^2} z_0\right) t \\ \bar{a} &= \left(1 + \frac{a}{c^2} z_0\right)^{-1} a \end{aligned} \tag{2.8}$$

where z_0 is some given fixed value. This transformation yields:

$$\begin{aligned} cT &= \left(\bar{z} + \frac{c^2}{\bar{a}}\right) \sinh\left(\frac{\bar{a}\bar{t}}{c}\right) \\ Z &= \left(\bar{z} + \frac{c^2}{\bar{a}}\right) \cosh\left(\frac{\bar{a}\bar{t}}{c}\right) - \frac{c^2}{\bar{a}} + z_0. \end{aligned} \tag{2.9}$$

Consequently, except for a trivial shift in the Z-variable, the relations between the inertial and the KM coordinates remain in the same form. This implies that for a given extended system in motion, attributing a different "uniform" acceleration $\bar{a}$ instead of a is equally valid, achieved simply by choosing $z = z_0$ rather than $z = 0$ as the reference of the system. Consequently, applying the same reasoning as before, we arrive at a distinct Unruh temperature

$$T_{\bar{a}} = \frac{\bar{a}}{a} T_a \tag{2.10}$$

This ambiguity challenges the very notion of the Unruh temperature of an extended system.

However, if the system is "small", i.e., the quantum system is strongly localized around some point $z = z_0$ (and thus remains in the accelerated frame for a sufficient amount of time), the choice of the reference point of the system is natural, being the system localized on a single point $z = z_0$, leading to the conclusion that the system is characterized by a single temperature.

Conversely, in the case of an extended system, we could choose any point inside the quantum system as the reference point. And since different points are associated with different proper accelerations, as expressed by Eq. (1.30), it becomes impossible to identify a single Unruh temperature. This implies that the very concept of the Unruh temperature of an extended system is ambiguous.

This ambiguity in temperature arises from an inherent uncertainty in both the unit of time and, consequently, the unit of energy. Notably, standard clocks attached to different points in the "uniformly" accelerated object lose synchrony. Consequently, we could, in fact, define a local temperature $T(z) \sim a/(1 + az/c^2)$ associated, at each point z. This local temperature would then vary across the object.

Some might argue that this scenario is not unprecedented: a similar situation arises for a classical object in thermal equilibrium within a static gravitational field [9, 83]. In such cases, the presence of gravitational redshifts introduces variations in the natural unit of time and energy between different heights, resulting in a temperature inhomogeneity across the body. Nevertheless, this analogy is not appropriate for our scenario.

Here, we deal with an extended quantum system, where the quantum states are not confined to specific locations but instead encompass the entirety of the system. The equilibrium state of the system is characterized by a distribution over these extended states. According to the modern understanding of thermal equilibrium in large systems, thermal equilibrium is typically a property of the extended states of the system, and under normal circumstances, they are associated with a unique thermodynamic temperature [37, 79].

However, in this context, this is not the case. So, as stressed by BHL, we are dealing here with an ambiguity rather than an inhomogeneity in temperature. This is a novel phenomenon without a classical or quantum analogue.

2.1.4 Modeling the Thermometer through Confined Electrons

Given the challenges mentioned earlier, it's natural to wonder if we can actually measure the thermal effect. The key lies in identifying the right measurable quantities, similar to a "temperature indicator", that can represent a sort of average temperature and maybe provide a result independent of any arbitrarily chosen "central point". Choosing this indicator depends on a more detailed model of the system acting as a thermometer, which we'll explore next.

So far, we've left the concept of the thermometer fairly broad. In theory, it could be any quantum system that has a finite size. However, to create a more practical and workable model, we'll follow the approach laid out by BHL, which treats the thermometer as a single confined electron. (This approach simplifies the analysis but sacrifices a more realistic portrayal of a macroscopic thermometer; we will delve into these complexities in future work).

To keep the confined electron moving with constant acceleration, we must apply special external fields, denoted by $A_\mu = (\varphi, \mathbf{A})$. These fields must remain constant across the series of inertial reference frames $\mathcal{F}(t)$ associated with the accelerated motion. Imagine these fields like a constantly moving box that traps the electron within its frame. (Neither the original work by BHL nor this discussion explores the complex engineering required to create and maintain these fields.)

With these external fields in place, the electron's behaviour can be described using a Dirac quantum field, denoted by ψ. This field follows specific rules (canonical anticommutation relations) compared to an empty space devoid of particles (Minkowski vacuum).

According to Eq. (2.2) the boosted Hamiltonian H^a of such a thermometer is given by the expression

$$H^a = H + \frac{a}{c} K \tag{2.11}$$

where, abusing notation, H^a, H and K now exclusively refer to the thermometer. The familiar expression for the fermionic boosted Hamiltonian H is

$$H = \int d^3x \;\; \mathcal{H} = \int d^3x \;\; \psi^\dagger H^{(1)} \psi \,, \tag{2.12}$$

where

$$\mathcal{H} = \psi^\dagger H^{(1)} \psi$$

and $H^{(1)}$ is the first quantization Dirac Hamiltonian:

$$H^{(1)} = -ic\hbar\boldsymbol{\alpha}\cdot\mathbf{D} + mc^2\beta + e\varphi. \tag{2.13}$$

Here, $\mathbf{D} = \boldsymbol{\nabla} + \frac{e}{i\hbar}\mathbf{A}$, m is the mass of the electron, φ is the electrostatic potential, $\boldsymbol{\alpha} = \gamma_0\boldsymbol{\gamma}$ and $\beta = \gamma_0$, where $(\gamma_0, \boldsymbol{\gamma})$ are the Dirac matrices. Furthermore, Eq. (2.12) and subsequent formulas rely on established regularization procedures for products of field operators evaluated at the same spacetime point.

The boost generator along z in the first quantization is

$$K^{(1)} = \frac{1}{2c}\left(zH^{(1)} + H^{(1)}z\right) \tag{2.14}$$

(see, e.g., [82]). Then, according to the standard rules (see, e.g., [16]), the generator of the boost on the Hilbert space of the quantum field is

$$K = \int d^3x\, \psi^\dagger K^{(1)}\psi. \tag{2.15}$$

Substituting Eq. (2.14) into the above equation and evaluating the expression $H^{(1)}z\psi$, where $H^{(1)}$ is defined by Eq. (2.13), we readily obtain

$$K = \frac{1}{c}\int d^3x\, \psi^\dagger\left(zH^{(1)} - \frac{ic\hbar}{2}\alpha_z\right)\psi\,. \tag{2.16}$$

Finally, upon substituting in Eq. (2.11) the expressions for H and K, we arrive at

$$H^a = \int d^3x\left[N(z)\mathcal{H} - \frac{ia\hbar}{2c}\psi^\dagger\alpha_z\psi\right], \tag{2.17}$$

where, recalling Eq. (1.29), we have grouped the terms proportional to $\mathcal{H}$. Because of the zero of $N(z) = 1 + az/c^2$–the limit in which the Rindler metric (1.28) is well defined–we restrict our analysis to the region where $N(z) > 0$, i.e. the right Rindler wedge. Henceforth, by H^a, we denote the restriction of the right-hand side (2.17) to this specific region.

The diagonalization of H^a can be brought back to solving the c-number time-independent Dirac equation in the region $N(z) > 0$ (see, e.g., [87]):

$$\left[N(z)\left(-ic\hbar\boldsymbol{\alpha}\cdot\mathbf{D} + mc^2\beta + e\varphi\right) - i\frac{a\hbar}{2c}\alpha_z\right]\Psi = E\Psi \tag{2.18}$$

where Ψ is a Dirac 4-spinor. Without the external fields φ and $\mathbf{A}$, the lowest non-negative energy state is the fermionic Rindler vacuum. In this case, the term $N(z) = 1 + az/c^2$ in Eq. (2.18) might cause excitations from negative to positive energy levels, indicating pair production (in alignment with Dirac's initial interpretation of his equation). However, these excitations can be disregarded if

$$\hbar a/c \ll mc^2 \quad \text{and} \quad az/c^2 \ll 1\,. \tag{2.19}$$

Then, the focus can shift solely to the excitation of the additional electron confined within the potential well around $z = 0$. Accordingly, within the regime defined by

Eqs. (2.19), and assuming that the external fields φ and $\mathbf{B}$ are not excessively strong, the positive energy solutions of Eq. (2.18) provide the eigenvalues of H^a that predominantly govern the populations of the energy levels in Eq. (2.6) in the right Rindler wedge.

Additionally, given the specified conditions, a suitable nonrelativistic approximation suffices (see Appendix 2.A), which further simplifies the problem of diagonalizing H^a_{R} to the diagonalization of the 1-particle 2-spinor nonrelativistic Hamiltonian

$$\frac{1}{2m}(i\hbar\boldsymbol{\nabla} + e\mathbf{A})^2 + e\varphi + maz - \frac{e\hbar}{2m}\boldsymbol{\sigma}\cdot\mathbf{B}\,. \tag{2.20}$$

A natural choice for our temperature indicator, as mentioned before, is the electron's spin along the z-axis (directly measured using a suitable macroscopic device or by observing indirect effects like depolarization in a beam of identically prepared electrons). In approximation (2.19), in fact, the spin and orbital motions decouple. Consequently, the thermal distribution across the energy levels implies a spin density matrix [9]

$$\exp\left(\frac{\hbar e}{2m}\frac{\sigma\cdot\mathbf{B}}{k_B T_a}\right) = \exp\left(\frac{\pi c e}{ma}\sigma\cdot\mathbf{B}\right), \tag{2.21}$$

where T_a is the Unruh temperature associated with the (single) acceleration a, i.e., the acceleration of the electron near $z = 0$.

The results obtained using the lowest order Hamiltonian (2.20) omit spin-orbit coupling. Consequently, the BHL model decouples the spin from the spatial degrees of freedom, preventing it from registering the effects of varying accelerations within the extended quantum system. This leads to a Unruh temperature that does not reflect the extended nature of the system, as shown by Eq. (2.21).

We conclude that the ambiguity of temperature doesn't pose a significant challenge in this simplified model and within this approximation. The main hurdle becomes the practical difficulty of confining the electron for an extended period.

2.2 Extended Thermometers with Spin-Spatial Degrees of Freedom Coupling

Recognizing the limitation of omitting the spin-orbit coupling, BHL suggested the presence of these effects in higher-order approximations. We address this by incorporating the next-order contributions in $1/c^2$ using a more straightforward approach. We assume that the magnetic field $\mathbf{B}$ is strong enough to make the higher order magnetic moment term from Eq. (2.20) the only relevant term at order $1/c^2$ (see Appendix 2.A for the full derivation, in particular Eq. (2.45)).

To ensure the validity of the regime characterized in Sec. 2.1.4 and avoid the phenomenon of pair production, conditions (2.19) must hold. The first condition $\hbar a/c \ll mc^2$ (for an electron) implies $a \ll 10^{29}\,\mathrm{m/s^2}$, which is comfortably satisfied by achievable Unruh accelerations, typically on the order of $10^{20}\,\mathrm{m/s^2}$. For this latter Unruh acceleration, the second condition $az/c^2 \ll 1$ requires $z \ll 10^{-3}\,\mathrm{m}$. This

means that we can have a quantum thermometer delocalized over a “macroscopic" length scale.

To simplify the treatment, we take **B** uniform (in the accelerated frame) and direct along z, so that the Hamiltonian H^a to be diagonalized becomes

$$H^a = -\frac{\hbar^2}{2m}\frac{\partial^2}{\partial z^2} + U(z) + maz + N(z)\hbar\omega\sigma_z\,, \tag{2.22}$$

where $\omega = |e|B/2m$, m and e denote the mass and charge of the electron, respectively, and σ_z is the third component of the Pauli matrices $\boldsymbol{\sigma}$. Since we selected the spin degrees of freedom as the temperature indicator, this Hamiltonian is the natural choice for modeling the accelerated extended quantum thermometer. Crucially, the presence of the lapse function $N(z)$ in Eq. (2.22) distinguishes our treatment from that of BHL [9]. This inclusion enables the spin to serve as a temperature indicator for a delocalized thermometer, as discussed below.

2.2.1 Tracing out the spatial degrees of freedom

In the regime we have been considering and under the assumption of weak-coupling and long-term interaction [21, 17], the density matrix (2.21) is expected to be replaced with

$$\widetilde{\rho}^a_{\beta_a} \propto \exp\left(-\beta_a H^a\right) \tag{2.23}$$

with H^a given by Eq. (2.22). As the spin along the magnetic field direction serves as our temperature indicator, we need to focus on the reduced density matrix in spin space. This quantity is obtained by tracing out the spatial degrees of freedom from the density matrix $\widetilde{\rho}^a_{\beta_a}$. Denoting the latter by $\widehat{\rho}^a$, the spin density matrix of the thermometer is given by

$$\widehat{\rho}^a \propto \mathrm{Tr}_{\mathrm{space}}\left[\exp\left(-\beta_a H^a\right)\right] = \sum_n \langle n|e^{-\beta_a H^a}|n\rangle \tag{2.24}$$

where $|n\rangle$ is any orthonormal basis in Hilbert space of the purely spatial degrees of freedom.

To compute $\widehat{\rho}^a$, we first need a tractable expression for $\exp\left(-\beta_a H^a\right)$. This can be readily achieved by making appropriate approximations based on the physical regime of interest. Recalling the definition in Eq. (1.29), we expand $N(z)\hbar\omega\sigma_z$ and decompose the total Hamiltonian H^a (Eq. (2.22)) into the following terms: $H_{\mathrm{spin}} = \hbar\omega\sigma_z$ (spin term), $H_{\mathrm{int}} = az/c^2\hbar\omega\sigma_z$ (interaction term), and H_{space} (implicitly defined by the remaining terms in Eq. (2.22)).

Given the separation of scales between the particle’s mass-energy and the interaction term ($mc^2 \gg \hbar\omega$), we can employ first-order perturbation theory to treat H_{int} as a small perturbation to $H_{\mathrm{space}} + H_{\mathrm{spin}}$. This allows us to solve for the eigenstates and eigenvalues approximately. To implement this, let us consider first the diagonal representation

$$\exp\left(-\beta_a H^a\right) = \sum_{n,\sigma} e^{-\beta_a \mathcal{E}^\sigma_n}|\Psi^\sigma_n\rangle|\sigma\rangle\langle\sigma|\langle\Psi^\sigma_n|\,, \tag{2.25}$$

where $\sigma = \pm 1$, with $|\sigma\rangle$ denoting the two eigenstates of σ_z, and $|\Psi_n^\sigma\rangle\,|\sigma\rangle$ being the eigenstates of H^a corresponding to the eigenvalues $\mathcal{E}_n^\sigma$.

The first-order approximation in $\hbar\omega/mc^2$ of the right-hand side of Eq. (2.25) is given by (see Appendix 2.B)

$$\sum_{n,\sigma} e^{-\beta_a E_n - \overline{\beta}_n \sigma \hbar\omega}\, |\Psi_n^{\sigma(1)}\rangle\,|\sigma\rangle\,\langle\sigma|\,\langle\Psi_n^{\sigma(1)}|\,, \tag{2.26}$$

where

- E_n are the eigenvalues of H_{space};
- $\overline{\beta}_n = \beta_a(\overline{z}_n)$, with $\beta_a(z) = \beta_a(1 + az/c^2)$, and

$$\overline{z}_n = \int z|\Phi_n(z)|^2 dz \tag{2.27}$$

  is the mean position of the particle in the n-th eigenstate Φ_n of H_{space}; equivalently, since $\beta_a = \beta_a(z)$ is a linear function, $\overline{\beta}_n$ can be regarded as the mean value of β in the state Φ_n, i.e.,

$$\overline{\beta}_n = \int \beta_a(z)|\Phi_n(z)|^2\, dz\,; \tag{2.28}$$

- $\Psi_n^{\sigma(1)}$ represents the first-order corrections to the eigenstates of H^a (see Eq. (2.49) in Appendix 2.B).

Finally, substituting the approximate expression for $\exp(-\beta_a H^a)$ (Eq. (2.26)) into Eq. (2.24) and choosing the basis states $|n\rangle$ in Eq. (2.24) to be the first-order corrected eigenstates $|\Psi_n^{\sigma(1)}\rangle$, we obtain the reduced density matrix in spin space up to the first order in $\hbar\omega/(mc^2)$:

$$\widehat{\rho}^a \propto \sum_\sigma c_\sigma |\sigma\rangle\langle\sigma|\,, \tag{2.29}$$

where c_σ are coefficients given by

$$c_\sigma = \sum_n e^{-\beta_a E_n - \overline{\beta}_n \hbar\omega\sigma}\,. \tag{2.30}$$

Let's summarize the key quantities in Eqs. (2.29) and (2.30) for clarity and future reference: β_a signifies the inverse Unruh temperature associated with the Rindler frame, $\overline{\beta}_n$ represents the mean inverse Unruh temperature in the spatial states Φ_n (the eigenstates of H_{space}) as determined by Eq. (2.28), and E_n corresponds to the energies of the states Φ_n (the eigenvalues of H_{space}).

In its present form, the spin state described by Eq. (2.29) is not thermal. However, as we shall elucidate in the following, through appropriate adjustments to the potential U and careful consideration of the order of magnitudes involved, we will demonstrate that the spin state described by Eq. (2.29) may closely approximate a thermal state.

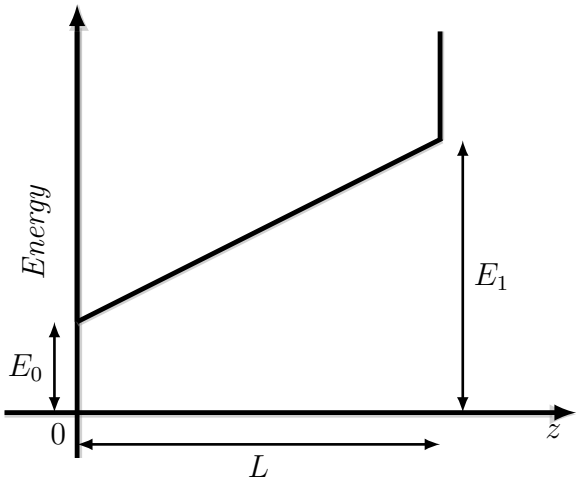

Figure 2.1: Infinitely deep well $U(z)$, with boundary energies E_0 and $E_1 \sim E_0 + maL$.

2.2.2 Nonlocal Unruh effect in an extended well

The spatial properties of the systems are determined by the confining potential $U(z)$ which ultimately determines the form of the eigenstates Φ_n of H_{space}.

Assuming $U(z)$ as an infinitely deep well with a linear size L, with its left side situated in $z = 0$, and tilted due to the lapse $N(z)$, the eigenvalues E_n of the spatial Hamiltonian H_{space} can be determined numerically from Eq. (2.30). It turns out that for an acceleration of the order $a \sim 2.5 \times 10^{20}$ m/s^2, and $L \sim 10^{-7}$ m, only the ground state of the spatial degrees of freedom is populated. That is, in the sum over n in Eq. (2.29), only the term $n = 0$, corresponding to the ground state of H_{space}, contributes. Consequently, the reduced density matrix $\widehat{\rho}^a$ becomes

$$\widehat{\rho}^a \propto \sum_{\sigma} e^{-\overline{\beta}_0 \hbar\omega\sigma} |\sigma\rangle\langle\sigma|. \tag{2.31}$$

This is the thermal state of the spin-thermometer at inverse temperature $\overline{\beta}_0$ with respect to the spin Hamiltonian H_{spin}. In this case, the thermometer registers a unique temperature despite experiencing different accelerations. Still, the thermometer keeps track of the nonlocal features and extensions of the wells since $\overline{\beta}_0$ represents the mean value of the inverse local Unruh temperatures (2.28) over the full spatial extension of the thermometer in the ground state. For a highly localized well, Eq. (2.31) reproduces the BHL result expressed by Eq. (2.20).

In other words, the spin-based thermometer measures an average inverse Unruh temperature, reflecting the influence of the extended quantum system's delocalization. This can be interpreted as if the particle is traversing a confined region with local temperature variations due to differences in acceleration. The spin thermometer essentially averages these local inverse temperatures, weighted by the particle's position within the system. It's essential to acknowledge the "as if" nature of this interpretation: attributing a genuinely spatially varying temperature is inappropriate (as elucidated in Sec. 2.1.3); moreover, within the confines of conventional quantum mechanics, genuine particle motion finds no place. Nevertheless, this effectively encapsulates the non-local character of the phenomenon.

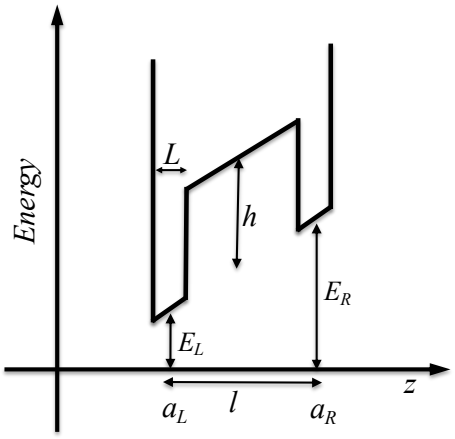

Figure 2.2: A pictorial representation of the double well-confining potential. The left and right wells have length L and are separated by a distance $l \gg L$. They are accelerated with proper acceleration a_L and a_R, respectively. The symmetric potential is tilted because of the relativistic effects.

2.2.3 Unruh effect in sharply localized multiple wells

Let us now consider a double-well confining potential. For simplicity, we assume to have two square wells of linear dimension L separated by l as shown in Fig. 2.2. As in the previous section, we take $a \sim 2.5 \times 10^{20}$ m/s^2, and $L \sim 10^{-7}$ m and assume that $L \ll l \lesssim 10^{-3}$ m (extending to the upper limit the second condition in Eq. (2.19)), so that the system can be delocalized over a macroscopic distance while still remaining within the non-relativistic regime. This would further support the considerations made at the end of the previous section.

The large separation of the two wells implies that there is no tunneling between them. For deep wells, only the lowest spatial eigenstates play a role in the dynamics, and these are strongly localized around the center of the wells. At the same time, following the results obtained in Sec. 2.2.2, for $L \sim 10^{-7}$ m, we expect only the ground states associated with the left and right wells to be populated. We denote these eigenstates and eigenvalues with $\phi_{L,R}$ and $E_{L,R}$, respectively. We also define the energy of the left (right) well in the inertial frame with E_L^0 (E_R^0) and the corresponding one with tilting due to the lapse with E_L (E_R).

To have an estimate of the energy scales, we take the left well in Fig. 2.2 as the reference frame, i.e., $a = a_L$ and $\beta_a = \beta_L$, and rescale the energy to have $E_L = E_L^0 = 0$. The right well ground state energy is $E_R = E_R^0 + mal$ so that the relativistic tilting increases the energy of the well.

For a symmetric double well $E_R^0 = E_L^0 = 0$, and $\beta_a E_R \sim 10^6$. Such value for the exponent implies that the right well is not populated, and, effectively, the particle is always found in the left well. As a consequence, the spin state is thermal with inverse temperature $\beta_a = \beta_L$ even if the system has a macroscopic extension $l \sim 10^{-3}$ m.

However, there are situations, as discussed in Sec. 2.2.2, where the thermometer registers an average inverse temperature. An example is the asymmetric well with $E_R^0 \sim -mal$ so that $E_R \sim E_L = 0$. In this case, the relativistic tilting cancels

the potential asymmetry, resulting in symmetric wells in the accelerated frame. Again, only the ground state is populated, but it is extended over the two wells, i.e., $\Phi_g \sim (\Phi_L + \Phi_R)/\sqrt{2}$. Consequently, from Eq. (2.28), the thermalizing inverse average temperature of the thermometer is

$$\overline{\beta}_0 = \frac{\beta_L + \beta_R}{2} \tag{2.32}$$

and, being $\beta_R \sim \beta_L(1 + al/c^2)$,

$$\overline{\beta}_0 = \beta_L \left(1 + \frac{a}{c^2}\frac{l}{2}\right). \tag{2.33}$$

And, written in terms of $a_R = a/(1 + al/c^2)$, from Eq. (2.32)

$$\overline{\beta}_0 = \frac{\beta_L + \beta_R}{2} = \frac{1}{2}\left(\frac{\beta_R}{1 + \frac{al}{c^2}} + \beta_R\right) = \beta_R \left(1 - \frac{\frac{al}{2c^2}}{1 + \frac{al}{c^2}}\right) = \beta_R \left(1 - \frac{a}{c^2}\frac{l}{2}\right). \tag{2.34}$$

Therefore, the mean inverse temperature is shifted by half the distance between the two wells $l/2$.

2.3 Summary of the results

We began by examining existing research on the Unruh effect in extended quantum systems. We then explored how the finite size of these systems becomes crucial. This analysis brings us closer to a realistic experimental setup, likely involving storage rings [1], where the Unruh effect could potentially be observed - although for the latter case, further study of uniform circular acceleration is needed. In this scenario, our thermometer is modeled as a single electron confined within a constantly accelerating box by external fields. This electron exists as a low-energy state of a zero-temperature fermionic field. The electron's spin interacts with a quantum field in its vacuum state, mimicking a thermal reservoir for the accelerated electron. While a true temperature cannot be definitively assigned to a delocalized electron, we can measure a unique value in a specific regime by carefully choosing the electron's spin as a temperature indicator.

This effect manifests itself most prominently when the electron's energy is low. Additionally, specific conditions are required to maintain its delocalization within the box. Under these circumstances, we can treat the electron's motion non-relativistically while retaining a remnant of relativistic effects through its spin degrees of freedom. This approach effectively captures the key aspects of the phenomenon without delving into all the complexities of a fully relativistic treatment.

Building on the arguments presented in Ref. [9], we show that the stationary solution for the reduced spin density matrix [see Eq. (2.29)] lacks a strictly thermal character. However, through a more refined approximation compared to Ref. [9], we identify and describe the precise conditions under which a form of thermalization can emerge, even for extended quantum systems. Our results indicate that under specific conditions, carefully designed measurements might lead to a reevaluation of our understanding

of Unruh thermalization. In particular, we analyzed two scenarios: a large confining well and sharply localized multiple wells. Notably, the calculated temperature in these cases represents an average across the entire confined region. This implies that while an extended system may not possess a single, well-defined temperature, specific measurements can still extract a unique effective temperature that reflects the nonlocal and extended nature of the quantum system.

2.A Non-relativistic approximation of Dirac equation in accelerated frames

The derivation of the non-relativistic approximation of Eq. (2.22) to yield Eq. (2.22) can be readily achieved by adapting standard methods (assuming $N(z) = 1$) to the specific case at hand ($N(z) = 1 + az/c^2$). We include it here for completeness. To simplify the analysis, we will focus on the time-dependent c-number Dirac equation

$$i\hbar\frac{\partial\Psi}{\partial t} = \left[\left(1+\frac{az}{c^2}\right)(-ic\hbar\alpha^i \mathrm{D}_i + mc^2\beta + e\phi) - i\frac{a\hbar}{2c}\alpha_z\right]\Psi. \tag{2.35}$$

where $\Psi = (\bar{\chi}, \bar{\phi})$ is a Dirac 4-spinor defined in terms of the 2-spinors $\bar{\chi}, \bar{\phi}$. Accordingly, Eq. (2.35) can be written as

$$i\hbar\frac{\partial\bar{\chi}}{\partial t} = -i\hbar c\left(1+\frac{az}{c^2}\right)\sigma\cdot\mathbf{D}\bar{\phi} - i\hbar\frac{a}{2c}\sigma_z\bar{\phi} + \left(1+\frac{az}{c^2}\right)(mc^2 + U(z))\bar{\chi} \tag{2.36}$$

$$i\hbar\frac{\partial\bar{\phi}}{\partial t} = -i\hbar c\left(1+\frac{az}{c^2}\right)\sigma\cdot\mathbf{D}\bar{\chi} - i\hbar\frac{a}{2c}\sigma_z\bar{\chi} - \left(1+\frac{az}{c^2}\right)(mc^2 - U(z))\bar{\phi}. \tag{2.37}$$

Let $N(z)$ be the lapse function defined by Eq. (1.29). Moreover, define

$$\begin{pmatrix}\bar{\chi}\\ \bar{\phi}\end{pmatrix} = \exp\left[-i\frac{tmc^2}{\hbar}N(z)\right]\begin{pmatrix}\chi\\ \phi\end{pmatrix}. \tag{2.38}$$

(see, e.g., [49]). Then the 2-spinors ϕ and χ satisfy the equations

$$i\hbar\frac{\partial\chi}{\partial t} = -i\hbar cN(z)\sigma\cdot\mathbf{D}\phi - macN(z)\sigma_z\phi - i\hbar\frac{a}{2c}\sigma_z\phi + N(z)U(z)\chi \tag{2.39}$$

$$i\hbar\frac{\partial\phi}{\partial t} = -i\hbar cN(z)\sigma\cdot\mathbf{D}\chi - macN(z)\sigma_z\chi - i\hbar\frac{a}{2c}\sigma_z\chi - N(z)(2mc^2 + U(z))\phi.$$

Assuming $\hbar\partial_t\phi \ll mc^2$ and $U(z) \ll mc^2$, the second equation becomes

$$\phi \simeq -\frac{1}{2mc^2}\left(i\hbar c\sigma\cdot\mathbf{D} + mac\sigma_z + i\hbar\frac{a}{2c}\frac{1}{N(z)}\sigma_z\right)\chi. \tag{2.40}$$

Substituting the relation between ϕ and χ into Eq. (2.39), it becomes

$$\begin{aligned}i\hbar\frac{\partial\chi}{\partial t} = N(z)\Bigg(&-\frac{\hbar^2}{2m}(\sigma\cdot\mathbf{D})^2 + i\frac{\hbar at}{2}(\sigma\cdot\mathbf{D})\sigma_z - \frac{\hbar^2 a}{4mc^2}\frac{1}{N(z)}(\sigma\cdot\mathbf{D})\sigma_z\\ &+\frac{\hbar^2a^2}{4mc^4}\frac{1}{N(z)^2}\Bigg)\chi + N(z)\sigma_z\left(i\frac{\hbar at}{2}\sigma\cdot\mathbf{D} + \frac{ma^2t^2}{2}\sigma_z + i\frac{\hbar a^2t}{4c^2}\frac{1}{N(z)}\sigma_z\right)\chi\\ &+\sigma_z\left(-\frac{\hbar^2a}{4mc^2}\sigma\cdot\mathbf{D} + i\frac{\hbar a^2t}{4c^2}\sigma_z - \frac{\hbar^2a^2}{8mc^4}\frac{1}{N(z)}\sigma_z\right)\chi + N(z)U(z)\chi.\end{aligned}$$

Then, using $\{\sigma^i, \sigma^j\} = 2\delta^{ij}\mathbb{1}$, we obtain

$$
\begin{aligned}
i\hbar\frac{\partial\chi}{\partial t} &= N(z)\Big(-\frac{\hbar^2}{2m}(\sigma\cdot\mathbf{D})^2 + i\hbar at\delta^{iz}\mathrm{D}_i\Big)\chi + \frac{ma^2t^2}{2}N(z)\chi \\
&\quad + \Big(-\frac{\hbar^2 a}{2mc^2}\delta^{iz}\mathrm{D}_i + i\frac{\hbar a^2 t}{2c^2} + \frac{\hbar^2 a^2}{8mc^4}\frac{1}{N(z)}\Big)\chi + N(z)U(z)\chi \\
i\hbar\frac{\partial\chi}{\partial t} &= \frac{1}{2m}N(z)\Big(-i\hbar(\sigma\cdot\mathbf{D}) - mat\sigma_z\Big)^2\chi \\
&\quad + \Big(-\frac{\hbar^2 a}{2mc^2}\mathrm{D}_z + i\frac{\hbar a^2 t}{2c^2} + \frac{\hbar^2 a^2}{8mc^4}\frac{1}{N(z)}\Big)\chi + N(z)U(z)\chi. \qquad (2.41)
\end{aligned}
$$

We now apply the transformation $\chi = e^{imazt/\hbar}\Psi$ (with abuse of notation Ψ is now denoting a 2-spinor). Thus, (2.41) becomes

$$
\begin{aligned}
i\hbar\frac{\partial\Psi}{\partial t} &= -\frac{\hbar^2}{2m}N(z)(\sigma\cdot\mathbf{D})^2\Psi - \frac{\hbar^2 a}{2mc^2}\mathrm{D}_z\Psi \\
&\quad + \frac{\hbar^2 a^2}{8mc^4}\frac{1}{N(z)}\Psi + N(z)U(z)\Psi + maz\Psi. \qquad (2.42)
\end{aligned}
$$

Using the well know Pauli vector identity for two vectors $\mathbf{u}, \mathbf{v}$

$$(\sigma\cdot\mathbf{u})(\sigma\cdot\mathbf{v}) = \mathbf{u}\cdot\mathbf{v} + i\sigma\cdot(\mathbf{u}\times\mathbf{v})$$

and given that

$$(i\hbar\nabla + e\mathbf{A})(i\hbar\nabla + e\mathbf{A})\Psi = ie\hbar\mathbf{B}\Psi$$

where $\mathbf{B} = \nabla\times\mathbf{A}$, the Pauli-like equation (2.42) becomes

$$
\begin{aligned}
i\hbar\frac{\partial\Psi}{\partial t} &= \frac{1}{2m}N(z)(i\hbar\boldsymbol{\nabla} + e\mathbf{A})^2\Psi - \frac{e\hbar}{2m}N(z)\boldsymbol{\sigma}\cdot\mathbf{B}\Psi \\
&\quad + \frac{i\hbar a}{2mc^2}\delta^{iz}(i\hbar\boldsymbol{\nabla} + e\mathbf{A})_i\Psi + \frac{\hbar^2 a^2}{8mc^4}\frac{1}{N(z)}\Psi + N(z)U(z)\Psi + maz\Psi. \qquad (2.43)
\end{aligned}
$$

At first order in $1/c$, Eq. (2.43) is

$$i\hbar\frac{\partial\Psi}{\partial t} = \frac{1}{2m}(i\hbar\boldsymbol{\nabla} + e\mathbf{A})^2\Psi - \frac{e\hbar}{2m}\boldsymbol{\sigma}\cdot\mathbf{B}\Psi + U(z)\Psi + maz\Psi \qquad (2.44)$$

which is the same obtained in Ref. [9].

However, in this approximation, the spin degrees of freedom, i.e., the ones used as a thermometer, are not affected by the lapse contribution that is of order $1/c^2$. We can then consider the next expansion contribution, i.e., to the order $1/c^2$, and, to simplify the problem, we make the following additional assumptions: *i*) we assume that the magnetic field B is strong enough to produce observable effects in the spin degrees of freedom and, *ii*) that the confining potential $U(z)$ induces localization of the lowest eigenstates of the Hamiltonian in Eq. (2.43). In this case, the equation becomes

$$i\hbar\frac{\partial\Psi}{\partial t} = \frac{1}{2m}(i\hbar\boldsymbol{\nabla} + e\mathbf{A})^2\Psi + U(z)\Psi + maz\Psi + N(z)\hbar\boldsymbol{\omega}\cdot\boldsymbol{\sigma}\Psi \qquad (2.45)$$

where we have substituted $\mathbf{B}$ with the corresponding $\boldsymbol{\omega} = -e\mathbf{B}/(2m)$. Note that, because we are considering a perturbative expansion on $1/c$, we are assuming $az/c^2 \ll 1$. Therefore, given that $a \approx 10^{20}\,\mathrm{m}\cdot\mathrm{sec}^{-2}$, the range of validity of Eq. (2.45) is $z \ll 10^{-3}\,\mathrm{m}$.

2.B Perturbative expansion of H

From Eq. (2.45), we obtain the Hamiltonian of the system H, respectively. We denote with $\mathcal{E}_n^\sigma$ and $|\Psi_n^\sigma\rangle\,|\sigma\rangle$ (with $\sigma = \pm$) its eigenvalues and eigenstates. With these notations, we can write the Hamiltonian H as

$$H = \sum_{n,\sigma} \mathcal{E}_n^\sigma |\Psi_n^\sigma\rangle|\sigma\rangle\langle\sigma|\langle\Psi_n^\sigma|. \tag{2.46}$$

As discussed in the main text, we separate the Hamiltonian (2.22) in three contributions: H_{space}, H_{spin} and H_{int} which include the spatial, the spin degrees of freedom and the interaction between the two. Explicitly, they read

$$\begin{aligned} H_{\text{space}} &= -\frac{\hbar^2}{2m}\frac{\partial^2}{\partial z^2} + U(z) + maz \\ H_{\text{spin}} &= \hbar\omega\sigma_z \\ H_{\text{int}} &= \frac{az}{c^2}\hbar\omega\sigma_z \end{aligned} \tag{2.47}$$

Projecting on the $|\pm\rangle$ spin sector, we obtain two eigenequations for the Hamiltonian (2.22)

$$H^\pm = -\frac{\hbar^2}{2m}\frac{\partial^2}{\partial z^2} + U(z) + maz \pm \hbar\omega \pm \frac{az}{c^2}\hbar\omega \tag{2.48}$$

Since in the realistic cases, $mc^2 \gg \hbar\omega$, the last term associated to H_{int} can be treated as a perturbation. This allows us to separate the spatial and spin degrees of freedom and keep the first-order correction in $\hbar\omega/(mc^2)$ to obtain the eigenvalues and eigenstates [49]

$$\begin{aligned} \mathcal{E}_n^\pm &= E_n \pm (1 + az_n/c^2)\hbar\omega \\ |\Psi_n^{\pm(1)}\rangle &= |\Phi_n\pm\rangle \pm \frac{\hbar a\omega}{c^2}\sum_k \frac{z_{k,n}}{E_n - E_k}\,|\Phi_k\pm\rangle\,, \end{aligned} \tag{2.49}$$

where $z_{k,n} = \langle\Phi_k|z|\Phi_n\rangle$, E_n and $|\Phi_n\rangle$ are eigenvalues and eigenstates of the space Hamiltonian, respectively. From this, we immediately obtain the stationary density matrix in Eq. (2.25) in the main text.

Chapter 3

Probing the Unruh effect in circular trajectories

3.1 Rotational Unruh effect: general setting and motivation

In the previous chapters we have developed the conceptual and technical framework required to describe the response of quantum detectors coupled to relativistic quantum fields along non-inertial trajectories. Special emphasis has been placed on the Unruh–DeWitt detector as an conceptual and operational probe of quantum field correlations along prescribed worldlines, and on the role of stationarity, Kubo–Martin–Schwinger (KMS) conditions, and detailed balance in characterizing equilibrium and near-equilibrium situations. Within this framework, the Unruh effect associated with uniform linear acceleration has emerged as a paradigmatic example in which the response of the detector admits a genuine thermal interpretation, with a universal temperature proportional to the proper acceleration.

The purpose of the present chapter is to move beyond this special case and to investigate a broader class of accelerated motions, focusing on general stationary trajectories and, in particular, on rotational motion, from the non-relativistic to the ultra-relativistic regime. The central object of study remains the detector response function, but the physical questions that arise are qualitatively different. In contrast to the standard Unruh effect, rotational motion does not generically lead to a strictly thermal spectrum, nor to a universal temperature independent of the detector's internal structure. Understanding the origin, interpretation, and limitations of this non-thermality is one of the main motivations of this chapter.

From a conceptual standpoint, investigations of observers undergoing non-linear acceleration offer an essential framework for disentangling which aspects of the Unruh effect are intrinsically associated with acceleration, and which instead depend on more delicate global characteristics of the observer's trajectory and the corresponding notion of time evolution. It is now well established that acceleration, by itself, does not suffice to ensure a strictly thermal response of a detector. This realization naturally motivates the question of whether one can formulate an operational notion of effective temperature, suitable for exploring the regimes in which such a quantity

meaningfully corresponds to a genuine thermal state.

A key development in extending the study of the Unruh effect beyond uniform acceleration is the systematic classification of stationary worldlines introduced by Letaw and reviewed in Chapter 1. The stationarity of the corresponding metric is closely connected to the fact that the generator of time evolution can be written as a linear combination of generators of the Poincaré group. As a result, this classification identifies the most general set of motions for which a steady-state detector response is well defined. Moreover, the stationarity of the detector ensures the existence of a well-defined asymptotic stationary limit, which is essential for a consistent statistical analysis of the system.

Among non-linearly accelerated motions, uniform circular motion occupies a distinguished position. On the one hand, it is conceptually simple and experimentally appealing, as it allows the detector to remain within a finite spatial region for arbitrarily long interaction times. On the other hand, it exhibits features that sharply distinguish it from the uniformly accelerated case. In circular motion, the detector experiences a constant proper acceleration, yet its response does not reduce to that of a thermal bath at the Unruh temperature associated with that acceleration. This immediately signals that the thermal character of the Unruh effect cannot be attributed solely to the local magnitude of the acceleration.

The physical relevance of circular motion was first emphasized in the context of electron storage rings, where the depolarization of relativistic electrons was interpreted as a manifestation of vacuum fluctuations experienced along a circular trajectory. This line of investigation, initiated by Bell and Leinaas [10, 53], highlighted both the similarities and the crucial differences between linear and circular acceleration. While vacuum fluctuations do lead to depolarization effects in both cases, the excitation spectrum in circular motion depends sensitively on additional parameters, such as the angular velocity and the internal structure of the detector, and does not possess the universal thermal form characteristic of the Unruh effect.

Like the standard Unruh effect, the circular motion can be formulated in terms of positive-frequency modes of a quantum field. The analysis of these features requires careful consideration of the notion of time evolution and energy in non-inertial frames involving rotation [55]. For stationary trajectories with rotation, the generator of proper-time translations is generally a linear combination of the Minkowski Hamiltonian and rotation generators [46]. As a consequence, the corresponding Hamiltonian is not a priori bounded from below, and the standard identification of the vacuum as the ground state becomes subtle. In this setting, the Minkowski vacuum remains a physically meaningful state, but the excitation of a detector may occur not only through the absorption of positive-energy quanta, but also through the emission of modes with negative energy with respect to the detector's notion of time. This mechanism plays a central role in the non-thermal features of the detector response in rotational motion.

These issues have been analyzed in detail by Unruh et al. [12], who clarified the structure of detector excitation in rotating frames and emphasized the importance of global causal properties, such as the presence of static limits and ergoregions. A key result of their analysis is that the response is governed by local properties of the trajectory and by the spectral content of field correlations sampled along it. This

reinforces the operational viewpoint adopted throughout this thesis, in which the detector response, rather than the notion of particles or vacua associated with a given coordinate system, is taken as the primary physical observable.

In recent years, the study of detector responses along stationary worldlines has been revisited in more systematic and quantitative perspectives [38]. In particular, several works have emphasized that, even in the absence of strict thermality–namely, when the state of the system cannot be described by a Gibbs distribution with a constant temperature parameter–it is often still possible to introduce an energy-dependent notion of temperature. Although this idea may seem a contradiction at first glance, it turns out to be particularly useful in various generalizations of the Unruh effect. As we shall see, there exist trajectories that give rise to states which can be described as asymptotically thermal, in a sense that will be clarified in the following sections. This notion is commonly referred to as an effective temperature.

Such temperatures typically depend on the detector's energy gap and on the geometric invariants of the trajectory, and reduce to the Unruh temperature only in the special case of uniform linear acceleration. This effective temperature provides a useful operational tool for comparing different stationary motions and for assessing their potential experimental relevance.

From this modern perspective, circular motion represents a prototypical example of an 'Unruh-like' effect without exact thermality. Analytic and numerical studies [12, 38] have shown that, in appropriate limits, the effective temperature associated with circular motion reaches the same order of magnitude as the Unruh temperature for linear acceleration, while displaying a nontrivial dependence on the detector's energy gap. These results have renewed interest in the possibility of observing Unruh-like phenomena in laboratory settings, including analogue gravity experiments and condensed-matter systems [28, 62].

The final aim of this chapter is to build upon this body of work and to present new results on the rotational Unruh effect for electrons rotating in storage rings, in which the detector's motion and internal dynamics are not treated as independent quantities. In particular, we shall consider a scenario in which the circular motion of the detector is generated by an external magnetic field, so that the kinematics of the trajectory, the proper acceleration, and the internal energy gap of the detector are all controlled by a common physical parameter. This coupling between dynamics and kinematics leads to qualitative differences with respect to previously studied models of circular motion and gives rise to novel features in the detector response, which will be analyzed in detail in the following sections.

The structure of the chapter is as follows. In Sec. 3.2 we give a proof of the fact that the KMS condition cannot be extended to uniform circular motion, setting the field for the UDW detector model and the notion of effective temperature. In Sec. 3.3 we review the classification of stationary worldlines and the general properties of detector response functions along such trajectories, following Letaw's seminal work. In particular, we will focus on the cuspide case, which is the only analytically solvable case among the more general stationary motions. In Sec. 3.4 we review the QFT interpretation of the lacking of a thermal spectrum for trajectories generated by the linear combination of time and rotation operators. In Sec. 3.5 we focus on uniform circular motion and review the main results obtained by Biermann et al., emphasizing

the physical origin of the non-thermal detector response. Finally, in Sec. 4.2 we present the original results of this thesis on rotational Unruh effect in magnetically induced circular motion and discuss their physical and experimental implications.

3.2 Absence of KMS Periodicity for Uniform Circular Motion

We consider an Unruh–DeWitt detector undergoing uniform circular motion with constant radius R and constant angular velocity ω. Following the discussion of Chapter 1, the detector worldline can be parametrized by the proper time τ as

$$x^\mu(\tau) = \big(cT(\tau),\, X(\tau),\, Y(\tau),\, Z(\tau)\big) = \big(c\,\gamma\tau,\, R\cos(\gamma\omega\tau),\, R\sin(\gamma\omega\tau),\, 0\big), \tag{3.1}$$

where

$$\gamma = \frac{1}{\sqrt{1-\frac{v^2}{c^2}}} = \frac{1}{\sqrt{1-\frac{R^2\omega^2}{c^2}}} \tag{3.2}$$

is the Lorentz factor associated with the constant tangential velocity $v = R\omega$. The coordinate time measured in the inertial laboratory frame is $T(\tau) = \gamma\tau$, while the azimuthal angle evolves as $\Phi(\tau) = \gamma\omega\tau$.

This motion is accelerated but does not possess a global event horizon: unlike the case of uniform linear acceleration, the rotating observer is not confined to a Rindler wedge. As a consequence, it is not a priori clear whether the Minkowski vacuum, when restricted to this trajectory, can be interpreted as a thermal equilibrium state.

To address this question, we analyze the Wightman function of a free massless scalar field along the circular worldline and study its analytic continuation to complex proper times, following the same rigorous strategy adopted in Sec. 1.6.4 for uniformly accelerated motion.

3.2.1 Wightman function along the circular trajectory

We recall that the Wightman function in the Minkowski vacuum, defined in Chapter 1, is given by

$$G(\tau,\tau') = \langle 0_{\rm M}|\phi(x(\tau))\,\phi(x(\tau'))\,|0_{\rm M}\rangle, \tag{3.3}$$

and for a massless scalar field in $3+1$ dimensions, its explicit form in SI units is given by Eq. (1.20), which we recall here for sake of clarity

$$G_0(\tau,\tau') = -\frac{\hbar}{4\pi^2}\frac{1}{c^2[T(\tau)-T(\tau')-i\epsilon]^2 - \big[\mathbf{X}(\tau)-\mathbf{X}(\tau')\big]^2}. \tag{3.4}$$

Since the trajectory is stationary, the Wightman function depends only on the proper–time difference. We therefore set $\tau' = 0$ without loss of generality and define $G_0(\tau) \equiv G_0(\tau,0)$. Substituting the explicit form of the worldline (3.1), we obtain

$$G_0(\tau) = -\frac{\hbar}{4\pi^2}\frac{1}{\big(c\gamma\tau\big)^2 - \big[R\cos(\gamma\omega\tau)-R\big]^2 - \big[R\sin(\gamma\omega\tau)\big]^2}. \tag{3.5}$$

The spatial terms in the denominator can be simplified using trigonometric identities. Indeed,

$$\begin{aligned}\big[R\cos(\gamma\omega\tau)-R\big]^2+\big[R\sin(\gamma\omega\tau)\big]^2 &= R^2\Big[(\cos\gamma\omega\tau-1)^2+\sin^2\gamma\omega\tau\Big]\\ &= 2R^2\big(1-\cos\gamma\omega\tau\big)\\ &= 4R^2\sin^2\Big(\frac{\gamma\omega\tau}{2}\Big).\end{aligned} \tag{3.6}$$

The Wightman function, with the $i\epsilon$ prescription, along the circular trajectory therefore takes the exact form

$$W(\tau)=\frac{\hbar}{4\pi^2}\frac{1}{\big(c\gamma(\tau-i\epsilon)\big)^2-4R^2\sin^2\big(\frac{\gamma\omega\tau}{2}\big)},\qquad \tau\in\mathbb{R}. \tag{3.7}$$

In the inertial limit $\omega\to 0$ (or $R\to 0$), one has $\gamma\to 1$ and the expression reduces to the standard inertial Wightman function, as expected. For nonzero angular velocity, however, the trigonometric structure of the denominator leads to a markedly different analytic behavior compared to the uniformly accelerated case.

3.2.2 Analytic continuation and singularities

We now promote τ to a complex variable and study the analytic structure of $W(\tau)$. Singularities arise from the zeros of the denominator in Eq. (3.7), which satisfy

$$(c\gamma\tau)^2-4R^2\sin^2\Big(\frac{\gamma\omega\tau}{2}\Big)=0. \tag{3.8}$$

Using the same strategy adopted in Chapter 1, Section 1.5, we extend τ to a complex variable, and introduce the auxiliary variable

$$z=\frac{\gamma\omega\tau}{2}. \tag{3.9}$$

Thus, Eq. (3.8) becomes

$$\sin^2 z=\frac{c^2}{v^2}z^2,\qquad v=R\omega. \tag{3.10}$$

For real z, the inequality $|\sin z|\le 1$ implies that Eq. (3.10) has no solutions other than $z=0$, confirming that no two distinct points on the circular worldline are lightlike separated. Nontrivial solutions must therefore satisfy $\mathrm{Im}(z)\neq 0$. In particular, we consider the case where $z=iy$ with $y\in\mathbb{R}$, Eq. (3.10) reduces to

$$\frac{\sinh y}{y}=\frac{c}{v}>1. \tag{3.11}$$

The function $\sinh y/y$ is even and strictly increasing for $y>0$, with $\sinh y/y=1$ at $y=0$ and diverging as $y\to+\infty$. Hence there exists a unique solution $y_0>0$ of Eq. (3.11). This gives rise to two purely imaginary solutions of Eq. (3.8),

$$\tau=\pm i\,\tau_*,\qquad \tau_*=\frac{2y_0}{\gamma\omega}, \tag{3.12}$$

and no further purely imaginary solutions exist. Consequently, the Wightman function is holomorphic in the open strip

$$-\tau_* < \mathrm{Im}(\tau) < \tau_*, \tag{3.13}$$

and cannot be analytically continued beyond these boundaries due to the presence of isolated singularities.

3.2.3 Failure of the KMS condition

We now prove that there is no inverse temperature β such that the vacuum state in a circular trajectory is a thermal equilibrium state. Such a state must satisfy the KMS condition, which requires the Wightman function to be analytic in the strip $0 < \mathrm{Im}(\tau) < \beta$ and to obey the periodicity relation

$$W(\tau + i\beta) = W(\tau - i0), \qquad \tau \in \mathbb{R}. \tag{3.14}$$

In the present case, the maximal strip of analyticity has finite width $2\tau_*$ and does not exhibit any imaginary–time periodicity. The singularities at $\mathrm{Im}(\tau) = \pm\tau_*$ are not repeated at integer multiples thereof, in contrast with the uniformly accelerated case, where periodic singularities give rise to the Unruh temperature.

Any assumption of a finite KMS period β therefore leads to a contradiction: if $\beta \geq 2\tau_*$, the analytic continuation necessarily crosses a singularity; if $\beta < 2\tau_*$, the periodicity condition cannot be satisfied.

We conclude that the Minkowski vacuum does not satisfy the KMS condition with respect to proper–time translations along a uniformly rotating trajectory. Consequently, an Unruh–DeWitt detector in uniform circular motion does not perceive a genuine thermal spectrum.

3.3 Letaw stationary worldlines and Unruh–DeWitt detector response

The result established in Sec. 3.2 shows, at the level of the Wightman function, that uniform circular motion does not admit a KMS interpretation with respect to proper–time translations along the trajectory. The operational counterpart of this analytic statement is provided by the Unruh–DeWitt (UDW) detector response: stationarity of the pullback correlator yields a time–translation–invariant transition rate, but in general the resulting spectrum is non–Planckian and does not obey exact detailed balance [54].

In Chapter 1 we reviewed Letaw's classification of stationary worldlines in Minkowski spacetime and its geometric characterization in terms of constant curvature invariants. In the present chapter, using the results reviewed in Chapter 1, we will first recall the UDW response formalism as needed for stationary trajectories and then focus on the one nontrivial Letaw worldline—besides uniform linear acceleration—for which the response can be computed fully analytically in elementary functions, namely the cusped trajectory. All intermediate derivations are collected in Appendix 3.A.

3.3.1 UDW detector response for stationary pullbacks

We consider a two–level UDW detector on a timelike worldline $x^\mu(\tau)$, linearly coupled to a real massless scalar field $\phi(x)$ through

$$H_{\rm int}(\tau) = \lambda\ \mu(\tau)\,\phi(x(\tau)), \tag{3.15}$$

where $\mu(\tau)$ the monopole operator in the interaction picture. Working in the Minkowski vacuum $|0\rangle$, we use the standard Wightman function given in Eq. (3.4). We recall that for Letaw–stationary worldlines the invariant interval between two points on the trajectory depends only on the proper–time separation $s = \tau - \tau'$, so that the pullback

$$G_0(s)\ :=\ G_0\big(x(\tau), x(\tau')\big)\Big|_{s=\tau-\tau'} \tag{3.16}$$

is a function of s alone. In the long–interaction–time limit one defines the stationary response function as the Fourier transform

$$\mathcal{G}(E)\ =\ \int_{-\infty}^{+\infty} ds\ \exp\!\left(-\frac{i}{\hbar}Es\right)\ G_0(s), \tag{3.17}$$

where E is the detector energy gap (excitation for $E > 0$, de–excitation for $E < 0$). Up to an overall detector–dependent prefactor, $\mathcal{G}(E)$ gives the transition probability per unit proper time.

As a benchmark, the inertial pullback yields

$$\mathcal{G}_{\rm inert}(E) = -\frac{E}{2\pi\hbar}\,\Theta(-E), \tag{3.18}$$

so that the Minkowski vacuum does not excite an inertial detector, see Appendix 3.A.2 for details.

3.3.2 Cusped worldline: results

Among Letaw's nontrivial stationary trajectories, discussed in Chapter 1, Sec. 2, the cusped worldline admits a fully closed analytic expression for $\mathcal{G}(E)$ in terms of elementary functions. The importance of this case is twofold: On the one hand, it represents an analytically solvable stationary motion beyond the Rindler motion; On the other hand, it is the ultra-relativistic limit of the circular motion. Therefore, it is of crucial relevance for the present discussion.

Using the parametrization

$$x^\mu(\tau) = \left(c\tau + \frac{a^2}{6c}\tau^3,\ \frac{a}{2}\tau^2,\ \frac{a^2}{6c}\tau^3,\ 0\right), \tag{3.19}$$

one finds that the Minkowski squared interval between two points on the worldline, depending only on $s = \tau - \tau'$, takes the form

$$\Delta s^2_{\rm M} = c^2 s^2 + \frac{a^2}{12c^2}s^4. \tag{3.20}$$

Hence the Wightman function (3.4) can be written as the rational function

$$G_{\rm cus}(s) = -\frac{\hbar}{4\pi^2}\,\frac{1}{c^2 s^2 + \frac{a^2}{12c^2}s^4}. \tag{3.21}$$

Its Fourier transform can be evaluated exactly (Appendix 3.A), yielding

$$\mathcal{G}_{\rm cus}(E) = -\frac{E}{2\pi}\,\Theta(-E) + \frac{\alpha}{4\pi}\,e^{-|E|/(\hbar\alpha)}, \qquad \alpha = \frac{a}{2\sqrt{3}\,c}. \tag{3.22}$$

The spectrum associated to this Wightman function is stationary but non–Planckian.

In such a situation, one may introduce a frequency–dependent effective temperature by imposing a generalized detailed balance definition

$$\frac{1}{T_{\rm eff}(E)} = \frac{k_B}{E}\ln\!\left(\frac{\mathcal{G}(-E)}{\mathcal{G}(E)}\right). \tag{3.23}$$

Obviously, in the cases in which the Wightman function satisfies the KMS condition, Eq. (3.23) reduces to the standard constant and well-defined inverse temperature β. Solving the ration (see Appendix 3.A) the explicit form of the effective temperature is given by

$$\frac{1}{T_{\rm cus}(E)} = \frac{k_B}{E}\,\ln\!\left(\frac{E\,\Theta(E) + \frac{\hbar\alpha}{2}\,e^{-|E|/(\hbar\alpha)}}{-E\,\Theta(-E) + \frac{\hbar\alpha}{2}\,e^{-|E|/(\hbar\alpha)}}\right). \tag{3.24}$$

3.4 Energy and time evolution: QFT intuition for the non-thermal character of rotation

The analysis of Sec. 3.2 established, directly from the Wightman function, that uniform circular motion does not exhibit KMS periodicity and therefore does not admit a genuine thermal interpretation. It is useful, however, to complement that explicit analytic result with a more qualitative point of view from quantum field theory. The purpose of the present section is not to add a second proof, but to explain why the failure of thermality in rotational motion is expected on general grounds once one asks what "energy" and "time evolution" mean for a rotating observer.

A standard lesson from QFT in curved spacetime (and, more generally, QFT in non-inertial settings) is that thermality is not merely a statement about time translation invariance. Rather, thermality is tied to the existence of a physically meaningful time flow with respect to which one can define equilibrium. In operational terms, a detector may have a stationary response simply because the trajectory is stationary, yet the corresponding spectrum need not be thermal because the notion of energy relevant to that time flow does not support a genuine equilibrium ensemble.

For stationary worldlines, the observer's motion is generated by a symmetry flow: one can think of the worldline as being transported into itself by a one-parameter family of isometries. In QFT this symmetry selects the notion of "time translations" relevant for the observer, and thus the notion of energy that would enter any equilibrium interpretation. For uniform linear acceleration this structure is exceptionally well behaved: the relevant time flow is associated with a Hamiltonian

that admits a sensible ground state in the appropriate wedge, and the Minkowski vacuum restricted to that wedge has the thermal (KMS) property.

Uniform rotation is different in a way that is conceptually simple. The time flow of a rotating observer mixes an inertial time translation with a spatial rotation. The corresponding energy is therefore not the usual inertial energy, but an "energy in the rotating frame" in which angular momentum contributes with an opposite sign. The qualitative consequence is that modes with sufficiently large angular momentum can carry arbitrarily negative energy with respect to the rotating time flow, even though their inertial energy is positive. This feature does not indicate any instability of the Minkowski vacuum in the inertial sense; it only reflects that the rotating observer's energy bookkeeping is fundamentally different.

Once this is appreciated, the thermodynamic conclusion is essentially immediate: a genuine thermal state in the strict sense would require an equilibrium ensemble with respect to the rotating time evolution. But equilibrium requires, at minimum, that the relevant energy notion behaves like a true Hamiltonian, in particular that it can serve as the basis of a Gibbs weight. If the rotating-frame energy can take arbitrarily negative values, then one should not expect an honest Gibbs description, and correspondingly one should not expect exact KMS periodicity. In this qualitative sense, QFT methods provide a clear structural reason for why rotation does not produce thermality in the same way as uniform linear acceleration.

This perspective is best regarded as a conceptual companion to the explicit Wightman analysis of Sec. 3.2. There, non-thermality appears as a precise statement about analyticity and the absence of imaginary-time periodicity; here, it is understood as a general obstruction to defining equilibrium with respect to the rotating time flow. In the following section we therefore shift attention away from the question of a unique temperature and focus instead on effective, operational notions extracted from specific regimes of the detector response in circular motion.

3.5 Circular motion as an ideal detector model: results in 3+1 dimensions

We now turn to the analysis of the Unruh–DeWitt detector response in uniform circular motion developed by Biermann et al [12] and further refined in subsequent work. Throughout this section we restrict attention to a massless scalar field in $3+1$-dimensional Minkowski spacetime and to the relativistic detector model, which is the setting directly relevant for the present discussion.

The purpose of this section is twofold. First, we present explicitly the main analytic results obtained by Biermann et al. for the effective temperature extracted from the detector response in circular motion, in the asymptotic regimes of large detector energy gap, small energy gap, and ultrarelativistic motion. Second, we emphasize the modeling assumptions under which these results are derived, in particular the separation between the detector's internal energy scale and the kinematic parameters of the motion.

3.5.1 Framework and definition of the circular temperature

In the paper, they consider an Unruh–DeWitt detector with fixed energy gap E in the comoving, i.e. rotating, reference frame, linearly coupled to a massless scalar field in the Minkowski vacuum, following a worldline of uniform circular motion with radius R and angular velocity Ω. The trajectory is stationary and admits a proper-time parametrization with constant Lorentz factor $\gamma = (1 - v^2/c^2)^{-1/2}$, where $v = R\Omega$ is the tangential velocity.

In this stationary setting, the detector response is characterized by the transition rate

$$\mathcal{G}(E) = \int_{-\infty}^{\infty} ds\, e^{-\frac{iEs}{\hbar}} W(s),$$

where $W(s)$ is the pullback of the Wightman function to the circular worldline. In this context, an effective temperature $T_{\mathrm{circ}}(E)$ can be defined operationally through the detailed balance relation

$$\frac{\mathcal{G}(-E)}{\mathcal{G}(E)} = \exp \frac{E}{k_B T_{\mathrm{circ}}(E)}.$$

In the uniformly accelerated case, this function corresponds to a well-defined (and therefore constant) notion of temperature in the usual statistical sense. More generally, it depends on the detector comoving energy gap E.

3.5.2 Large-gap regime

Biermann et al. [12] first analyze the limit of large detector energy gap, $|E| \to \infty$, at fixed v and R. In this regime the detector probes the short-distance structure of the field correlations along the trajectory. In $3 + 1$ dimensions, the response function splits naturally into an inertial contribution and a finite correction due to the acceleration.

In the large-gap limit, the dominant contribution to the excitation rate arises from an exponential suppression controlled by the nearest singularity of the Wightman function in the complex proper-time plane. This leads to an effective circular temperature

$$T_{\mathrm{circ}} = \frac{\hbar c}{k_B} \frac{\gamma v}{2\alpha_0 R},$$

where the parameter α_0 is defined implicitly by $v = (\alpha_0 / \sinh \alpha_0)c$.

It is instructive to compare this temperature with the linear Unruh temperature associated with the same proper acceleration,

$$T_{\mathrm{lin}} = \frac{\hbar a}{2\pi c k_B} = \frac{v^2}{2\pi(1 - v^2/c^2)R}.$$

The ratio $T_{\mathrm{circ}}/T_{\mathrm{lin}}$ is a function of v alone and remains of order unity for all admissible velocities. In particular, in the ultrarelativistic limit $v \to c$ this ratio approaches $\pi/\sqrt{3} \simeq 1.8$.

Small-gap regime

A qualitatively different behavior emerges in the opposite limit of small detector energy gap, $E \to 0$, at fixed v and R. In this regime the detector becomes sensitive to long-time correlations of the field along the circular trajectory, with respect to the characteristic time $\bar{\tau} = \hbar/E$.

In $3+1$ dimensions, the response function remains finite and that the effective temperature approaches a nonzero limit as $E \to 0$. More precisely, the ratio of the circular temperature to the linear Unruh temperature tends to a velocity-dependent constant,

$$\frac{T_{\rm circ}}{T_{\rm lin}} = \frac{c}{v}\sqrt{1-\frac{v^2}{c^2}}\int_0^\infty dz\,\frac{1}{z^2-1}\frac{z^2-\frac{v^2}{c^2}}{z^2-\frac{v^2}{c^2}\sin^2 z}, \tag{3.25}$$

which is finite and strictly positive for all $0 < v < c$. Here $z = \frac{\gamma v}{2R}s$ is a dimensionless parameter.

This result highlights a key feature of the circular motion Unruh effect in $3+1$ dimensions: even at arbitrarily small energy gaps, the detector does not become blind to the acceleration, in contrast with what happens in lower spacetime dimensions [12].

3.5.3 Ultrarelativistic regime

The most striking results concern the ultrarelativistic limit, $v \to c$, in which the detector's tangential velocity approaches the speed of light. In this limit the proper acceleration diverges as $a \simeq \gamma^2 c^2/R$, while the detector gap E is held fixed.

In $3+1$ dimensions, the effective temperature admits a closed asymptotic expression that is uniform in the ratio $Ec/(\hbar a)$. To leading order in $\hbar a/(cE)$, the circular temperature is given by

$$T_{\rm circ} = \frac{|E|}{k_B \ln\!\left(1+\frac{4\sqrt{3}|E|c}{\hbar a}e^{2\sqrt{3}\frac{|E|c}{\hbar a}}\right)},$$

which interpolates smoothly between two simple limits. For $|E|c \ll \hbar a$,

$$T_{\rm circ} \simeq \frac{\hbar a}{4\sqrt{3}k_B c},$$

while for $|E|c \gg \hbar a$, one finds the plateau

$$T_{\rm circ} \simeq \frac{\hbar a}{2\sqrt{3}k_B c}.$$

Expressed in units of the linear Unruh temperature, these limits correspond respectively to

$$\frac{T_{\rm circ}}{T_{\rm lin}} \to \frac{\pi}{2\sqrt{3}} \quad \text{and} \quad \frac{T_{\rm circ}}{T_{\rm lin}} \to \frac{\pi}{\sqrt{3}},$$

in agreement with earlier results [54, 80]. Importantly, these expressions coincide with the effective temperature obtained for the cusped trajectory in the corresponding limits, a result that was already anticipated and discussed in Sec. 3.3.

3.5.4 Interpretation and scope of the model

The analysis of Biermann et al. [12] demonstrates that, within the Unruh–DeWitt detector model, uniform circular motion in $3+1$ dimensions gives rise to well-defined and analytically controlled effective temperatures in several asymptotic regimes. At the same time, these results rely crucially on the assumption that the detector energy gap E is an independent parameter, unrelated to the kinematic quantities R, Ω, and a that characterize the motion.

In this idealized framework, the detector serves as a probe whose internal dynamics can be tuned independently of the external forces required to maintain the circular trajectory. The emergence of a temperature plateau in the ultrarelativistic regime and their agreement with the cusped trajectory should therefore be understood as promising ways to probe the Unruh effect in realistic experimental settings. This distinction between internal dynamics and external forces will be central in the next chapter.

In realistic experimental settings, such as storage rings, the internal energy scale of the detector and the kinematic parameters of the motion are not independent, but are instead jointly determined by the external electromagnetic fields. The consequences of this coupling between dynamics and kinematics will be explored in the following chapter.

3.A Technical derivations for stationary UDW response and the cusped spectrum

This appendix collects the intermediate calculations omitted in Sec. 3.3. We derive the inertial response (3.18) and present a complete analytic evaluation of the UDW response for the cusped stationary worldline, leading to the closed form (3.22).

3.A.1 Stationary pullback and response function

For a prescribed timelike worldline $x^\mu(\tau)$, the pulled–back Wightman function is

$$G_0(s) := G_0\big(x(\tau), x(\tau')\big)\Big|_{s=\tau-\tau'}. \tag{3.26}$$

For stationary worldlines, the invariant interval between $x(\tau)$ and $x(\tau')$ depends only on s, so $G_0(s)$ is independent of τ and the stationary response function is defined by the Fourier transform

$$\mathcal{G}(E) = \int_{-\infty}^{+\infty} ds\, \exp\left(-\frac{i}{\hbar}Es\right) G_0(s). \tag{3.27}$$

The sign convention is such that $E > 0$ corresponds to excitation and $E < 0$ to de–excitation.

3.A.2 Inertial benchmark

For an inertial trajectory $x^\mu(\tau) = (c\tau, 0, 0, 0)$, the pullback of (3.4) is

$$G_{\rm inert}(s) = -\frac{\hbar c}{4\pi^2}\,\frac{1}{(cs - i\epsilon)^2}. \tag{3.28}$$

Hence

$$\mathcal{G}_{\rm inert}(E) = -\frac{\hbar}{4\pi^2 c}\int_{-\infty}^{+\infty} ds\, \frac{e^{-iEs/\hbar}}{(s - i\epsilon)^2}. \tag{3.29}$$

To evaluate the integral, consider $E \neq 0$ and close the contour in the half–plane where $e^{-iEs/\hbar}$ decays. For $E > 0$, decay occurs in the lower half–plane and the pole at $s = i\epsilon$ lies in the upper half–plane, so the contour encloses no singularities and the integral vanishes. For $E < 0$, decay occurs in the upper half–plane and the contour encloses the second–order pole at $s = i\epsilon$. Using

$$\mathrm{Res}\left(\frac{e^{-iEs/\hbar}}{(s - i\epsilon)^2},\, s = i\epsilon\right) = \left|\frac{d}{ds}\, e^{-iEs/\hbar}\right|_{s=i\epsilon} = -\frac{iE}{\hbar}\, e^{E\epsilon/\hbar}, \tag{3.30}$$

and taking $\epsilon \to 0^+$, one obtains

$$\int_{-\infty}^{+\infty} ds\, \frac{e^{-iEs/\hbar}}{(s - i\epsilon)^2} = 2\pi i\left(-\frac{iE}{\hbar}\right)\Theta(-E) = \frac{2\pi E}{\hbar}\,\Theta(-E). \tag{3.31}$$

Substituting into (3.29) yields the inertial result

$$\mathcal{G}_{\rm inert}(E) = -\frac{E}{2\pi}\,\Theta(-E). \tag{3.32}$$

3.A.3 Cusped worldline: invariant interval and pullback

We consider the cusped parametrization

$$x^\mu(\tau) = \Big(cT(\tau),\, X(\tau),\, Y(\tau),\, Z(\tau)\Big) = \left(c\tau + \frac{a^2}{6c}\tau^3,\, \frac{a}{2}\tau^2,\, \frac{a^2}{6c}\tau^3,\, 0\right). \tag{3.33}$$

Fix τ and $\tau' = \tau - s$ and define $\Delta(cT) := cT(\tau) - cT(\tau')$, and similarly ΔX, ΔY, ΔZ. A direct expansion gives

$$\Delta(cT) = cs + \frac{a^2}{6c}\Big(\tau^3 - (\tau - s)^3\Big) = cs + \frac{a^2}{2c}\tau^2 s - \frac{a^2}{2c}\tau s^2 + \frac{a^2}{6c}s^3, \tag{3.34}$$

$$\Delta X = \frac{a}{2}\Big(\tau^2 - (\tau - s)^2\Big) = a\tau s - \frac{a}{2}s^2, \tag{3.35}$$

$$\Delta Y = \frac{a^2}{6c}\Big(\tau^3 - (\tau - s)^3\Big) = \frac{a^2}{2c}\tau^2 s - \frac{a^2}{2c}\tau s^2 + \frac{a^2}{6c}s^3, \tag{3.36}$$

and $\Delta Z = 0$. In particular,

$$\Delta(cT) = cs + \Delta Y. \tag{3.37}$$

With $(+,-,-,-)$ signature, the squared interval is

$$\Delta s_{\mathrm{M}}^2 = \big(\Delta(cT) - i\epsilon\big)^2 - (\Delta X)^2 - (\Delta Y)^2 - (\Delta Z)^2. \tag{3.38}$$

Using (3.37),

$$\begin{aligned}\big(\Delta(cT) - i\epsilon\big)^2 - (\Delta Y)^2 &= (cs - i\epsilon + \Delta Y)^2 - (\Delta Y)^2 \\ &= (cs - i\epsilon)^2 + 2(cs - i\epsilon)\Delta Y,\end{aligned} \tag{3.39}$$

so that

$$\Delta s_{\mathrm{M}}^2 = (cs - i\epsilon)^2 + 2(cs - i\epsilon)\Delta Y - (\Delta X)^2. \tag{3.40}$$

Substituting the explicit expressions for ΔX and ΔY into (3.40), one finds that all τ–dependent polynomial terms cancel identically (the regulator affects only the causal prescription and does not alter the algebraic cancellation). The result is the purely s–dependent expression

$$\Delta s_{\mathrm{M}}^2 = (cs - i\epsilon)^2 + \frac{a^2}{12}s^4. \tag{3.41}$$

Inserting (3.41) into (3.4) yields the cusped pullback

$$G_{\mathrm{cus}}(s) = -\frac{\hbar}{4\pi^2}\,\frac{1}{(cs - i\epsilon)^2 + \frac{a^2}{12}s^4}. \tag{3.42}$$

3.A.4 Cusped response: computing the Fourier transform

Define

$$\alpha^2 := \frac{a^2}{12c^2}, \qquad \alpha = \frac{a}{2\sqrt{3}c}. \tag{3.43}$$

Then

$$\frac{1}{(cs-i\epsilon)^2+\frac{a^2}{12}s^4}=\frac{1}{c^2}\,\frac{1}{(s-i\epsilon)^2\big(1+\alpha^2 s^2\big)}. \tag{3.44}$$

Using the identity

$$\frac{1}{s^2\big(1+\alpha^2 s^2\big)}=\frac{1}{s^2}-\frac{\alpha^2}{1+\alpha^2 s^2}, \tag{3.45}$$

we write

$$G_{\rm cus}(s)=-\frac{\hbar}{4\pi^2 c^2}\left[\frac{1}{(s-i\epsilon)^2}-\frac{\alpha^2}{1+\alpha^2 s^2}\right], \tag{3.46}$$

where the $i\epsilon$ prescription is only required in the first (universal) term.

The response is therefore

$$\mathcal{G}_{\rm cus}(E)=-\frac{\hbar}{4\pi^2 c^2}\int_{-\infty}^{+\infty}ds\,e^{-iEs/\hbar}\left[\frac{1}{(s-i\epsilon)^2}-\frac{\alpha^2}{1+\alpha^2 s^2}\right]. \tag{3.47}$$

The first term reproduces the inertial contribution (3.18). It remains to evaluate

$$I(E):=\int_{-\infty}^{+\infty}ds\,e^{-iEs/\hbar}\,\frac{\alpha^2}{1+\alpha^2 s^2}=\int_{-\infty}^{+\infty}ds\,e^{-iEs/\hbar}\,\frac{1}{s^2+\frac{1}{\alpha^2}}. \tag{3.48}$$

The integrand has simple poles at $s=\pm i/\alpha$. For $E>0$ one closes the contour in the lower half–plane (exponential decay) and encloses the pole at $s=-i/\alpha$, with residue

$$\operatorname{Res}\left[\frac{e^{-iEs/\hbar}}{s^2+\frac{1}{\alpha^2}},\,s=-\frac{i}{\alpha}\right]=\frac{e^{-iE(-i/\alpha)/\hbar}}{2(-i/\alpha)}=\frac{e^{-E/(\hbar\alpha)}}{-2i/\alpha}. \tag{3.49}$$

Hence

$$I(E)=2\pi i\left(\frac{e^{-E/(\hbar\alpha)}}{-2i/\alpha}\right)=\pi\alpha\,e^{-E/(\hbar\alpha)},\qquad E>0. \tag{3.50}$$

For $E<0$ one closes in the upper half–plane and encloses the pole at $s=+i/\alpha$, obtaining the same expression with $|E|$:

$$I(E)=\pi\alpha\,e^{-|E|/(\hbar\alpha)},\qquad E\in\mathbb{R}. \tag{3.51}$$

Assembling the inertial contribution with (3.51), one finds

$$\begin{aligned}\mathcal{G}_{\rm cus}(E)&=-\frac{E}{2\pi}\,\Theta(-E)+\frac{\hbar}{4\pi^2}\,I(E)\\&=-\frac{E}{2\pi}\,\Theta(-E)+\frac{\hbar}{4\pi^2}\,\pi\alpha\,e^{-|E|/(\hbar\alpha)}\\&=-\frac{E}{2\pi}\,\Theta(-E)+\frac{\hbar\alpha}{4\pi}\,e^{-|E|/(\hbar\alpha)}.\end{aligned} \tag{3.52}$$

3.A.5 Effective temperature from generalized detailed balance

For stationary spectra one may define an E–dependent effective temperature by

$$\frac{1}{T_{\rm eff}(E)}=\frac{k_B}{E}\ln\!\left(\frac{\mathcal{G}(-E)}{\mathcal{G}(E)}\right). \tag{3.53}$$

For the cusped spectrum (3.52), a convenient explicit form is obtained by treating $E > 0$ and $E < 0$ separately and then combining the results. One finds

$$\frac{1}{T_{\mathrm{cus}}(E)} = \frac{k_B}{E} \ln\left(\frac{E\,\Theta(E) + \frac{\hbar\alpha}{2}\, e^{-|E|/(\hbar\alpha)}}{-E\,\Theta(-E) + \frac{\hbar\alpha}{2}\, e^{-|E|/(\hbar\alpha)}} \right). \tag{3.54}$$

The limits $E \to 0$ and $|E| \to \infty$ follow directly from the above expression.

Chapter 4

Circular Unruh–DeWitt detector driven by a magnetic field

4.1 Introduction

This chapter presents new results on a laboratory realisation of a circular Unruh–DeWitt detector in which the detector trajectory and the detector's internal energy scale are generated by the same external control field. The system we focus on is a charged spin-1/2 particle undergoing uniform circular motion in a plane, sustained by a static homogeneous magnetic field. The detector is identified with the spin degree of freedom: the magnetic field generates the Zeeman splitting, i.e. a natural two-level structure, as well as sets the circular motion. This "single-knob" feature is the key difference with respect to more idealised UDW analyses in which the detector gap and the trajectory can be tuned independently, and constitutes the defining element of the present approach.

A first original result of this chapter is the identification of a reduced description of the detector response entirely in terms of laboratory control parameters. To this end, we express the worldline in proper-time parametrisation, derive the invariant separations between two points on the orbit, and obtain the Wightman function restricted to the trajectory as a stationary correlator. The resulting expression depends on the magnetic field and on the orbital radius only through a small set of experimentally meaningful combinations, which allow one to organise the dynamics in terms of a single dimensionless parameter controlling the relativistic regime. This reduction is not merely a simplification, but implies that the stationary response is approximately constant along curves of fixed magnetic rigidity in the control plane, providing a direct link between theoretical predictions and experimentally accessible configurations.

A second central result concerns the structure of the ultrarelativistic limit in this magnetic implementation. In circular motion, ultrarelativistic response functions are often discussed in terms of an effective detailed-balance temperature. In the present setup, however, increasing the relativistic parameter by strengthening the magnetic field (or enlarging the radius) modifies both the proper acceleration and the detector gap, since the Zeeman splitting is set by the same field that drives the motion. As a consequence, the relevant dimensionless ratio comparing the gap to the non-inertial

scale does not vary freely, but approaches a constant in the deep ultrarelativistic regime.

We show that this magnetic scaling leads to a qualitatively different behaviour with respect to standard expectations: the stationary excited-state population does not decay at large non-inertiality, but instead approaches a field- and radius-independent plateau, whose value is controlled predominantly by an effective gyromagnetic factor. This provides a sharp and experimentally testable prediction, directly tied to the physical constraints of the laboratory implementation.

After establishing the analytic structure, we present numerical color maps of the stationary excitation probability in the plane of laboratory parameters. The maps exhibit a suppressed probability at lower values of the control parameter and a domain in which the excitation probability saturates to the predicted plateau. These results provide an explicit visualization of the scaling behaviour and confirm the analytic predictions within a realistic parameter space.

We then extend the analysis beyond electrons to protons and to selected nuclei, showing that two competing requirements govern feasibility: access to the ultrarelativistic regime (set mainly by charge-to-mass ratio and rigidity), and the plateau height (set mainly by the effective gyromagnetic factor). This establishes a quantitative criterion for species optimisation and highlights how different particles probe distinct regions of the same underlying scaling structure.

4.2 UDW detector model for an electron in magnetic relativistic circular motion

In this section we implement the Unruh–DeWitt (UDW) detector framework for a concrete realization in which both the kinematics and the internal detector scale are controlled by the same laboratory field. We consider an electron of mass m and charge $q = -|q|$ constrained to uniform circular motion in the plane $z = 0$ by a static and homogeneous magnetic field $\mathbf{B} = B\,\hat{\mathbf{z}}$. The two-level detector is identified with the electron spin, with a Zeeman energy gap. A central goal is to write the Wightman function along the electron worldline in a form that depends only on the control parameters (B, R), with no intermediate kinematical symbols left implicit.

4.2.1 Magnetic circular motion and proper angular frequency

It is convenient to introduce the dimensionless control parameter

$$k \equiv \frac{|q|BR}{mc}, \tag{4.1}$$

which completely characterizes the relativistic regime of the motion. Using the expression for the Lorentz force, we can obtain the speed v as

$$v = \frac{|q|BR}{\gamma m}, \tag{4.2}$$

from which the relativistic parameters read

$$\gamma(B,R) = \sqrt{1+k^2}, \qquad \frac{v}{c} = \frac{k}{\sqrt{1+k^2}}, \tag{4.3}$$

so that the ultra-relativistic regime corresponds to $k \gg 1$.

The cyclotron frequency measured in the laboratory frame is

$$\omega_{\text{lab}} = \frac{|q|B}{\gamma m} = \frac{|q|B}{m\sqrt{1+k^2}}, \tag{4.4}$$

while the angular frequency with respect to the detector proper time is

$$\omega_{\text{p}} \equiv \gamma\,\omega_{\text{lab}} = \frac{|q|B}{m}. \tag{4.5}$$

As expected for purely magnetic circular motion, the proper angular frequency ω_{p} is independent of the Lorentz factor and depends only on B and m.

The magnitude of the proper acceleration is constant and given by

$$a = \gamma^2 \frac{v^2}{R} = \left(\frac{|q|B}{m}\right)^2 R, \tag{4.6}$$

which depends on B and R but not explicitly on γ once written in this form.

4.2.2 Worldline and invariant separations in terms of B, R, and k

Building on the results of Chapter 1, Eq. (1.8), we adopt the circular trajectory introduced by Letaw. Expressed in terms of the proper time τ and the control parameter k, the worldline takes the form

$$\begin{aligned} cT(\tau) &= \sqrt{1+k^2}\, c\tau \\ X(\tau) &= R\cos\left(\frac{|q|B}{m}\,\tau\right) \\ Y(\tau) &= R\sin\left(\frac{|q|B}{m}\,\tau\right) \\ Z(\tau) &= 0. \end{aligned} \tag{4.7}$$

For two points on the worldline separated by $s = \tau - \tau'$, the temporal and spatial separations are

$$\Delta T = \gamma s = \sqrt{1+k^2}\, s, \tag{4.8}$$

$$|\Delta \mathbf{X}|^2 = 4R^2 \sin^2(\omega_{\text{p}} s/2) = 4R^2 \sin^2\left(\frac{|q|B}{2m}\, s\right). \tag{4.9}$$

The invariant interval is therefore

$$c^2\Delta T^2 - |\Delta X|^2 = c^2(1+k^2)(s)^2 - 4R^2 \sin^2\left(\frac{|q|B}{2m}\, s\right). \tag{4.10}$$

4.2.3 Wightman function along the magnetic circular worldline

For a real massless scalar field in the Minkowski vacuum, the positive-frequency Wightman function is

$$G_0(x,x') = -\frac{1}{4\pi^2}\,\frac{1}{c^2(\Delta T - i\epsilon)^2 - |\Delta \mathbf{X}|^2}. \tag{4.11}$$

Restricting this expression to the trajectory (4.7) yields a stationary correlator depending only on s and on the control parameter k:

$$G_{(k)}(s) = -\frac{1}{4\pi^2}\left[\left(c\sqrt{1+k^2}\,(s-i\epsilon)\right)^2 - 4R^2\sin^2\!\left(\frac{|q|B}{2m}\,s\right)\right]^{-1}. \tag{4.12}$$

The single dimensionless parameter k controls the qualitative behaviour of the correlator. In particular, the regime $k \gg 1$ corresponds to ultra-relativistic circular motion, which will play a central role in the asymptotic analysis of the detector response.

4.2.4 Ultrarelativistic probability plateau for a magnetic circular electron detector

In the magnetic realization of circular motion introduced in Sec. 3.6, the kinematics of the trajectory and the internal energy scale of the Unruh–DeWitt (UDW) detector are not independent. The proper angular frequency, given by Eq. (4.5) is independent of γ, while the constant proper acceleration, given by Eq. (4.6), can be written exclusively in terms of (B,R) as

$$a(B,R) = \omega_{\rm p}^2(B)\,R. \tag{4.13}$$

The two-level detector is identified with the electron spin. In the comoving frame, the Zeeman splitting defines the detector gap

$$\begin{aligned} E &= \hbar\,\Omega \\ \Omega &= \frac{g}{2}\,\gamma\,\omega_{\rm p}, \end{aligned} \tag{4.14}$$

where $g \simeq 2$ is the electron g-factor (in the numerical estimates below we take $g \simeq 2$). An important consequence of (4.13)–(4.14) is that, in the limit $k \gg 1$, the ratio $|E|/a$ saturates to a constant:

$$\frac{|E|}{a} = \frac{\hbar\Omega}{a} = \frac{\hbar}{c}\,\frac{g\gamma c}{2\omega_{\rm p}R} = \frac{\hbar}{c}\,\frac{g}{2}\,\frac{\gamma}{k} \xrightarrow{k\gg 1} \frac{\hbar}{c}\,\frac{g}{2}. \tag{4.15}$$

Equivalently, the dimensionless quantity $\Omega c/a$ tends to $g/2$:

$$\frac{\Omega c}{a} = \frac{g}{2}\,\frac{\gamma}{k} \xrightarrow{k\gg 1} \frac{g}{2}. \tag{4.16}$$

As discussed in Chapter 1, Sec. 1.6, because the motion is stationary, the UDW response is encoded in the transition rate

$$\mathcal{G}(E) = \int_{-\infty}^{+\infty} ds\, e^{-iEs/\hbar}\, G_{(k)}(s) \tag{4.17}$$

and the effective detailed-balance temperature $T_{\mathrm{circ}}(E)$ is defined by

$$\frac{\mathcal{G}(E)}{\mathcal{G}(-E)} = \exp\Big(-\frac{E}{T_{\mathrm{circ}}(E)}\Big). \tag{4.18}$$

In the ultrarelativistic regime $k \gg 1$, the magnetic model falls precisely into the uniform asymptotic regime of [12], introduced in this thesis in Chapter 3, Sec. 3.5, in which T_{circ} admits a closed expression that is uniform in the ratio $|E|c/(\hbar a)$. Specializing that uniform asymptotic form to the present magnetic scaling (4.16), one finds (see Appendix 4.A for the full derivation) that the ratio $\mathcal{G}(E)/\mathcal{G}(-E)$ converges to a constant independent of B and R:

$$\frac{\mathcal{G}(E)}{\mathcal{G}(-E)} \xrightarrow{k\gg 1} \exp\big(-g\,\chi_\infty\big), \tag{4.19}$$

with

$$\chi_\infty = \frac{1}{g}\,\ln\Big(1 + 2g\sqrt{3}\,e^{g\sqrt{3}}\Big). \tag{4.20}$$

For an electron ($g \simeq 2$), $\chi_\infty \simeq 2.70$, numerically very close to $\pi\sqrt{3}/2 \simeq 2.72$, and hence (4.19) yields the plateau value

$$\frac{\mathcal{G}(E)}{\mathcal{G}(-E)} \;\approx\; e^{-g\,\pi\sqrt{3}/2}. \tag{4.21}$$

Finally, the observable excitation probability of the two-level system in the stationary regime is not the bare ratio $\mathcal{G}(E)/\mathcal{G}(-E)$, but the population of the excited level obtained from the balance of excitation and de-excitation channels:

$$p_\uparrow = \frac{\mathcal{G}(E)}{\mathcal{G}(E)+\mathcal{G}(-E)} = \frac{1}{1+\mathcal{G}(-E)/\mathcal{G}(E)} = \frac{1}{1+\exp\big(g\chi_\infty\big)}. \tag{4.22}$$

Therefore, in the ultrarelativistic magnetic regime $k \gg 1$,

$$p_\uparrow \xrightarrow{k\gg 1} p_\uparrow^{(\infty)} = \frac{1}{1+\exp\big(g\chi_\infty\big)} \;\approx\; \frac{1}{1+\exp\big(g\pi\sqrt{3}/2\big)}. \tag{4.23}$$

For $g \simeq 2$, this gives $p_\uparrow^{(\infty)} \simeq 4\times 10^{-3}$, i.e. a plateau at the sub-percent level, consistent with the numerical findings of Sec. 4.3.

Condition for reaching the plateau. The plateau is reached when k is sufficiently large. A conservative criterion is $k \gtrsim 30$ (already $\gamma \simeq k$ and $\beta \simeq 1$ to per-mille accuracy). Solving for R gives

$$R \gtrsim \frac{k\,mc}{|q|\,B}. \tag{4.24}$$

For an electron, $mc/|q| \simeq 1.70 \times 10^{-3}\,\mathrm{T\,m}$, hence

$$R \gtrsim 5.1 \times 10^{-3}\,\mathrm{m}\left(\frac{k}{30}\right)\left(\frac{10\,\mathrm{T}}{B}\right). \tag{4.25}$$

Thus, for $B \sim 10\,\mathrm{T}$ one needs radii of order millimeters to centimeters to enter the deep ultrarelativistic regime in this magnetic model, whereas for weaker fields the required radius grows proportionally as $R \propto 1/B$.

Discussion: why is the excitation probability non-thermal in the (B, R) variables?

We now relate this result with the ultrarelativistic regime discussed in Chapter 3. According to [12], the ultrarelativistic regime shows an asymptotic thermal behaviour. Therefore, the asymptotic probability should be of the form

$$p_{\uparrow}^{(\mathrm{th})}(E,T) = \frac{1}{1+e^{E/(k_B T)}}, \tag{4.26}$$

which tends to 0 for $E \gg k_B T$ and to 1/2 for $E \ll k_B T$.

Large k (large B and/or large R): One might expect that, as B and R increase, the detector probes higher energy scales, leading to a suppression of excitation analogous to that in a thermal bath. The magnetic circular model behaves differently because, in the ultrarelativistic regime $k \gg 1$, if we fix R and vary B, both the energy and the acceleration change. In particular, the detector gap and the acceleration grow together:

$$\Omega = \frac{g}{2}\gamma\omega_{\mathrm{p}} \simeq \frac{g}{2}\frac{a}{c}, \qquad (k \gg 1), \tag{4.27}$$

equivalently

$$\frac{\Omega c}{a} \xrightarrow[k\gg 1]{} \frac{g}{2}. \tag{4.28}$$

Thus, taking $k \gg 1$ does not correspond to varying the internal dynamics only, as considered in [12]; instead, for each value of k, both kinematics and dynamics change in the same way, leaving the probability constant. A useful way to phrase this is to compare to the Unruh scale $T_U = \hbar a/(2\pi c)$: in the present magnetic scaling,

$$\frac{E}{k_B T_U} = \frac{\hbar\Omega}{\hbar a/(2\pi c)} = 2\pi\,\frac{\Omega c}{a} \xrightarrow[k\gg 1]{} \pi g, \tag{4.29}$$

which is a constant. Therefore, increasing B and/or R does not drive the system into the large gap regime; it drives it into a regime where both the gap and the non-inertial frequency content of the sampled vacuum correlations increase together, leaving the excitation balance asymptotically unchanged. This is precisely the mechanism behind the derived plateau $p_{\uparrow} \to p_{\uparrow}^{(\infty)}$: the response becomes controlled by a constant effective exponent of the form $\exp[-\mathrm{const} \times (Ec)/(\hbar a)]$, and since $(Ec)/(\hbar a)$ saturates, so does $p_{\uparrow}$.

In this sense, the absence of a high-(B, R) decay is a direct consequence of the model: the increase of B that, in turn, increases the non-inertiality (through a),

simultaneously increases the detector gap (through Ω). To recover the familiar thermal limits (decay to zero at high energy and approach to 1/2 at low energy), one would need a setup in which the internal splitting can be tuned independently of the trajectory, so that $\Omega c/a$ can be taken to ∞ or to 0 without simultaneously changing the sampling of the field along the worldline.

Small B (and/or small BR): In the opposite case, taking $B \to 0$ at fixed R simultaneously drives the motion and the internal splitting to zero:

$$\omega_{\mathrm{p}} = \frac{|q|B}{m} \to 0, \qquad \Omega \simeq \frac{g}{2}\omega_{\mathrm{p}} \to 0, \qquad a = \omega_{\mathrm{p}}^2 R \to 0. \tag{4.30}$$

From a thermal viewpoint one might be tempted to call this a "low-energy" limit and expect $p_\uparrow \to 1/2$. However, what matters is not Ω alone, but the comparison of the gap to the characteristic scale of the field fluctuations as sampled along the trajectory. As $B \to 0$ the worldline becomes progressively indistinguishable from an inertial line over any fixed interaction time: for a fixed proper-time window s relevant to an excitation/de-excitation event, the angular deflection is

$$\Delta\varphi = \omega_{\mathrm{p}}\, s \xrightarrow[B\to 0]{} 0, \tag{4.31}$$

so the arc traversed during the transition becomes arbitrarily well approximated by its tangent. In other words, within the time support that contributes dominantly to the response, the motion becomes effectively inertial: the detector samples Minkowski vacuum correlations as an inertial observer would. In the stationary limit of an eternally coupled inertial detector, the excitation rate in the vacuum vanishes for any positive gap, and the corresponding steady-state population is therefore driven to

$$p_\uparrow \to 0, \qquad (B \to 0 \text{ at fixed } R). \tag{4.32}$$

This provides a physical explanation for the low-B corner of the numerical maps: the system does not thermalise to equipartition because the non-inertial character of the trajectory itself disappears.

This behaviour sharply contrasts with uniform linear acceleration: even if one focuses on any finite proper-time interval, a uniformly accelerated trajectory exhibits a nonzero change in velocity over that interval. Therefore, one never reaches an inertial limit by taking a small while keeping a fixed "transition window"; correspondingly, the KMS property persists (with $T_U \propto a$), and the thermal intuition remains applicable.

4.3 Numerical results

4.3.1 Plot in the laboratory control plane and reduction to a single parameter

The numerical results below are presented as color maps of the stationary excited-state population $p_\uparrow$ in the (B, R) control plane, computed from the excitation and de-excitation response functions through Eq. (4.22). The magnetic circular realization

has an important built-in scaling property: although the correlator (4.12) contains both B and R, the observable $p_\uparrow$ depends, to a very good approximation, only on the dimensionless combination

$$k = \frac{|q|BR}{mc}. \tag{4.33}$$

This can be seen by rescaling the proper-time difference as $u = \omega_{\rm p} s$, with $\omega_{\rm p} = |q|B/m$. Using $k = \omega_{\rm p} R/c$, the Wightman function restricted to the worldline can be written as an overall factor times a dimensionless function of k, while the Fourier phase depends on $E/(\hbar\omega_{\rm p}) = (g/2)\gamma(k)$. As a consequence, the ratio $\mathcal{G}(-E)/\mathcal{G}(E)$ and hence $p_\uparrow$ are controlled predominantly by the single parameter k (for fixed g), implying that contour lines of constant $p_\uparrow$ should align with lines of constant BR in the $(\log B, \log R)$ plane. This is exactly what is observed in Figs. 4.1–4.2.

4.3.2 Electron: emergence of the ultrarelativistic excitation plateau

Figure 4.1 shows $p_\uparrow(B, R)$ for an electron detector, taking $g = 2.002$ in the Zeeman gap (4.14). The color map displays two clearly separated regions: a strongly suppressed domain at small k (blue), and an ultrarelativistic domain at large k in which $p_\uparrow$ saturates to a B- and R-independent plateau (red). The transition between the two regimes follows a straight diagonal in log-log scales, consistent with a threshold at approximately constant BR (i.e. constant k). For the electron, $mc/|q| \simeq 1.70 \times 10^{-3}\,\mathrm{T\,m}$, so already moderate laboratory fields and millimeter-to-centimeter radii can reach $k \gtrsim \mathcal{O}(10)$, where the saturation becomes apparent.

In the large-k region the numerical plateau matches the analytic prediction (4.23). For $g = 2.002$, Eq. (4.23) gives

$$p_\uparrow^{(\infty)}\big|_{g=2} \simeq 4.48 \times 10^{-3}, \tag{4.34}$$

in agreement with the saturated value reached across the upper-right portion of Fig. 4.1. This confirms that the magnetic scaling $\Omega c/a \to g/2$ (Eq. (4.16)) places the electron detector precisely in the uniform asymptotic regime underlying the ultra-relativistic spectrum discussed in Chapter 3.

Since $k = |q|BR/(mc)$, entering the plateau requires the product BR to exceed a particle-dependent scale set by $mc/|q|$.

4.3.3 Proton: shifted access to the plateau and stronger suppression

We now observe that it is possible to extend the discussion made for the electron to other charged spin-1/2 particles. The most simple case is the proton. Figure 4.2 reports it probability of excitation, using the proton g-factor $g_p \simeq 5.586$ in Eq. (4.14). The qualitative structure remains the same—suppressed region at small k and a large-k plateau. However, two key differences emerge. First, because of the $k \propto 1/m$ scaling, achieving a given relativistic regime requires a much larger value of BR for

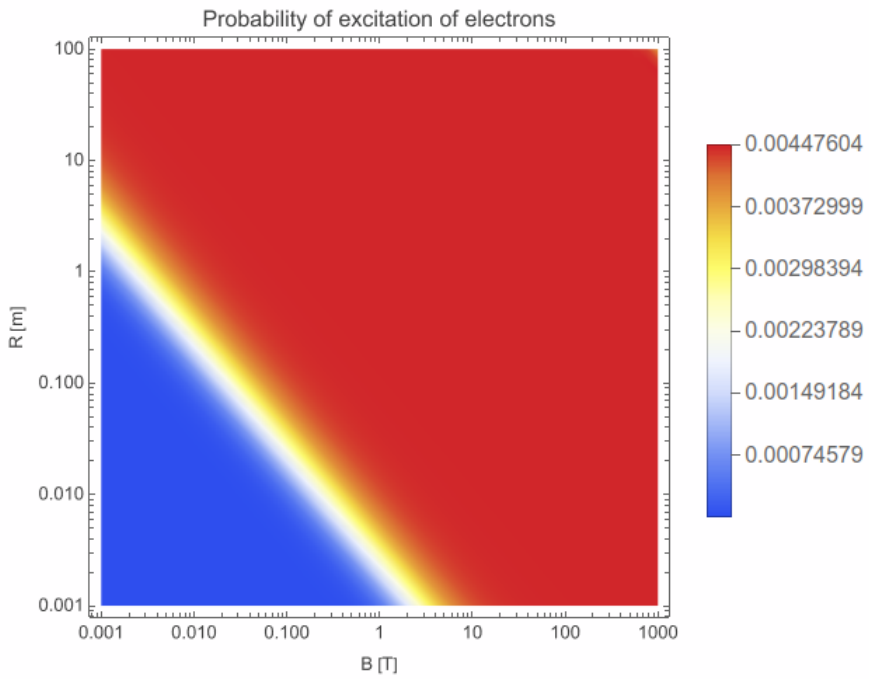

Figure 4.1: Stationary excited-state population $p_\uparrow$ for an electron spin detector in magnetic circular motion, shown as a function of the laboratory controls (B, R) (on logarithmic axes). The diagonal transition band follows approximately $k = |q|BR/(mc) = \text{const.}$. For large k the probability saturates to the ultrarelativistic plateau $p_\uparrow^{(\infty)} \simeq 4.5 \times 10^{-3}$ predicted by Eq. (4.23) (with $g \simeq 2$).

protons than for electrons. Quantitatively,

$$\frac{k_p}{k_e} = \frac{m_e}{m_p} \simeq \frac{1}{1836}, \tag{4.35}$$

so the white diagonal transition band in Figure 4.1 is shifted toward the upper-right corner of the plot. Equivalently, the characteristic scale is now $mc/|q| \simeq 3.13\,\mathrm{T\,m}$, implying that the onset of the plateau demands either very strong magnetic fields, very large radii, or both.

Second, even when the plateau is reached, the saturation value is dramatically smaller. This is not a mass effect (which only controls how fast one reaches large k) but a g-dependence, as we showed that the ultrarelativistic plateau (4.23) depends only on g. For $g = g_p \simeq 5.585$ one finds

$$p_\uparrow^{(\infty)}\big|_{g=g_p} \simeq 2.7 \times 10^{-6}, \tag{4.36}$$

consistent with the red saturation level in Fig. 4.2. Therefore, the proton case is doubly challenging: it requires much more extreme (B, R) to enter the ultrarelativistic regime, and it yields an intrinsically smaller steady-state excitation probability once there.

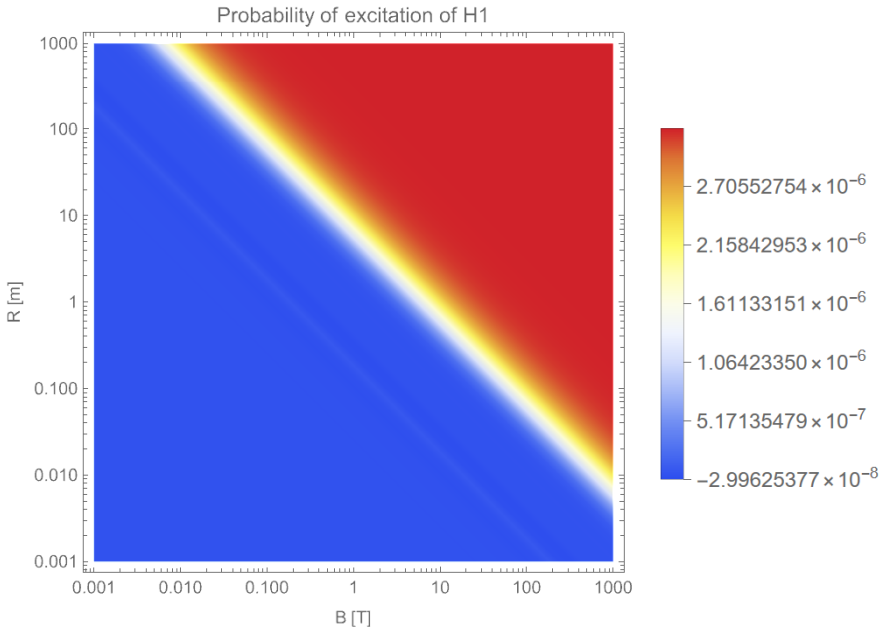

Figure 4.2: Stationary excited-state population $p_\uparrow$ for a proton spin detector in magnetic circular motion, shown in the same (B, R) control plane (logarithmic axes). The diagonal transition again follows approximately $k = \text{const.}$, but is shifted to larger BR because $k \propto 1/m$. The ultrarelativistic plateau exists as in the electron case, but its value is much smaller, $p_\uparrow^{(\infty)} \simeq 2.7 \times 10^{-6}$, reflecting the dependence of Eq. (4.23) on the g-factor.

4.4 Beyond electrons and protons

The electron and proton results shown in Figs. 4.1–4.2 illustrate a key structural feature of the magnetic circular model: in the ultrarelativistic regime $k \gg 1$, the stationary excited–state population is controlled predominantly by an effective gyromagnetic factor, rather than by B and R separately. In particular, the magnetic scaling of Sec. 4.2.4 implies

$$\frac{\Omega c}{a} \xrightarrow{k\gg 1} \frac{g}{2}, \tag{4.37}$$

and therefore the plateau population can be written, asymptotically, as a closed function of g only,

$$p_\uparrow^{(\infty)}(g) = \frac{1}{1+\exp\big(g\chi_\infty(g)\big)} = \frac{1}{2+2g\sqrt{3}\,e^{g\sqrt{3}}}, \tag{4.38}$$

where we used $\exp(g\chi_\infty) = 1 + 2g\sqrt{3}\,e^{g\sqrt{3}}$. This explains the dramatic suppression observed for the proton compared to the electron: increasing g drives an essentially exponential decrease of $p_\uparrow^{(\infty)}$.

4.4.1 Species optimisation for larger excitation probability: Heavy ions and an effective g-factor

One possible way to counteract the lower probability of excitation of the proton is to work on the gyromagnetic factor g, as lower g-factors are associated to higher excitation probabilities. It is possible to consider the gyromagnetic factors of heavy nucleus and consider the coupling of the magnetic field with their nuclear spin I from their measured magnetic dipole moment μ. Defining the nuclear g-factor $g_{\rm ion}$ by $g_I \equiv \mu/(I\mu_N)$, one can map to the effective g entering the Zeeman gap in Eq. (4.14) by comparing it with the nuclear msgnetic moment $\mu_N = q\hbar/(2m_p)$

$$\mu = g_{\rm ion}\mu_N = g_{\rm ion}\frac{q\hbar}{2m_p}. \tag{4.39}$$

Using the tabulated nuclear moments, one finds several stable spin-1/2 nuclei for which $|g_{\rm ion}|$ is significantly smaller than the electron value, and hence $p_\uparrow^{(\infty)}$ can be orders of magnitude larger. Here we list some of the ions with the highest excitation probability:

- **Carbon-13 nucleus** ($^{13}C^+$, $A/Z = 13/6$): $g_{\rm ion} \simeq 1.404738$, giving $p_\uparrow^{(\infty)} \approx 4.9 \times 10^{-4} \approx 0.05\%$.
- **Oxygen-17 nucleus** ($^{17}O^+$, $A/Z = 17/8$): $g_{\rm ion} \simeq 0.757$, hence $p_\uparrow^{(\infty)} \approx 2.3 \times 10^{-2} \approx 2.3\%$.
- **Nitrogen-15 nucleus** ($^{15}N^+$, $A/Z = 15/7$): $g_{\rm ion} \simeq 0.566114$, hence $p_\uparrow^{(\infty)} \approx 2.3 \times 10^{-2} \approx 2.3\%$.
- **Thulium-169 nucleus** ($^{169}Tm^+$, $A/Z = 169/69$): $g_{\rm ion} \simeq 0.4620$, hence $p_\uparrow^{(\infty)} \approx 2.8 \times 10^{-2} \approx 2.8\%$.
- **Iron-57 nucleus** ($^{57}Fe^+$, $A/Z = 57/26$): $g_{\rm Fe-57} \simeq 0.18128$, hence $p_\uparrow^{(\infty)} \approx 2.11 \times 10^{-1} \approx 21.1\%$.
- **Osmium-187 nucleus** ($^{187}Os^+$, $A/Z = 187/76$): $g_{\rm Os-187} \simeq 0.1288$, hence $p_\uparrow^{(\infty)} \approx 2.14 \times 10^{-1} \approx 21.4\%$.

The relative color maps are plotted in Figs 4.3, 4.4, 4.5. These examples show that, within the same magnetic circular scheme, replacing the proton spin by a nuclear spin with a smaller magnetic moment-to-spin ratio can raise the asymptotic excitation probability from the proton level ($\sim 10^{-6}$) up to the 10^{-2}–10^{-1} range, leading to a relevant probability of excitation.

Trade-off: reaching $k \gg 1$ is harder for heavy ions. The gain in $p_\uparrow^{(\infty)}$ must be balanced against the fact that the ultrarelativistic control parameter becomes

$$k = \frac{|q|BR}{mc} \simeq \frac{Z}{A}\frac{eBR}{m_p c}, \tag{4.40}$$

so that all nuclei considered are characterized by $A/Z \approx 2$, having k roughly a factor ~ 2 smaller than the proton for the same (B, R). Equivalently, the condition $k \gtrsim k_*$ translates into a larger rigidity requirement,

$$BR \gtrsim k_* \frac{Am_p c}{Ze}. \tag{4.41}$$

Therefore, species optimisation is a two-parameter problem: one seeks small $|g_{\text{eff}}|$ to raise the plateau, while keeping Z/A sufficiently large (or BR sufficiently high) to actually access the regime where the plateau approximation is accurate. The examples proposed above represent realistic candidates for experimental realizations of such setup in storage rings that accelerate heavy ions.

Other routes. The strong g-dependence in Eq. (4.38) also suggests a different strategy: engineer a smaller effective Zeeman splitting without changing the circulating charge-to-mass ratio, e.g. by using internal transitions with a small differential magnetic moment ("clock-like" transitions) so that the detector gap is no longer rigidly tied to ω_{p}. This moves beyond the minimal "spin-as-detector" identification, but it provides a systematic handle to increase $p_\uparrow$ by driving $\Omega c/a \ll 1$ at fixed kinematics.

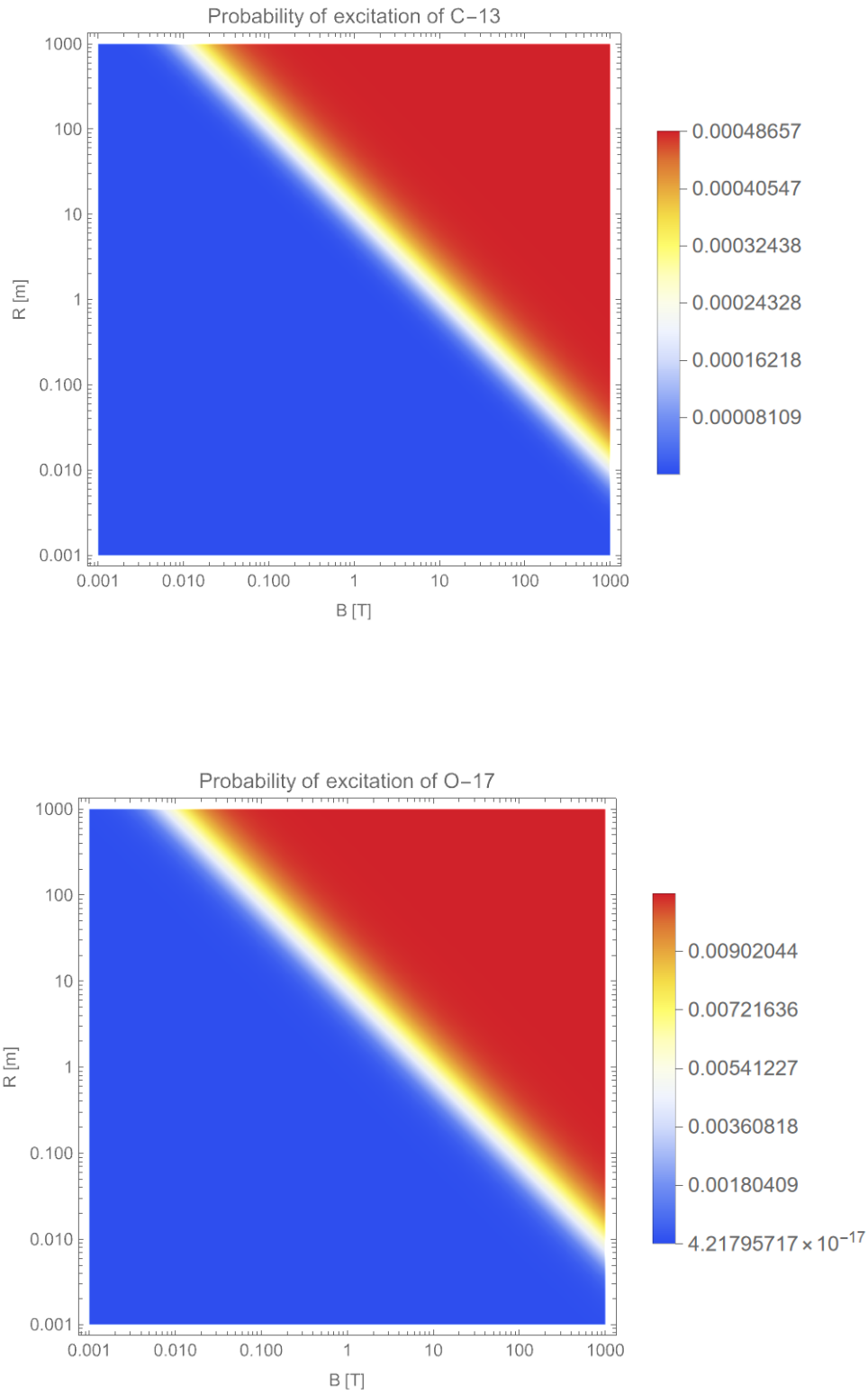

Figure 4.3: Probability of excitation for the Carbon-13 and the Oxygen-17 nuclei.

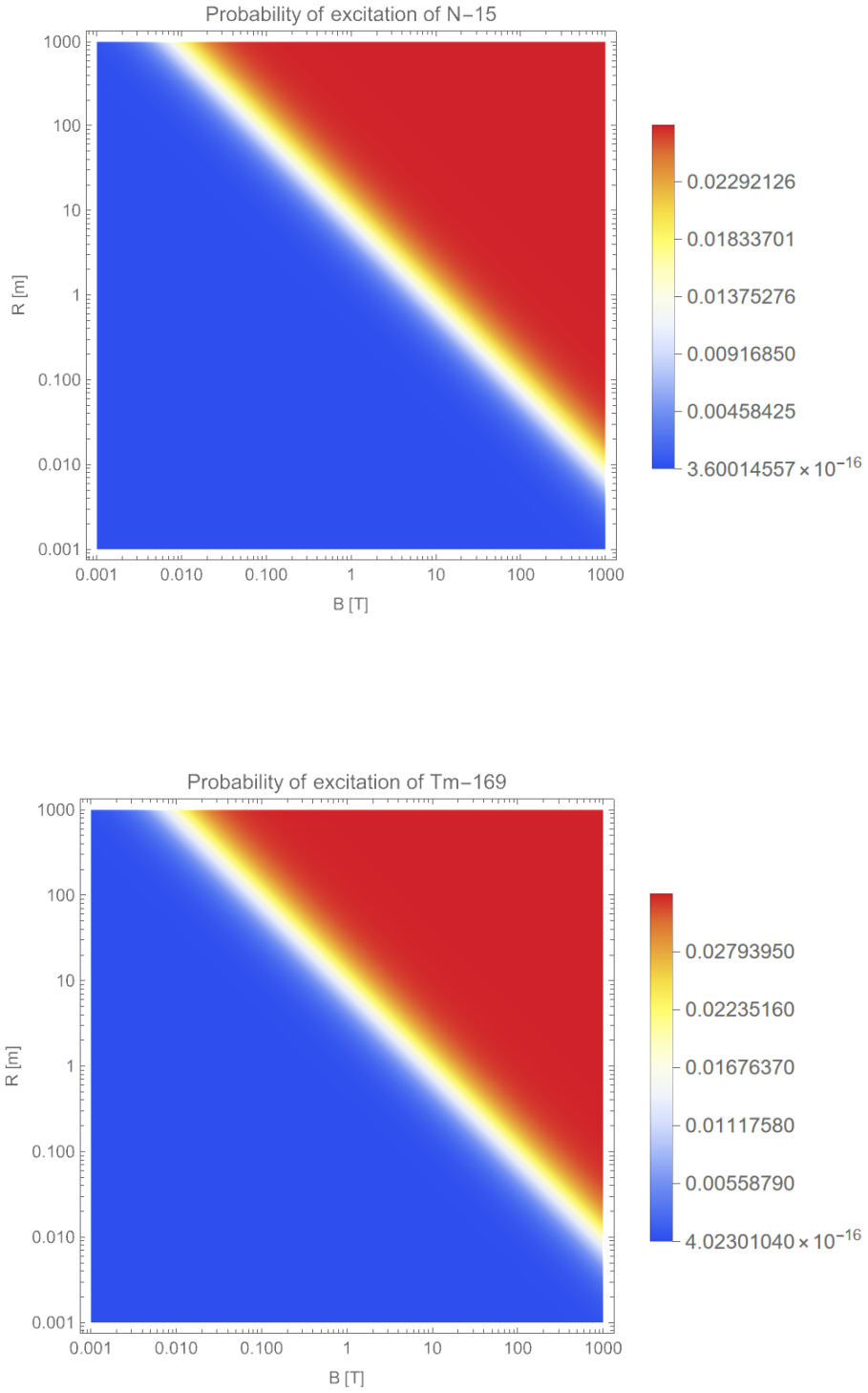

Figure 4.4: Probability of excitation for the Nitrogen-15 and the Thulium-169 nuclei.

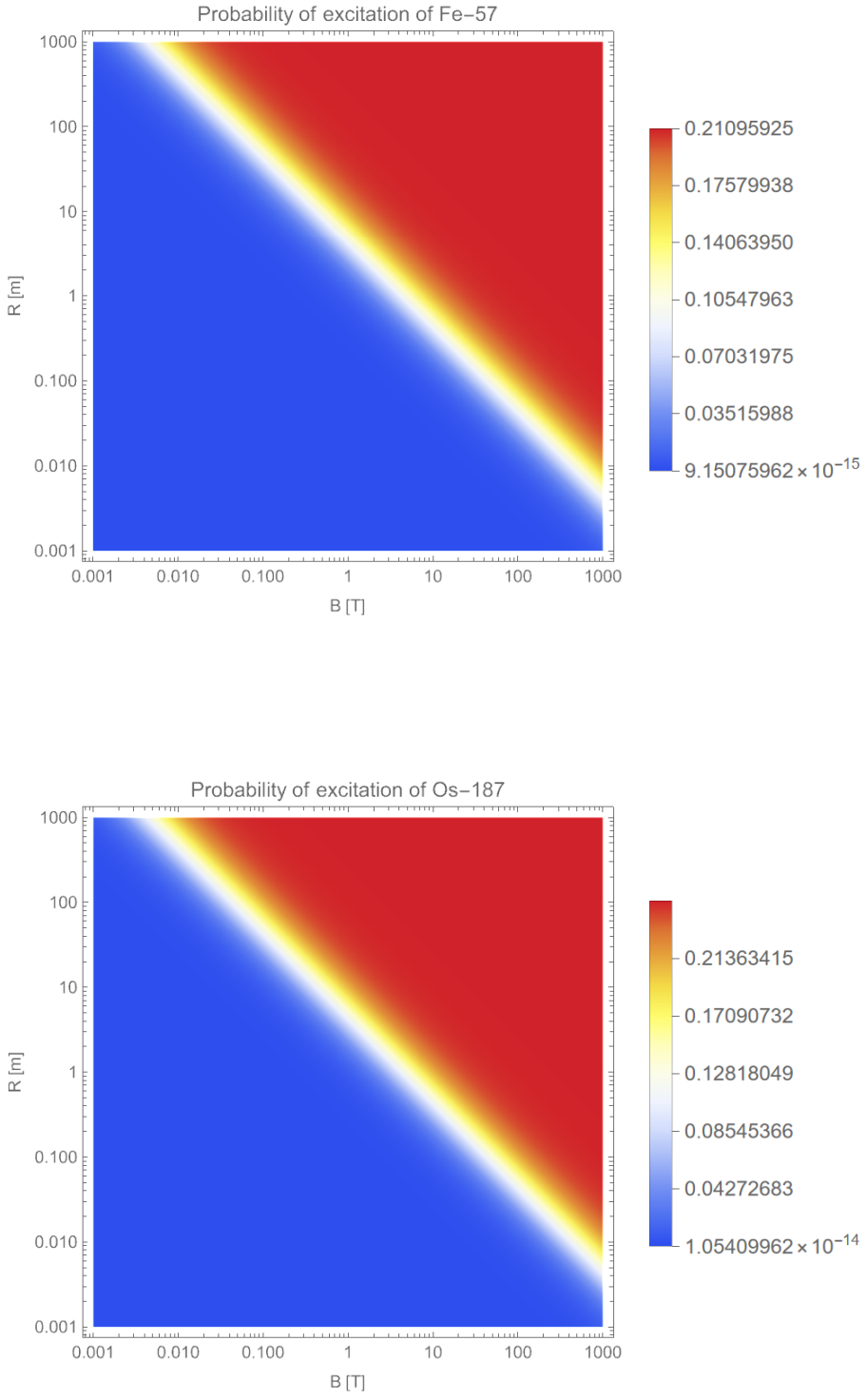

Figure 4.5: Probability of excitation for the Iron-57 and the Osmium-187 nuclei.

4.A Asymptotic derivation of the ultrarelativistic plateau in the magnetic circular model

This appendix provides a complete derivation of the ultrarelativistic plateau (4.19)–(4.23) for the magnetic circular realization of a UDW detector. We work throughout with a real massless scalar field in $3+1$ dimensions and no switching, so that the response is defined by the stationary transition rate (4.17).

4.A.1 Magnetic worldline, invariant separation, and Wightman pullback

Consider an electron of mass m and charge $q = -|q|$ undergoing uniform circular motion of radius R in the plane $z = 0$, sustained by a static uniform magnetic field $\mathbf{B} = B\,\hat{\mathbf{z}}$. Introduce the dimensionless control parameter

$$k \equiv \frac{|q|BR}{mc}. \tag{4.42}$$

As shown in Sec. 3.6.1, the Lorentz factor and velocity are

$$\gamma = \sqrt{1+k^2}, \qquad \beta = \frac{k}{\sqrt{1+k^2}}, \tag{4.43}$$

and the proper angular frequency is

$$\omega_{\mathrm{p}} = \frac{|q|B}{m}. \tag{4.44}$$

Parametrizing by proper time τ, the worldline is

$$t(\tau) = \gamma\tau, \qquad x(\tau) = R\cos(\omega_{\mathrm{p}}\tau), \qquad y(\tau) = R\sin(\omega_{\mathrm{p}}\tau), \qquad z(\tau) = 0. \tag{4.45}$$

For two points separated by $s = \tau - \tau'$, the separations are

$$\Delta t = \gamma s, \qquad |\Delta\mathbf{x}|^2 = \big(x(\tau) - x(\tau')\big)^2 + \big(y(\tau) - y(\tau')\big)^2 = 4R^2\sin^2\Big(\frac{\omega_{\mathrm{p}} s}{2}\Big). \tag{4.46}$$

The Minkowski vacuum Wightman function for a real massless scalar field is

$$G_0(x,x') = -\frac{1}{4\pi^2}\,\frac{1}{c^2\Delta T^2 - |\Delta\mathbf{X}|^2}. \tag{4.47}$$

Restricting (4.47) to (4.45) gives the stationary pullback

$$G_{(k)}(s) = -\frac{1}{4\pi^2}\,\frac{1}{c^2\gamma^2 s^2 - 4R^2\sin^2\Big(\frac{\omega_{\mathrm{p}} s}{2}\Big)}. \tag{4.48}$$

All dependence on (B,R) enters through ω_{p}, R, and k.

4.A.2 Detector gap and the magnetic scaling of E/a

The two-level detector is the electron spin. In the comoving frame the Zeeman gap is

$$E = \hbar\Omega, \qquad \Omega = \frac{g}{2}\,\gamma\,\omega_{\mathrm{p}}, \tag{4.49}$$

where g is the electron g-factor. The proper acceleration is

$$a = \gamma^2 \frac{v^2}{R} = \omega_{\mathrm{p}}^2 R. \tag{4.50}$$

Combining (4.49)–(4.50) and using $k = \omega_{\mathrm{p}} R/c$ (equivalent to (4.42)) yields the key magnetic scaling

$$\frac{\Omega c}{a} = \frac{\frac{g}{2}\gamma\omega_{\mathrm{p}} c}{\omega_{\mathrm{p}}^2 R} = \frac{g}{2}\,\frac{\gamma}{k} \xrightarrow{k\gg 1} \frac{g}{2}. \tag{4.51}$$

Hence, in the ultrarelativistic limit $k \gg 1$, the detector probes the circular spectrum in a regime where the ratio $\Omega c/a$ is fixed (and equal to $g/2$), rather than being an independently tunable parameter.

4.A.3 Response function and detailed balance

The stationary transition rate is

$$\mathcal{G}(E) = \int_{-\infty}^{+\infty} ds\, e^{-iEs/\hbar}\, G_{(k)}(s), \tag{4.52}$$

and the effective detailed-balance temperature is defined by

$$\frac{\mathcal{G}(-E)}{\mathcal{G}(E)} = \exp\!\Big(\frac{E}{T_{\mathrm{circ}}(E)}\Big). \tag{4.53}$$

Our goal is to show that, when $k \gg 1$ in the magnetic scaling (4.51), the ratio $\mathcal{G}(E)/\mathcal{G}(-E)$ tends to a constant, and therefore the excitation probability $p_\uparrow = \mathcal{G}(E)/(\mathcal{G}(E) + \mathcal{G}(-E))$ develops a plateau.

4.A.4 Complex singularities

A common heuristic in large-parameter limits is to replace $\sin(\omega_{\mathrm{p}} s/2)$ by its Taylor expansion. This is not legitimate here because the integration variable s runs over the whole real line and the oscillatory weight $e^{-iEs/\hbar}$ does not localize the integral at small s. The correct approach is instead complex-analytic: the asymptotics of Fourier-type integrals such as (4.52) are controlled by the analytic structure of the integrand in the complex s-plane.

The singularities of $G_{(k)}(s)$ are the zeros of the denominator

$$D(s) \equiv c^2\gamma^2 s^2 - 4R^2 \sin^2\!\Big(\frac{\omega_{\mathrm{p}} s}{2}\Big) = 0 \tag{4.54}$$

Introduce the dimensionless complex variable

$$z \equiv \frac{\omega_{\mathrm{p}} s}{2}, \qquad \text{so that} \qquad s = \frac{2z}{\omega_{\mathrm{p}}}, \tag{4.55}$$

and recall that $\beta = \omega_{\rm p} R/(\gamma c)$. Then (4.54) becomes

$$\sin^2 z = \frac{1}{\beta^2}\, z^2. \tag{4.56}$$

Equation (4.56) has no nonzero real solutions because $|\sin z| \le 1$ while $|z|/\beta$ grows unboundedly. Therefore all nontrivial solutions satisfy $\mathrm{Im}(z) \neq 0$.

4.A.5 Existence, uniqueness, and location of the nearest singularity

Set $z = x + iy$. Using

$$\sin(x+iy) = \sin x\, \cosh y + i \cos x\, \sinh y, \qquad |\sin(x+iy)|^2 = \sin^2 x + \sinh^2 y, \tag{4.57}$$

the singularity condition (4.56) can be written as

$$\sin^2 x + \sinh^2 y = \frac{1}{\beta^2}\,(x^2 + y^2). \tag{4.58}$$

We now show that the solution with smallest $|\mathrm{Im}(z)|$ is purely imaginary.

Lemma 1 (purely imaginary minimizer). Let $\beta \in (0,1)$. Among all nonzero solutions of (4.58), the one(s) with minimal $|y|$ satisfy $x = 0$.

Proof. Fix $y > 0$. The left-hand side of (4.58) satisfies $\sin^2 x + \sinh^2 y \ge \sinh^2 y$, with equality at $x = 0$. The right-hand side satisfies $(x^2 + y^2)/\beta^2 \ge y^2/\beta^2$, with equality at $x = 0$. Therefore, for given y, the equality (4.58) is hardest to satisfy when $x = 0$ in the sense that increasing x increases the right-hand side at least quadratically but changes the left-hand side by a bounded amount ($\sin^2 x \le 1$). Consequently, if (4.58) has a solution at some (x, y) with $y > 0$, then there exists a solution at $(0, y_0)$ with $0 < y_0 \le y$. This shows that the minimal y must occur at $x = 0$. □

Setting $x = 0$ gives $z = iy$ and (4.56) becomes

$$\sinh^2 y = \frac{1}{\beta^2}\, y^2 \qquad \Longleftrightarrow \qquad \frac{\sinh y}{y} = \frac{1}{\beta}. \tag{4.59}$$

Since $\sinh y/y$ is strictly increasing for $y > 0$, with $(\sinh y)/y \to 1$ as $y \to 0$ and $(\sinh y)/y \to \infty$ as $y \to \infty$, there exists a unique $y_0(\beta) > 0$ solving (4.59). Thus the nearest singularities to the real axis are located at

$$z = \pm i y_0(\beta), \qquad s = \pm i s_*(\beta), \qquad s_*(\beta) = \frac{2 y_0(\beta)}{\omega_{\rm p}}. \tag{4.60}$$

4.A.6 Ultrarelativistic asymptotics of the singularity: $y_0(\beta) \sim \sqrt{3}/\gamma$

We now obtain the ultrarelativistic behavior of $y_0(\beta)$ as $\beta \to 1^-$ (equivalently $k \gg 1$, $\gamma \to \infty$). Let $\delta \equiv 1 - \beta$ and note that

$$1 - \beta^2 = \frac{1}{\gamma^2} \qquad \Longrightarrow \qquad \beta = 1 - \frac{1}{2\gamma^2} + O(\gamma^{-4}). \tag{4.61}$$

We look for a solution of (4.59) in the form $y_0 \ll 1$ when $\gamma \gg 1$. Using the Taylor series

$$\sinh y = y + \frac{y^3}{6} + O(y^5) \qquad \Longrightarrow \qquad \frac{\sinh y}{y} = 1 + \frac{y^2}{6} + O(y^4), \tag{4.62}$$

equation (4.59) becomes

$$1 + \frac{y_0^2}{6} + O(y_0^4) = \frac{1}{\beta} = 1 + \frac{1-\beta}{\beta} = 1 + (1-\beta) + O\big((1-\beta)^2\big). \tag{4.63}$$

Using (4.61), $1 - \beta = 1/(2\gamma^2) + O(\gamma^{-4})$, hence

$$\frac{y_0^2}{6} = \frac{1}{2\gamma^2} + O(\gamma^{-4}) \qquad \Longrightarrow \qquad y_0(\beta) = \frac{\sqrt{3}}{\gamma} + O(\gamma^{-3}). \tag{4.64}$$

This step is controlled: the assumption $y_0 \ll 1$ is consistent because $y_0 \sim \gamma^{-1}$.

4.A.7 From the nearest singularity to the detailed-balance plateau

The exponential suppression of excitation in stationary trajectories is governed by the distance s_* of the nearest singularity to the real axis. The rigorous statement is that, under mild regularity assumptions satisfied by (4.48), the large-$|E|$ behavior of $\mathcal{G}(E)$ is controlled by the singularity closest to the real axis. However, in the present magnetic ultrarelativistic scaling we do not take $|E| \to \infty$ at fixed kinematics: instead we take $k \gg 1$ while the dimensionless ratio $\Omega c/a$ tends to a fixed constant (4.51). This is precisely the regime where the Biermann uniform asymptotic expression applies, yielding a closed formula for the effective temperature in terms of $|E|/a$ that is uniform in that ratio.

Concretely, in the ultrarelativistic circular spectrum one has the uniform asymptotic form

$$T_{\mathrm{circ}}(E) = \frac{|E|}{\ln\!\left(1 + 4\sqrt{3}\,\frac{|E|}{a}\,e^{2\sqrt{3}|E|/a}\right)} \qquad (\beta \to 1^-), \tag{4.65}$$

which interpolates between the limits $T_{\mathrm{circ}} \simeq a/(4\sqrt{3})$ for $|E| \ll a$ and $T_{\mathrm{circ}} \simeq a/(2\sqrt{3})$ for $|E| \gg a$ (see Sec. 3.5). Using (4.53), this implies

$$\begin{aligned} \frac{\mathcal{G}(E)}{\mathcal{G}(-E)} = \exp\!\Big(-\frac{E}{T_{\mathrm{circ}}(E)}\Big) &= \exp\!\left[-\ln\!\left(1 + 4\sqrt{3}\,\frac{|E|}{a}\,e^{2\sqrt{3}|E|/a}\right)\right] \\ &= \left(1 + 4\sqrt{3}\,\frac{|E|}{a}\,e^{2\sqrt{3}|E|/a}\right)^{-1}. \end{aligned} \tag{4.66}$$

We now specialize to the magnetic model. From (4.51),

$$\frac{|E|}{a} = \frac{\hbar\Omega}{a} = \frac{\hbar}{c}\,\frac{\Omega c}{a} \xrightarrow{k\gg 1} \frac{\hbar}{c}\,\frac{g}{2}, \qquad \text{or equivalently} \qquad \frac{\Omega c}{a} \xrightarrow{k\gg 1} \frac{g}{2}. \tag{4.67}$$

In the standard relativistic conventions used in Eq. (4.65) (the same conventions already used in Sec. 3.5), it is the dimensionless ratio $|E|/a$ that enters. Therefore,

in the magnetic ultrarelativistic regime the argument $|E|/a$ becomes a constant, and (4.66) converges to a constant:

$$\frac{\mathcal{G}(E)}{\mathcal{G}(-E)} \xrightarrow{k\gg 1} \left(1+2g\sqrt{3}\,e^{g\sqrt{3}}\right)^{-1} = \exp\big(-g\,\chi_\infty\big), \tag{4.68}$$

where

$$\chi_\infty \equiv \frac{1}{g}\ln\Big(1+2g\sqrt{3}\,e^{g\sqrt{3}}\Big). \tag{4.69}$$

For an electron ($g \simeq 2$), $\chi_\infty \simeq 2.70$, numerically very close to $\pi\sqrt{3}/2 \simeq 2.72$. This is the origin of the practically relevant approximation

$$\chi_\infty \simeq \frac{\pi\sqrt{3}}{2}, \qquad (g \simeq 2), \tag{4.70}$$

and hence

$$\frac{\mathcal{G}(E)}{\mathcal{G}(-E)} \simeq e^{-g\pi\sqrt{3}/2}. \tag{4.71}$$

4.A.8 Plateau of the excitation probability

The excitation probability in the stationary regime is

$$p_\uparrow = \frac{\mathcal{G}(E)}{\mathcal{G}(E)+\mathcal{G}(-E)} = \frac{1}{1+\exp\big(g\chi_\infty\big)}. \tag{4.72}$$

Using (4.70) gives the practical closed estimate

$$p_\uparrow^{(\infty)} \simeq \frac{1}{1+\exp\big(g\pi\sqrt{3}/2\big)}. \tag{4.73}$$

For $g \simeq 2$ this is $p_\uparrow^{(\infty)} \sim 4\times 10^{-3}$, i.e. a plateau at the $\sim 0.4\%$ level.

4.A.9 When is the ultrarelativistic plateau reached in terms of B and R?

Since $k = |q|BR/(mc)$, the approach to the plateau is controlled entirely by the magnitude of BR. A convenient practical threshold is $k \gtrsim 30$, for which $\beta \simeq 1-1/(2k^2)$ and $\gamma \simeq k$ at per-mille level. This implies

$$R \gtrsim \frac{k\,mc}{|q|\,B}. \tag{4.74}$$

For an electron, $mc/|q| \simeq 1.70\times 10^{-3}\,\mathrm{T\,m}$, hence

$$R \gtrsim 5.1\times 10^{-3}\,\mathrm{m}\,\Big(\frac{k}{30}\Big)\Big(\frac{10\,\mathrm{T}}{B}\Big). \tag{4.75}$$

Therefore, for laboratory fields of order 10 T the plateau requires radii in the millimeter-to-centimeter range, while for $B \sim 1$ T one needs radii larger by an order of magnitude.

Remark (consistency with numerical implementations). In numerical evaluations based on the decomposition $\mathcal{G}(E) = \mathcal{G}_{\text{inert}}(E) + \mathcal{G}_{\text{corr}}(E)$, care must be taken when forming ratios: the inertial term contributes only for $E < 0$ (de-excitation), whereas excitation at $E > 0$ is purely due to the circular correction. The population $p_\uparrow$ is therefore not equal to $\mathcal{G}(E)/\mathcal{G}(-E)$, but is given by (4.72). This distinction is essential when comparing to a numerical code that computes $\mathcal{G}(E)/\mathcal{G}(-E)$ directly.

Chapter 5

Leggett-Garg Inequalities: Foundations, Formulation and Significance

In the previous chapters, quantum detectors have been introduced as operational tools to probe physical properties that are not directly accessible through local field observables alone. In particular, the Unruh–DeWitt detector provided a concrete realization of how a localized quantum system, coupled to a field along a prescribed trajectory, can encode information about the state of the field and about the observer's motion in its internal dynamics.

In this chapter, the concept of a quantum detector is explored further in a different but closely related direction. Rather than being used to investigate observer-dependent particle content or thermal features of quantum fields, the detector is now employed as a tool to address questions concerning the temporal structure of quantum dynamics and the validity of classical descriptions of physical systems over time. This shift of focus naturally leads to the framework of the Leggett–Garg inequalities and to the broader notion of macrorealism.

The central idea underlying the Leggett–Garg program is that a classical system should admit a description in which physical quantities possess well-defined values at all times and evolve according to dynamics that can, at least in principle, be monitored without inducing significant back-action. Quantum mechanics challenges this picture, not through spatial nonlocality as in Bell-type scenarios, but through the structure of temporal correlations associated with sequential measurements on a single system. Quantum detectors play a crucial role in this context, as they provide a controlled and operationally meaningful way to access such temporal correlations.

From this perspective, the Leggett–Garg inequalities can be understood as consistency conditions imposed on the outcomes recorded by a detector monitoring the system at different times. Their violation signals the impossibility of embedding the observed dynamics into a classical description. At the same time, the analysis of these inequalities highlights the delicate role played by measurement invasiveness, detector back-action, and the operational definition of what it means to observe a system without disturbing it.

The purpose of this chapter is to develop this detector-based viewpoint in a

systematic way. After reviewing the historical motivations and original formulation of the Leggett–Garg inequalities, the discussion will progressively move toward more refined measurement protocols in which quantum detectors are coupled to the system in a non-demolition fashion. This approach ultimately allows one to characterize violations of classicality in terms of quasi-probability distributions and to go beyond the limitations inherent in inequality-based tests.

5.1 Introduction and Historical Motivation

Extrapolating the laws of quantum mechanics to the scale of everyday objects inevitably leads to the prospect of macroscopic coherence, where systems composed of a vast number of atoms could exist in quantum superpositions of macroscopically distinct states. The famous Schrödinger's cat paradox [69], simultaneously dead and alive, is the embodiment of this idea. This scenario runs completely counter to our intuitive understanding of how the macroscopic world operates.

In their 1985 paper, Leggett and Garg were concerned with whether macroscopic coherence could be realized in the laboratory and, if so, how one might demonstrate its presence [52]. Their approach was to first codify our classical intuition about the macroscopic world into two principles: macroscopic realism per sé (MRps) and noninvasive measurability (NIM). Based on these assumptions, they derived a class of inequalities, now known as the Leggett-Garg inequalities (LGIs), which any system behaving in accord with macroscopic classical intuition must obey.

An experimental violation of an LGI implies that at least one of the two fundamental postulates fails, forcing us to abandon a realistic and noninvasive description of the system. In this way, LGIs provide a method to investigate the existence of quantum coherence at increasingly larger scales and to test the limits of quantum mechanics as we move from the microscopic to the macroscopic world [51].

Structurally, LGIs are closely related to Bell inequalities [8]. However, while Bell inequalities impose constraints on correlations between measurements performed on spatially separated systems, in LGIs the separation is along the time axis. For this reason, LGIs are often referred to as temporal Bell inequalities [63]. In both cases, to obtain testable inequalities that can be violated by quantum mechanics, the assumption of realism is combined with the principle of locality (for Bell) or with NIM (for Leggett-Garg), which play analogous formal roles in their respective derivations.

5.2 The Postulates of Macroscopic Realism

The conceptual core of the Leggett-Garg program lies in the rigorous codification of the expected intuitive behavior of a macroscopic object. Following the original formulation [52], the fundamental principles are:

(A1) Macroscopic Realism per sé. A macroscopic system with two or more macroscopically distinct states available to it will at all times be in one or the other of these states. In other words, the measured physical quantity has a

well-defined value at every instant, independent of the act of measurement. This assumption answers in the affirmative the provocative question: "Is the flux there when nobody looks?" in the original Leggett and Garg's paper [52].

(A2) Noninvasive Measurability (NIM). It is possible, in principle, to determine the state of the system with arbitrarily small perturbation on its subsequent dynamics. In a classical context, this is a natural expectation: we can "observe" a system without significantly disturbing it.

(A3) Induction. The outcome of a measurement on the system cannot be affected by what will or will not be measured on it later. This assumption, made explicit in later works [45, 50], reflects our notion of causality and the arrow of time and is rarely challenged in the analysis of LGI violations.

The conjunction of properties (A1)–(A3) has sometimes been referred to as "classicity" [11] or as "macrorealism in the broader sense". In the present treatment, such terminology will be avoided in favor of an explicit reference to the individual assumptions, in order to prevent ambiguities and to keep the logical structure of the argument transparent. Within a theory obeying (A1)–(A3), Schrödinger's cat is, at each instant of time, either dead or alive, and which of these two alternatives actually holds can, in principle, be ascertained by measurements that neither disturb the system nor are influenced by its future evolution.

The definition of macrorealism relies on the notion of macroscopically distinct states, although the precise meaning of macroscopic distinctness has been the subject of considerable discussion. Various criteria have been proposed to formalize this notion, such as the "extensive difference" $\mathfrak{L}$ and the "disconnectivity" $\mathfrak{D}$ introduced by Leggett [51]. Nevertheless, it has been pointed out by Maroney that macroscopicity is not strictly required for the formal derivation of the Leggett–Garg inequalities [58]. What is essential is instead the assumption that the theory is ontic, in the sense that physical quantities possess definite values at all times, together with the validity of assumptions (A2) and (A3).

Among these assumptions, non-invasive measurability, expressed by (A2), plays a particularly subtle role and has been the focus of extensive debate in the literature [71, 64, 85]. This assumption presupposes macrorealism per se, since a measurement is supposed to reveal a pre-existing property of the system. In the context of quantum mechanics, however, the statement of non-invasive measurability is inherently counterfactual: it refers to a property that the system would possess if it admitted a macrorealistic description, which is precisely what is being tested. As a result, a measurement may be regarded as non-invasive from the perspective of a macrorealist theory, while still being invasive in quantum mechanics due to the collapse of the wave function, a notion that has no counterpart within a macrorealistic framework.

Leggett and Garg themselves proposed the use of so-called ideal negative measurements as a possible strategy to approximate the condition of non-invasive measurability. In such a scheme, the detector is designed to interact only with the state corresponding to $Q = +1$, so that the absence of a detector response, together with the assumption of macrorealism, allows one to infer that the system was in the state $Q = -1$ without any direct interaction. Despite this classical intuition, even ideal

negative measurements induce wave-function collapse within quantum mechanics [31], and therefore do not fully resolve the problem of measurement invasiveness at the quantum level. It is worth pointing out, though, that the formal definition of NIM remains under debate. In recent years, the notion of NIM as been replaced by a weaker condition, which states that 'A measurement does not change the outcome statistics of a later measurement', known as the 'No-Signaling in Time' (NSIT), as proposed by Kofler and Brukner [45].

Given the assumptions A1-2 and 3, the logical structure of the Leggett–Garg inequalities closely mirrors that of Bell inequalities. In both cases, realism alone is not in conflict with the predictions of quantum mechanics. It is only when realism is supplemented by an additional assumption—locality in the Bell scenario, or non-invasive measurability in the Leggett–Garg framework—that one obtains inequalities which can be experimentally tested and potentially violated. The violation of such inequalities therefore signals the incompatibility of quantum predictions with the conjunction of these assumptions, rather than with realism taken in isolation.

5.3 Formal Derivation of the Leggett-Garg Inequalities

5.3.1 Leggett–Garg inequalities as constraints on temporal correlations

The Leggett–Garg inequalities emerge from the attempt to formalize, in experimentally testable terms, the assumptions underlying a macrorealistic description of temporal evolution. Consider a physical system on which a dichotomic observable $Q(t)$, taking values ± 1, can be measured at different instants of time. Under the assumptions of macrorealism per se, non-invasive measurability, and induction, it is possible to assign to the system a set of classical random variables $Q(t_1), Q(t_2), \ldots$, all defined on a single probability space and governed by a joint probability distribution $p(Q_1, Q_2, \ldots)$.

The existence of such a joint probability distribution implies nontrivial constraints on the measurable temporal correlations. In particular, the two-time correlation functions $C_{ij} = \langle Q(t_i)Q(t_j)\rangle$, obtained as marginals of the underlying joint distribution, cannot be chosen independently. Their allowed values are restricted by the positivity and normalization of the joint probability, and these restrictions can be expressed in the form of inequalities involving linear combinations of the correlators. The Leggett–Garg inequalities represent precisely these consistency conditions.

A paradigmatic example is provided by three sequential measurement times $t_1 < t_2 < t_3$, for which macrorealism implies the inequality (see e. g. [32])

$$K = C_{12} + C_{23} - C_{13} \leq 1,$$

together with analogous inequalities obtained by permutations of signs and indices. The derivation of these bounds relies solely on classical probability theory and does not invoke any specifically quantum-mechanical postulate. In this sense, the Leggett–

Garg inequalities delineate the region of temporal correlations compatible with a macrorealistic description, independently of the microscopic details of the system.

When the same correlators are computed within quantum mechanics, using the standard projection postulate and unitary time evolution, the resulting values may exceed the macrorealistic bounds. Such violations demonstrate that the observed temporal correlations cannot be embedded into a classical stochastic process satisfying the assumptions of macrorealism and non-invasive measurability. As in the case of Bell inequalities, the violation of a Leggett–Garg inequality therefore provides a clear and unambiguous witness of the failure of the conjunction of these assumptions.

At the same time, an important structural limitation of the Leggett–Garg framework must be recognized. The inequalities constrain only specific combinations of two-time correlation functions and thus probe only a limited portion of the full temporal statistics of the system. In particular, they do not test directly the existence of a global joint probability distribution for all measurement outcomes, but only certain marginal constraints derived from it. As a consequence, the violation of a Leggett–Garg inequality constitutes a sufficient condition for the violation of macrorealism, but not a necessary one.

This asymmetry has significant conceptual implications. It implies that the absence of a violation cannot be interpreted as evidence that a macrorealistic description is valid, but merely that the particular inequalities considered are not sensitive to the form of non-classical temporal correlations present in the system. There exist quantum evolutions for which the assumptions of macrorealism are violated, while all Leggett–Garg inequalities remain satisfied. In such cases, the failure of macrorealism is encoded in aspects of the temporal statistics that are not captured by inequality-based tests.

The recognition of this limitation motivates the development of alternative approaches capable of probing the full temporal structure of quantum dynamics. Rather than relying exclusively on correlators and inequalities, these approaches aim at reconstructing, in an operationally meaningful way, the underlying temporal quasi-probability distributions associated with sequential measurements. As will be shown in the following sections, it is possible to create a Quantum Non-Demolition Measurement (QNDM) protocol that provides both necessary and sufficient criteria for the violation of macrorealism, allowing one to overcome the intrinsic limitations of the Leggett–Garg inequalities.

For completeness, we note that alternative formulations providing necessary and sufficient conditions for macrorealism have been proposed. Notably, approaches based on NSIT hierarchies have been developed by Clemente [26, 27], as well as by Halliwell [40].

However, these approaches are typically formulated in terms of constraints on experimentally observed statistics, and therefore the corresponding NSIT conditions are verified a posteriori from the measured multi-time distributions. As a consequence, it is not guaranteed in advance whether these conditions will be satisfied or violated for a given protocol.

In contrast, the QNDM-based approach considered here is constructed so that the non-disturbance condition is enforced at the dynamical level. In this sense, it provides an alternative route to testing macrorealism, where the NSIT condition is

implemented operationally by design rather than verified retrospectively from the measured statistics.

5.3.2 Leggett–Garg inequalities from classical temporal statistics

A precise way to formalize the content of macrorealism, together with non-invasive measurability and induction, is to require that the values of a monitored observable at different times can be described by classical random variables defined on a single probability space. For a dichotomic observable $Q(t)$, such that at three times $t_1 < t_2 < t_3$ the associated outcomes are $q_i = q(t_i) \in \{\pm 1\}$, it is possible to define a joint probability distribution $p(q_1, q_2, q_3)$ [32]

$$p(q_1, q_2, q_3) \geq 0, \qquad \sum_{q_1,q_2,q_3} p(q_1, q_2, q_3) = 1,$$

such that all measurable marginals and correlation functions are obtained from it by standard marginalization. In particular, the two-time correlators are

$$C_{ij} = \langle Q_i Q_j \rangle = \sum_{q_1,q_2,q_3} q_i q_j \, p(q_1, q_2, q_3), \qquad (i, j) \in \{(1, 2), (2, 3), (1, 3)\},$$

where $Q_i \equiv Q(t_i)$. The Leggett–Garg inequalities are then nothing but necessary constraints on the admissible values of (C_{12}, C_{23}, C_{13}) implied by the positivity of $p(q_1, q_2, q_3)$.

To derive the simplest three-time inequality, consider the random variable

$$K \equiv Q_1 Q_2 + Q_2 Q_3 - Q_1 Q_3, \tag{5.1}$$

which is itself a classical random variable on the same probability space. Since each Q_i takes only the values ± 1, one can evaluate K pointwise for every realization (q_1, q_2, q_3). Using $q_i^2 = 1$, one may rewrite

$$K = q_2(q_1 + q_3) - q_1 q_3.$$

If $q_1 = q_3$, then $q_1 + q_3 = \pm 2$ and $q_1 q_3 = 1$, hence $K = \pm 2q_2 - 1$, which can only take the values 1 or -3. If instead $q_1 = -q_3$, then $q_1 + q_3 = 0$ and $q_1 q_3 = -1$, hence $K = 1$. Therefore, for any triple (q_1, q_2, q_3) one has the pointwise bound

$$K(q_1, q_2, q_3) \leq 1.$$

Taking the expectation value with respect to the joint distribution $p(q_1, q_2, q_3)$, linearity of the average yields

$$\langle K \rangle = \langle Q_1 Q_2 \rangle + \langle Q_2 Q_3 \rangle - \langle Q_1 Q_3 \rangle = C_{12} + C_{23} - C_{13} \leq 1.$$

This is the standard three-time Leggett–Garg inequality [52]. By considering instead the combinations obtained by changing the sign in front of one of the terms $Q_i Q_j$, one obtains the usual family of inequalities that delimit the polytope of correlations compatible with a single underlying joint probability distribution.

The logical content of the inequality can now be stated with complete clarity. If a theory satisfies macrorealism per se, non-invasive measurability and induction in the strong sense that they imply the existence of a non-negative joint probability distribution for (Q_1, Q_2, Q_3), then the inequality $C_{12} + C_{23} - C_{13} \leq 1$ must hold. Consequently, an experimentally observed value

$$C_{12} + C_{23} - C_{13} > 1$$

is incompatible with any classical temporal statistics based on a single joint distribution $p(q_1, q_2, q_3)$. In other words, a violation of the Leggett–Garg inequality certifies that no macrorealistic, non-invasively measurable description exists for the measured temporal correlations, regardless of the microscopic details of the system.

At the same time, it is important to keep track of what has, and has not, been established by this argument. The derivation shows that the inequalities are necessary conditions for the existence of a classical joint distribution, hence their violation is a sufficient witness of the failure of macrorealism. However, because the inequalities constrain only specific linear combinations of low-order correlators, their satisfaction does not by itself guarantee that a positive joint probability distribution exists, nor that the full temporal statistics admit a macrorealistic embedding. This distinction between sufficiency and necessity will become central when moving beyond inequality-based tests toward approaches that interrogate the temporal statistics more directly.

The derivation above has a clear logical content. The assumption that the temporal outcomes (Q_1, Q_2, Q_3) admit a non-negative joint probability distribution $p(q_1, q_2, q_3)$ implies the Leggett–Garg bound

$$C_{12} + C_{23} - C_{13} \leq 1,$$

together with the analogous sign-variants. Hence, an experimental violation of any of these inequalities is incompatible with the existence of such a classical temporal statistics, and therefore certifies the failure of the conjunction of macrorealism and non-invasive measurability. In this precise sense, the violation of a Leggett–Garg inequality is a sufficient witness of macrorealism breakdown.

5.3.3 Leggett–Garg inequalities as sufficient tests of macrorealism

A natural response to this limitation is to enlarge the set of tested constraints. If one considers n measurement times $t_1 < \cdots < t_n$, macrorealism in its strong probabilistic form requires the existence of a global joint distribution $p(q_1, \ldots, q_n) \geq 0$ for the entire sequence of outcomes, from which all marginals and correlators are obtained. From this assumption one can derive families of higher-order Leggett–Garg inequalities, involving more times and more correlators, that must be satisfied by any such classical model. In this way, one obtains a hierarchy of tests: increasing n and enlarging the class of inequalities imposes progressively stronger necessary conditions on the admissibility of the temporal correlations within a macrorealistic framework.

Despite this refinement, the fundamental logical asymmetry remains. For any fixed and finite set of inequalities, "no violation" cannot be promoted to a positive

verification of macrorealism. Operationally, this is because a finite inequality set constrains only a finite collection of statistical features of the temporal process, while a macrorealistic description entails the existence of a fully consistent classical probability structure for the entire time-ordered measurement record. Conceptually, it is also because the statement that measurements are non-invasive is not a purely statistical property of the observed correlators, but depends on the measurement protocol and on how information about the system is acquired. Consequently, even an arbitrarily extensive battery of Leggett–Garg inequalities, while valuable as a collection of necessary constraints, does not by itself provide a definitive criterion of macrorealism validity when no violation is observed.

This motivates the search for operational criteria that probe macrorealism more directly than correlator inequalities. Rather than inferring the existence or non-existence of a classical temporal statistics indirectly through a hierarchy of bounds, one may attempt to reconstruct a temporal (quasi-)probability structure associated with sequential monitoring of the system. Such an approach can, in principle, distinguish classical from non-classical temporal statistics at a more fundamental level and can yield diagnostics that are closer to being necessary and sufficient. In the following sections, this perspective will be developed by introducing detector-assisted non-demolition measurement schemes, which provide an explicit operational approach to sharper witnesses of macrorealism violation.

The above discussion can be further analysed by phrasing macrorealism as a problem for classical probability distributions [35, 33, 57]. Fix a sequence of times $t_1 < \cdots < t_n$ and define the sample space $\Omega_n = \{\pm 1\}^n$, whose elements are deterministic outcome strings $\omega = (q_1, \ldots, q_n)$. A macrorealistic temporal model at order n is a probability distribution $p_n : \Omega_n \to [0, 1]$ with $\sum_{\omega \in \Omega_n} p_n(\omega) = 1$. Any experimentally accessible statistic derived from measurements at those times—single-time probabilities, multi-time joint probabilities, and correlators—must be obtainable as marginals of p_n. For instance, for any subset $S \subset \{1, \ldots, n\}$ one defines the marginal

$$p_S(\{q_i\}_{i \in S}) = \sum_{\{q_j\}_{j \notin S}} p_n(q_1, \ldots, q_n),$$

and any correlation function is then an affine functional of the appropriate marginal, e.g.

$$C_{ij} = \sum_{q_i, q_j = \pm 1} q_i q_j \, p_{\{i,j\}}(q_i, q_j).$$

In this language, the Leggett–Garg inequalities are linear constraints on low-order marginals that are implied by the positivity of p_n. The derivation in the previous section is exactly of this type: if there exists a non-negative joint distribution $p_3(q_1, q_2, q_3)$, then for the function $K = C_{12} + C_{23} - C_{13}$ one has $K \leq 1$. Therefore, a violation $K > 1$ implies that no such p_3 exists, i.e. the observed statistics cannot arise from any classical joint distribution over (Q_1, Q_2, Q_3). This establishes, in a mathematically sharp sense, that Leggett–Garg violations are incompatible with classical temporal statistics of the macrorealistic type.

The converse direction is more subtle and it is precisely here that the "sufficient but not necessary" character of LGIs originates. Macrorealism is not merely the existence of some distribution consistent with a selected set of correlators; rather, it

is the existence of a fully consistent classical probability structure for the temporal measurement record [45]. Formally, this means that, for each n, there should exist a distribution p_n on Ω_n whose marginals reproduce the entire family of experimentally relevant statistics at order n, and that these distributions should be mutually compatible under marginalization, in the sense that for $m < n$ one has

$$p_m(q_1, \ldots, q_m) = \sum_{q_{m+1}, \ldots, q_n} p_n(q_1, \ldots, q_n).$$

This consistency requirement is the temporal analogue of the classical marginal problem: one is given a collection of marginals (e.g. all pairwise distributions, or all k-time distributions up to some k) and asks whether there exists a global non-negative distribution whose marginals coincide with the given ones. In general, constraining only a restricted subset of marginals—for instance a few two-time correlators [33], as in the simplest LG tests—does not solve the extension problem uniquely and does not rule out the possibility that incompatibilities reside in higher-order marginals that are not being tested [35].

Even in the idealized limit, however, the inference "no violation" $\Rightarrow$ "macrorealism holds" would require controlling not just one inequality family at one order, but the full consistency of the temporal statistics under extension and marginalization across all relevant timescales and all relevant marginals. Operationally, this is prohibitively demanding because the number of independent marginals and corresponding facet constraints grows rapidly with the number of times, and because the mapping from experimental protocols to the underlying classical marginals is itself affected by measurement back-action. These structural facts explain why Leggett–Garg inequalities are best regarded as powerful sufficient witnesses of macrorealism violation, but not as a logically complete criterion for macrorealism.

5.3.4 Limits of inequality-based tests: a simple example

This distinction can be illustrated explicitly with a simple but instructive example. Consider a dichotomic observable $Q(t) \in \{\pm 1\}$ measured at three times $t_1 < t_2 < t_3$. Suppose that the experimentally accessible statistics are such that all single-time averages vanish,

$$\langle Q(t_i) \rangle = 0 \qquad \text{for } i = 1, 2, 3,$$

and that the two-time correlators take the symmetric values

$$C_{12} = C_{23} = C_{13} = \frac{1}{2}.$$

With these values, all three-time Leggett–Garg inequalities are satisfied. For instance,

$$C_{12} + C_{23} - C_{13} = \frac{1}{2} \leq 1,$$

and analogous combinations obtained by permuting indices or changing signs also lie strictly within the macrorealistic bounds. From the point of view of inequality-based tests at this order, no violation is detected.

Nevertheless, the satisfaction of these inequalities does not guarantee the existence of a non-negative joint probability distribution $p(q_1, q_2, q_3)$ reproducing these correlators. To see this, note that for dichotomic variables with vanishing means the two-time marginals are uniquely fixed by the correlators,

$$p_{ij}(q_i, q_j) = \frac{1}{4}\big(1 + q_i q_j C_{ij}\big).$$

For the values above, this yields three pairwise distributions that are mutually inconsistent with any distribution on the whole sample space Ω_3. In particular, attempting to reconstruct $p(q_1, q_2, q_3)$ from these marginals leads to negative values for some outcome strings, signaling the impossibility of a classical joint distribution.

This inconsistency can be traced back to the fact that pairwise correlations alone do not uniquely determine a valid three-variable distribution [35], and that compatibility of all pairwise marginals is a strictly stronger requirement than the satisfaction of Leggett–Garg inequalities. In the present example, the correlators lie inside the region allowed by the inequalities, yet the corresponding marginal problem admits no non-negative solution. The failure of macrorealism is therefore encoded in higher-order compatibility conditions that are invisible at the level of the tested inequalities.

The example highlights in concrete terms the logical asymmetry discussed above. Violating a Leggett–Garg inequality excludes any macrorealistic model, but satisfying all inequalities at a given order does not establish the existence of a consistent classical temporal statistics. Detecting such inconsistencies requires either access to higher-order temporal correlations or, more fundamentally, a framework in which the temporal probability structure itself is probed directly rather than through a limited set of correlators. This observation motivates the search for measurement protocols capable of revealing the full temporal statistics of the system.

5.3.5 Four-time Leggett–Garg inequalities and the hierarchy of constraints

The passage from three to four measurement times provides a concrete illustration of how Leggett–Garg tests can be strengthened by enlarging the temporal structure that is being constrained [6, 7]. Consider a dichotomic observable $Q(t) \in \{\pm 1\}$ measured at four times $t_1 < t_2 < t_3 < t_4$, and assume, in the macrorealistic sense, that there exists a non-negative joint distribution $p(q_1, q_2, q_3, q_4)$ on $\{\pm 1\}^4$. As before, define the two-time correlators $C_{ij} = \langle Q_i Q_j \rangle$, where $Q_i \equiv Q(t_i)$.

A standard four-time Leggett–Garg combination is obtained by considering the random variable

$$K_4 \equiv Q_1 Q_2 + Q_2 Q_3 + Q_3 Q_4 - Q_1 Q_4,$$

which is well-defined pointwise on the same probability space. For any deterministic assignment $(q_1, q_2, q_3, q_4) \in \{\pm 1\}^4$, one can rewrite

$$K_4 = q_2(q_1 + q_3) + q_4(q_3 - q_1).$$

If $q_1 = q_3$, then $q_1 + q_3 = \pm 2$ and $q_3 - q_1 = 0$, hence $K_4 = \pm 2 q_2$, so $K_4 = \pm 2$. If $q_1 = -q_3$, then $q_1 + q_3 = 0$ and $q_3 - q_1 = \pm 2$, hence $K_4 = \pm 2 q_4$, so again $K_4 = \pm 2$.

Therefore one has the pointwise bound

$$K_4(q_1, q_2, q_3, q_4) \leq 2,$$

and taking the expectation value yields the four-time Leggett–Garg inequality

$$\langle K_4 \rangle = C_{12} + C_{23} + C_{34} - C_{14} \leq 2.$$

As in the three-time case, one obtains a family of related inequalities by changing the pattern of signs, corresponding to other linear combinations that are likewise bounded by 2 under any non-negative joint distribution. Any experimental violation of one of these bounds is incompatible with the existence of a classical temporal statistics for (Q_1, Q_2, Q_3, Q_4), and hence constitutes a sufficient witness of the breakdown of the macrorealistic assumptions.

The relevance of the four-time inequality is that it can rule out temporal statistics that may remain compatible with all three-time inequalities tested on overlapping triples [32]. This can be seen by an explicit consistency example. Suppose one observes strong nearest-neighbour correlations and an anticorrelation between the endpoints, namely

$$C_{12} = C_{23} = C_{34} = 1, \qquad C_{14} = -1.$$

Then the four-time combination gives

$$C_{12} + C_{23} + C_{34} - C_{14} = 1 + 1 + 1 - (-1) = 4,$$

which violates the four-time Leggett–Garg bound $4 \leq 2$. On the other hand, if one restricts attention only to three-time tests on the triples (t_1, t_2, t_3) and (t_2, t_3, t_4), these would involve C_{12}, C_{23}, C_{13} and C_{23}, C_{34}, C_{24}, respectively. By choosing, for instance, $C_{13} = 1$ and $C_{24} = 1$, the corresponding three-time combinations $C_{12} + C_{23} - C_{13}$ and $C_{23} + C_{34} - C_{24}$ both saturate the macrorealistic bound without violation. This illustrates that increasing the number of times introduces genuinely new classical consistency constraints that are invisible to lower-order tests, even when those lower-order tests are applied to overlapping time windows.

At the same time, the logical asymmetry emphasized earlier persists at four times, and in fact becomes sharper as the order increases. The inequality $C_{12} + C_{23} + C_{34} - C_{14} \leq 2$ is a necessary condition for the existence of a non-negative $p(q_1, q_2, q_3, q_4)$, but it is not, by itself, sufficient [35]. Passing this inequality only constrains one particular linear functional of a small subset of correlators. A macrorealistic model, however, entails the existence of a single global joint distribution reproducing all experimentally relevant temporal marginals. In particular, if additional correlators such as C_{13} and C_{24} (or higher-order temporal marginals) are also accessible, their values must be jointly compatible with the same $p(q_1, q_2, q_3, q_4)$. It is therefore possible for a given dataset to satisfy the chain inequality above while still failing to admit a non-negative joint distribution once the full temporal statistics are taken into account. In this precise sense, four-time Leggett–Garg inequalities strengthen the set of necessary constraints, but do not remove the fundamental fact that inequality-based tests provide, at any fixed order, only sufficient witnesses of macrorealism violation.

This motivates the hierarchical viewpoint. As one increases the number of measurement times and enlarges the class of inequalities tested, one imposes progressively stronger necessary conditions on the existence of a classical joint distribution. However, establishing macrorealism in the affirmative would require, in principle, controlling a complete set of compatibility conditions for the full temporal measurement record, which quickly becomes impractical and, more importantly, remains conceptually entangled with measurement back-action.

5.3.6 Beyond inequality-based tests: motivation for non demolition protocols

The analysis developed in the previous sections clarifies both the power and the intrinsic limitations of Leggett–Garg inequalities as tests of macrorealism. On the one hand, any observed violation of an LGI is incompatible with the existence of a classical temporal statistics based on a non-negative joint probability distribution for the measurement outcomes. In this precise sense, LGI violations provide unambiguous and experimentally accessible witnesses of the failure of macrorealism. On the other hand, the absence of a violation, even when considering inequalities of increasing order, cannot be promoted to a positive verification of macrorealism. Inequality-based tests constrain only selected projections of the full temporal statistics and therefore furnish, at any fixed order, only necessary conditions for the existence of a classical joint distribution.

This situation is further complicated by the operational meaning of non-invasive measurability. The LGI framework assumes that the measured correlators faithfully reflect properties of the system that pre-exist the act of measurement, yet in quantum mechanics the statistics of sequential measurements depend explicitly on the measurement protocol and on the associated back-action. As a consequence, even when LGIs are not violated, it remains ambiguous whether the observed statistics reflect an underlying macrorealistic dynamics or are instead shaped by measurement-induced disturbances that are not captured at the level of correlators alone.

These considerations point toward the need for a different diagnostic strategy. Rather than inferring the failure of macrorealism indirectly from bounds on selected correlators, one may seek protocols that provide direct operational access to the temporal probability structure itself. In particular, it is natural to ask whether one can construct, from measurable quantities, a temporal distribution whose properties unambiguously signal the presence or absence of an underlying classical joint probability model. If such a distribution were to exhibit features incompatible with classical probability theory, such as negativity, this would constitute a direct witness of macrorealism violation, potentially overcoming the sufficiency-only character of inequality-based tests.

In the following sections, this perspective is developed by introducing quantum non-demolition measurement schemes. These protocols employ an ancillary quantum detector that is sequentially coupled to the system in such a way that temporal information is encoded without destroying the system's intrinsic dynamics. As will be shown, the resulting detector-based temporal quasi-probability distributions provide a more complete characterization of temporal quantum correlations and lead

to criteria for macrorealism violation that go beyond the scope of Leggett–Garg inequalities.

5.4 Quantum Non-Demolition Measurements and Phase Accumulation

5.4.1 Motivation and conceptual framework

A central conceptual difficulty in the analysis of Leggett–Garg inequalities concerns the operational meaning of measurements. The derivation of these inequalities relies not only on the assumption of macroscopic realism, but also on the possibility of performing non-invasive measurements, namely measurements that reveal the value of a dynamical variable without perturbing its subsequent evolution. As discussed in the previous sections, this requirement is essential for the existence of an underlying classical joint probability distribution, yet it cannot be verified solely at the level of temporal correlators. Within quantum mechanics, moreover, the notion of non-invasive measurability is intrinsically problematic, since standard measurement schemes are generically accompanied by state disturbance.

Quantum non-demolition measurements (QNDMs) provide a framework in which these issues can be addressed in a controlled and operationally precise manner. Rather than postulating NSIT as an abstract assumption, QNDMs enforce it at the level of the measurement dynamics itself. Information about a system observable is extracted indirectly by coupling it to an auxiliary quantum system, referred to as a detector or ancilla, through an interaction designed to preserve the statistics of the measured observable. In this way, the measurement back-action is confined to degrees of freedom that commute with the monitored observable, while the intrinsic system dynamics remains unaffected.

In protocols relevant for the study of temporal correlations, the essential physical mechanism underlying QNDMs is the coherent accumulation of a quantum phase in the detector. This phase encodes information about the value of the system observable at one or multiple times, without requiring direct projective measurements on the system. As will be shown in this section, this detector-based encoding provides access to the temporal statistics of the system in a form that goes beyond individual correlators, allowing one to probe the structure of the underlying temporal probability distribution while maintaining a well-defined notion of non-demolition measurement.

5.4.2 Hamiltonian conditions for non-demolition measurements

We consider a quantum system S described by a Hilbert space $\mathcal{H}_S$ and a Hamiltonian $\hat{H}_S$. Let $\hat{Q}$ be a Hermitian operator on $\mathcal{H}_S$ representing the observable to be measured. A necessary condition for a measurement of $\hat{Q}$ to be of the non-demolition type is that the measurement interaction does not induce transitions between different eigenstates of $\hat{Q}$.

This requirement can be expressed at the Hamiltonian level. Introducing an auxiliary detector system D with Hilbert space $\mathcal{H}_D$ and Hamiltonian $\hat{H}_D$, the total Hamiltonian reads

$$\hat{H}(t) = \hat{H}_S + \hat{H}_D + \hat{H}_{\text{int}}(t). \tag{5.2}$$

The measurement interaction is of the quantum non-demolition type if

$$[\hat{Q}, \hat{H}_{\text{int}}(t_i)] = 0, \tag{5.3}$$

where t_i are the times associated with the measurements. It guarantees that the measurement interaction itself does not alter the value of $\hat{Q}$.

5.4.3 Detector-based measurement and phase imprinting

A standard choice for the interaction Hamiltonian in a QND measurement is

$$\hat{H}_{\text{int}}(t) = g(t)\,\hat{Q} \otimes \hat{P}_D, \tag{5.4}$$

where $g(t)$ is a controllable coupling function and $\hat{P}_D$ is a detector operator canonically conjugate to a detector phase variable. We emphasize that this is a strong assumption: the fact that $\hat{Q}$ and $\hat{P}_D$ are time-independent implies that $[\hat{H}_{int}(t), \hat{Q}] = 0\ \forall t$. The crucial feature of this interaction is that $\hat{Q}$ acts as a control parameter for the detector dynamics.

Assuming that the interaction is switched on for a short time interval Δt, such that the free-evolution terms H_S and H_D are negligible during Δt, the corresponding unitary evolution operator is ($\hbar = 1$)

$$\hat{u} = \exp\left(-i \int_{t_0}^{t_0+\Delta t} dt\, g(t)\,\hat{Q} \otimes \hat{P}_D\right). \tag{5.5}$$

Defining the effective coupling strength

$$\Lambda = \int_{t_0}^{t_0+\Delta t} dt\, g(t), \tag{5.6}$$

one obtains

$$\hat{u} = \exp\left(-i\Lambda\,\hat{Q} \otimes \hat{P}_D\right). \tag{5.7}$$

If the detector is prepared in a superposition of eigenstates of the operator conjugate to $\hat{P}_D$, the effect of the interaction is to generate a phase shift proportional to the eigenvalue of $\hat{Q}$. The information about the system observable is thus transferred to the detector as a relative phase, while the system remains in an eigenstate of $\hat{Q}$.

5.4.4 Two-level detector and conditional phase shifts

In many quantum simulation and quantum information settings, the detector is chosen to be a two-level system, or qubit. In this case, the interaction Hamiltonian can be written as

$$\hat{H}_{\text{int}} = \frac{\lambda}{2}\,\hat{Q} \otimes \hat{\sigma}_z^{(D)}, \tag{5.8}$$

where $\hat{\sigma}_z^{(D)}$ is a Pauli operator acting on the detector.

The corresponding unitary evolution is

$$\hat{u} = \exp\left(-i\frac{\lambda}{2}\,\hat{Q}\otimes\hat{\sigma}_z^{(D)}\right). \tag{5.9}$$

Preparing the detector in the state

$$|+\rangle_D = \frac{1}{\sqrt{2}}\left(|0\rangle_D + |1\rangle_D\right), \tag{5.10}$$

one finds that, for an eigenstate $|q\rangle$ of $\hat{Q}$,

$$|q\rangle_S \otimes |+\rangle_D \;\longrightarrow\; |q\rangle_S \otimes \frac{1}{\sqrt{2}}\left(e^{-i\lambda q/2}|0\rangle_D + e^{+i\lambda q/2}|1\rangle_D\right). \tag{5.11}$$

The system state is unchanged, while the detector acquires a relative phase that depends on the value of the system observable.

5.4.5 Phase accumulation at multiple times

The key advantage of QND measurements in the context of Leggett–Garg inequalities is their natural extension to sequences of measurements at different times. Let the system evolve freely under $\hat{H}_S$, and let QND interactions occur at times $t_1, t_2, \ldots, t_n$. The total evolution operator takes the form

$$\hat{U}_{tot} = \hat{U}_{\rm int}(t_n)\,\hat{U}_S(t_n, t_{n-1})\cdots\hat{U}_{\rm int}(t_1)\,\hat{U}_S(t_1, 0) \tag{5.12}$$

$$\hat{U}_S(t_i, t_{i-1}) = \exp(-iH_S(t_i - t_{i-1})) \tag{5.13}$$

Each interaction imprints a phase proportional to the instantaneous eigenvalue of the Heisenberg-picture operator $\hat{Q}(t_i)$, weighted by the probability of the path.

Let's consider a simple example in $n = 2$.

The total unitary evolution (5.12) is

$$\hat{U}_{\rm tot} = \hat{U}_{\rm int}(t_2)\,\hat{U}_S(t_2, t_1)\,\hat{U}_{\rm int}(t_1)\,\hat{U}_S(t_1, 0). \tag{5.14}$$

We assume an interaction of the form

$$\hat{U}_{\rm int}(t_i) = \exp\Big[-i\lambda\, t_i\,\hat{Q}(t_i)\otimes\hat{P}\Big]. \tag{5.15}$$

Let $\hat{Q}(t_i)$ have spectral decomposition

$$\hat{Q}(t_i) = \sum_{q_i} q_i\,\hat{\Pi}_{q_i}(t_i). \tag{5.16}$$

Using the functional calculus, the interaction operator can be written as

$$\hat{U}_{\rm int}(t_i) = \sum_{q_i}\hat{\Pi}_{q_i}(t_i)\otimes\exp\Big[-i\lambda\, t_i q_i\hat{P}\Big]. \tag{5.17}$$

Inserting these decompositions into $\hat{U}_{\text{tot}}$ yields a path decomposition over the eigenvalue histories (q_1, q_2),

$$\hat{U}_{\text{tot}} = \sum_{q_1,q_2} \Big[\hat{\Pi}_{q_2}(t_2)\,\hat{U}_S(t_2,t_1)\,\hat{\Pi}_{q_1}(t_1)\,\hat{U}_S(t_1,0)\Big] \otimes \exp\Big[-i\lambda(t_1 q_1 + t_2 q_2)\hat{P}\Big]. \quad (5.18)$$

Each history (q_1, q_2) therefore imprints on the detector a phase shift determined by

$$\Phi(q_1, q_2) = \lambda_1 q_1 + \lambda_2 q_2, \quad (5.19)$$

where $\lambda_i = \lambda\, t_i$

Generalizing this example, we say that the detector accumulates a total phase

$$\Phi = \sum_{i=1}^{n} \lambda_i\, Q(t_i). \quad (5.20)$$

The detector thus acts as a coherent quantum memory of the temporal history of the system observable.

5.4.6 Extraction of temporal correlation functions

After the sequence of interactions, the detector is measured in an appropriate basis. Expectation values of detector observables yield quantities of the form

$$\left\langle \exp\left(i \sum_i \lambda_i \hat{Q}(t_i) \right) \right\rangle. \quad (5.21)$$

By choosing the coupling strengths λ_i and expanding perturbatively, one can reconstruct temporal correlation functions such as

$$\langle \hat{Q}(t_i)\, \hat{Q}(t_j) \rangle, \quad (5.22)$$

which are the fundamental building blocks of the Leggett–Garg inequalities.

This approach allows one to access temporal correlations without performing direct projective measurements on the system at intermediate times.

5.4.7 Non-invasiveness and relevance for Leggett–Garg tests

From an operational perspective, QND measurements realize a notion of NSIT: the statistic of $\hat{Q}$ and the marginals are not altered by the measurement interaction, and no projection is performed on the system during the evolution. Nevertheless, the system becomes entangled with the detector, and information is stored in the detector phase. However, it does not realise a NSIT in the strict sense, as the marginals are compute from the quasi-probability rather then from the probability distribution.

This distinction is essential for the interpretation of Leggett–Garg violations. If a violation persists in a protocol based on QND measurements, it cannot be attributed to a trivial measurement disturbance, but reflects the incompatibility between macroscopic realism and the quantum structure of temporal correlations.

5.5 Quantum non-demolition protocol for witnessing violations of macrorealism

In this section, we summarize the key achievement of Solinas and Gherardini's paper [77]: there exists a sequential measurement scheme that (i) satisfies NSIT condition and (ii) yields a necessary and sufficient condition for MRps violation. The proposed protocol is based on the analysis of a quasi-probability distribution, namely the Wigner function, which is shown to take negative values if and only if the postulates defining Macrorealism are not simultaneously fulfilled, namely MRps, NIM, and the induction principle introduced in Section 5.2.

5.5.1 System, observable, and probing times

We consider a system with Hilbert space $\mathcal{H}_S$, evolving under a time-independent Hamiltonian $\hat{H}$. The monitored observable $\hat{A}$ has eigenstates $\{|i\rangle\}$ and eigenvalues $\{a_i\}$. The system is prepared at $t_0 = 0$ in $\hat{\rho}_0$ (pure or mixed). We probe the dynamics at three times,

$$t_0 = 0, \qquad t_1, \qquad t_2 = T. \tag{5.23}$$

The corresponding free evolution operators are

$$\hat{U}_1 = e^{-i\hat{H}t_1}, \qquad \hat{U}_2 = e^{-i\hat{H}(T-t_1)}. \tag{5.24}$$

No commutation between $\hat{A}$ and $\hat{H}$ is assumed.

5.5.2 QND detector and impulsive couplings

The protocol employs an auxiliary detector with a continuous degree of freedom, described by canonical operators $\hat{q}$ and $\hat{p}$ (units $\hbar = 1$),

$$[\hat{q}, \hat{p}] = i. \tag{5.25}$$

At each probing time t_0, t_1, t_2, the system and detector interact impulsively through the QND unitary

$$\hat{u} = \exp\left(i\frac{\lambda}{2}\,\hat{A} \otimes \hat{p}\right), \tag{5.26}$$

with dimensionless coupling strength λ. Since $[\hat{A}, \hat{u}] = 0$, the interaction does not induce transitions between eigenstates of $\hat{A}$; it only imprints a phase on the detector conditioned on the instantaneous eigenvalue of $\hat{A}$. The non-demolition character refers to the measurement interaction, not to the free dynamics generated by $\hat{H}$.

5.5.3 Total evolution and path expansion

The global unitary acting on system+detector reads

$$\hat{U}_{\text{tot}} = \hat{u}\,\hat{U}_2\,\hat{u}\,\hat{U}_1\,\hat{u}. \tag{5.27}$$

For a factorized system consisting of a detector initial state $\hat{r}_0$ and system initial state $\hat{\rho}_0$, ($\rho_{tot} = \hat{r}_0 \otimes \hat{\rho}_0$), the final joint density operator is

$$\hat{R} = \hat{U}_{\text{tot}} \, (\hat{\rho}_0 \otimes \hat{r}_0) \, \hat{U}_{\text{tot}}^{\dagger}. \tag{5.28}$$

Inserting resolutions of the identity in the $\hat{A}$ eigenbasis at each interaction time yields a sum over sequences of outcomes ($i \to j \to k$), naturally interpreted as quantum trajectories in outcome space.

5.5.4 Detector readout: ND quasi-characteristic function

The experimentally accessible quantity is extracted from an off-diagonal detector matrix element in the $\hat{p}$-basis, between $|p\rangle$ and $|-p\rangle$. Following Ref. [77], define the ND quasi-characteristic function

$$G_\lambda = \frac{\text{Tr}\Big[(\mathbb{I} \otimes \langle p|) \, \hat{R} \, (\mathbb{I} \otimes |-p\rangle)\Big]}{\langle p| \, \hat{r}_0 \, |-p\rangle}. \tag{5.29}$$

Choosing units such that G_λ is properly normalized, one obtains the explicit form

$$G_\lambda = \sum_{i,l} \sum_{j,m} \sum_{k} e^{i\lambda \, \Delta_{k,j,m,i,l}} \, U_{2,kj} \, U_{1,ji} \, \rho_{0,il} \, U_{1,lm}^{*} \, U_{2,mk}^{*}, \tag{5.30}$$

where $U_{1,ji} = \langle j| \, \hat{U}_1 \, |i\rangle$, $U_{2,kj} = \langle k| \, \hat{U}_2 \, |j\rangle$, and $\rho_{0,il} = \langle i| \, \hat{\rho}_0 \, |l\rangle$. The phase variable is

$$\Delta_{k,j,m,i,l} = a_k + \frac{a_j + a_m + a_i + a_l}{2}. \tag{5.31}$$

5.5.5 ND quasi-probability distribution

The ND quasi-probability distribution is defined as the inverse Fourier transform of G_λ,

$$\mathcal{P}_{\text{ND}}(\Delta) = \frac{1}{2\pi} \int d\lambda \; e^{-i\lambda\Delta} \, G_\lambda. \tag{5.32}$$

Introducing the projectors $\hat{\Pi}_i = |i\rangle\langle i|$ and using $\sum_k \hat{\Pi}_k = \mathbb{I}$, $\hat{\Pi}_j \hat{\Pi}_m = \delta_{jm} \hat{\Pi}_j$, one can rewrite $\mathcal{P}_{\text{ND}}(\Delta)$ as a discrete sum over path-interference amplitudes,

$$\mathcal{P}_{\text{ND}}(\Delta) = \sum_{i,l} \sum_{j,m} \sum_{k} P_{\text{ND}}(k,j,m,i,l) \, \delta[\Delta - \Delta_{k,j,m,i,l}] \, , \tag{5.33}$$

with

$$\begin{aligned} P_{\text{ND}}(k,j,m,i,l) &= \text{Tr}\Big[\hat{\Pi}_k \, \hat{U}_2 \, \hat{\Pi}_j \, \hat{U}_1 \, \hat{\Pi}_i \, \hat{\rho}_0 \, \hat{\Pi}_l \, \hat{U}_1^{\dagger} \, \hat{\Pi}_m \, \hat{U}_2^{\dagger}\Big] \\ &= U_{2,kj} \, U_{1,ji} \, \rho_{0,il} \, U_{1,lm}^{*} \, U_{2,mk}^{*}. \end{aligned} \tag{5.34}$$

By construction, $\mathcal{P}_{\text{ND}}(\Delta)$ is real and normalized (see Appendix 5.A).

5.5.6 Classical versus quantum contributions

Equation (5.33) admits a natural decomposition into a classical and a quantum part,

$$\mathcal{P}_{\mathrm{ND}}(\Delta) = \mathcal{P}_{\mathrm{cl}}(\Delta) + \mathcal{P}_{\mathrm{q}}(\Delta). \tag{5.35}$$

Classical contribution. The classical part corresponds to paths without interference, i.e. the terms with $m = j$ and $l = i$,

$$\mathcal{P}_{\mathrm{cl}}(\Delta) = \sum_{i,j,k} P_{\mathrm{ND}}(k, j, j, i, i)\, \delta[\Delta - \Delta_{k,j,j,i,i}]\,, \tag{5.36}$$

where

$$P_{\mathrm{ND}}(k, j, j, i, i) = \rho_{0,ii}\, |U_{1,ji}|^2\, |U_{2,kj}|^2 \geq 0, \qquad \Delta_{k,j,j,i,i} = a_k + a_j + a_i. \tag{5.37}$$

Thus, $\mathcal{P}_{\mathrm{cl}}$ admits a bona fide classical probabilistic interpretation as a product of preparation and transition probabilities.

For the dichotomic case $a_i = \pm 1$, the classical (non-interfering) values of Δ obtained from Eq. (5.37) are

$$\Delta_{\mathrm{cl}} = a_k + a_j + a_i \in \{-3, -1, 1, 3\}. \tag{5.38}$$

Quantum (interference) contribution. The quantum part collects all remaining terms,

$$\mathcal{P}_{\mathrm{q}}(\Delta) = \sum_{i,l} \sum_{j,m} {\sum_{k}}' P_{\mathrm{ND}}(k, j, m, i, l)\, \delta[\Delta - \Delta_{k,j,m,i,l}]\,, \tag{5.39}$$

where the prime denotes that the terms for which both $m = j$ and $l = i$ hold are excluded from the sum. These contributions encode interference between distinct temporal trajectories $(i \to j \to k)$ and $(l \to m \to k)$, and they have no counterpart within classical probability theory.

Applying this result to the dichotomic case, the interference term $\mathcal{P}_{\mathrm{q}}(\Delta)$ can contribute at classically forbidden values such as $\Delta = \pm 2$ or $\Delta = 0$. For example, using Eq. (5.31) one may obtain $\Delta = 2$ with $(a_k, a_j, a_m, a_i, a_l) = (1, 1, 1, 1, -1)$, and $\Delta = 0$ with $(a_k, a_j, a_m, a_i, a_l) = (1, 1, -1, -1, -1)$ [77]. The appearance of weight at these values is a direct operational signature of path interference in the ND reconstruction.

5.5.7 NSIT as operational non-invasiveness

The central requirement of any proposal is to verify whether the protocol satisfies the NSIT condition. In the proposed protocol, this requirement is fulfilled for a NSIT in the sense given in Subsection 5.4.7. Operationally, NSIT imposes single-time probabilities to coincide with the marginals of the corresponding multi-time statistics, i.e., with the Born-rule probabilities generated by the undisturbed unitary evolution [45, 27]. Quantum non-demolition measurements are specifically designed to realize this notion of non-disturbance, ensuring that repeated or sequential measurements reproduce the statistics of the freely evolved observable [19].

For instance, the probability of observing a_k at t_2 is obtained by summing $P_{\mathrm{ND}}(k,j,m,i,l)$ over the intermediate indices (i,l,j,m),

$$P(a_k) = \sum_{i,l} \sum_{j,m} P_{\mathrm{ND}}(k,j,m,i,l) = \mathrm{Tr}\left[\hat{\Pi}_k \left(\hat{U}_2\hat{U}_1\right) \hat{\rho}_0 \left(\hat{U}_2\hat{U}_1\right)^\dagger\right], \tag{5.40}$$

where the completeness relation for the projectors has been used. Similar expressions apply to the single-time probabilities at t_0 and t_1. Hence, any non-classical features of $\mathcal{P}_{\mathrm{ND}}(\Delta)$ cannot be attributed to classical measurement disturbance.

5.5.8 Negativity as a necessary and sufficient witness of MRps violation

The central theorem of Ref. [77] can be stated as follows.

Theorem. *The ND quasi-probability distribution $\mathcal{P}_{\mathrm{ND}}(\Delta)$ attains negative values if and only if MRps is violated.*

A detailed proof is provided in Appendix 5.A. Here we emphasize the physical mechanism: negativity originates from interference among distinct temporal trajectories, which is possible only in the presence of coherences in the $\hat{A}$ eigenbasis. Because the protocol is NSIT, the negativity cannot be reinterpreted as measurement-induced invasiveness.

5.5.9 Relation to Leggett–Garg inequalities

Leggett–Garg inequalities (LGIs) detect macrorealism violations via constraints on two-time correlators. The ND framework is more informative: it reconstructs a full three-time quasi-probability distribution compatible with NSIT, and its negativity is equivalent to MRps violation. Consequently, there exist regimes in which $\mathcal{P}_{\mathrm{ND}}(\Delta)$ is negative while all standard LGIs remain satisfied, showing that LGIs provide only sufficient (not necessary) conditions for macrorealism violation, whereas ND negativity constitutes a necessary-and-sufficient criterion [77].

5.A Negativity of $\mathcal{P}_{\mathrm{ND}}(\Delta)$ and macrorealism per se

This appendix provides a detailed proof that negativity of the ND quasi-probability distribution $\mathcal{P}_{\mathrm{ND}}(\Delta)$ is necessary and sufficient for the violation of MRps, closely following Ref. [77].

5.A.1 Reality and normalization

Reality. From Eq. (5.34) one has the conjugation symmetry

$$P_{\mathrm{ND}}(k,j,m,i,l)^* = P_{\mathrm{ND}}(k,m,j,l,i). \tag{5.41}$$

Moreover, $\Delta_{k,j,m,i,l} = \Delta_{k,m,j,l,i}$ follows immediately from Eq. (5.31). Therefore, terms appear in Eq. (5.33) in complex-conjugate pairs multiplying the same δ-peak, implying $\mathcal{P}_{\mathrm{ND}}(\Delta) \in \mathbb{R}$.

Normalization. Integrating Eq. (5.33) yields

$$\begin{aligned}\int d\Delta\, \mathcal{P}_{\mathrm{ND}}(\Delta) &= \sum_{i,l}\sum_{j,m}\sum_{k} P_{\mathrm{ND}}(k,j,m,i,l) \\ &= \mathrm{Tr}\left[\left(\sum_k \hat{\Pi}_k\right)\hat{U}_2\left(\sum_j \hat{\Pi}_j\right)\hat{U}_1\left(\sum_i \hat{\Pi}_i\right)\hat{\rho}_0\left(\sum_l \hat{\Pi}_l\right)\hat{U}_1^\dagger\left(\sum_m \hat{\Pi}_m\right)\hat{U}_2^\dagger\right] \\ &= \mathrm{Tr}\left[\hat{U}_2\hat{U}_1\,\hat{\rho}_0\,(\hat{U}_2\hat{U}_1)^\dagger\right] = \mathrm{Tr}[\hat{\rho}_0] = 1. \end{aligned} \tag{5.42}$$

5.A.2 Classical and quantum parts: integral constraint on P_{q}

By definition, the classical part $\mathcal{P}_{\mathrm{cl}}$ collects the $(m = j, l = i)$ terms, Eqs. (5.36)–(5.37), hence it is non-negative and normalized:

$$\int d\Delta\, \mathcal{P}_{\mathrm{cl}}(\Delta) = \sum_{i,j,k} \rho_{0,ii}|U_{1,ji}|^2|U_{2,kj}|^2 = \sum_i \rho_{0,ii} = 1. \tag{5.43}$$

Since $\int \mathcal{P}_{\mathrm{ND}} = 1$ by Eq. (5.42), it follows that

$$\int d\Delta\, \mathcal{P}_{\mathrm{q}}(\Delta) = 0. \tag{5.44}$$

Because $\mathcal{P}_{\mathrm{q}}(\Delta)$ is real (Appendix 5.A.1), any non-vanishing $\mathcal{P}_{\mathrm{q}}$ must take both positive and negative values.

5.A.3 Equivalence between ND negativity and MRps violation

(Negativity $\Rightarrow$ MRps violation). Assume that $\mathcal{P}_{\mathrm{ND}}(\Delta)$ attains negative values. Since $\mathcal{P}_{\mathrm{cl}}(\Delta) \geq 0$, this requires $\mathcal{P}_{\mathrm{q}}(\Delta) \neq 0$, hence the sum in Eq. (5.39) contains at least one non-zero term with $l \neq i$ and/or $m \neq j$. From Eq. (5.34), such terms are proportional to the off-diagonal matrix elements $\rho_{0,il}$ (and, more generally, to coherences of the state at the probing times when expressed in the $\hat{A}$ basis). This is incompatible with the MRps requirement (5.37). Therefore, negativity implies violation of MRps.

(MRps violation ⇒ negativity). Assume that MRps is violated. Then, at least at one probing time, the system state has coherences in the eigenbasis of $\hat{A}$. In particular, in the Schrödinger picture this implies that $\hat{\rho}_0$ contains off-diagonal elements $\rho_{0,il} \neq 0$ for some $i \neq l$ in the $\hat{A}$ basis (or, equivalently, that coherences appear in the corresponding interaction-picture states at the coupling times). Through Eq. (5.34) this generates a non-zero quantum contribution $\mathcal{P}_{\mathrm{q}}(\Delta) \neq 0$. Since $\mathcal{P}_{\mathrm{q}}(\Delta)$ is real and integrates to zero by Eq. (5.44), it must necessarily attain negative values. Hence $\mathcal{P}_{\mathrm{ND}}(\Delta)$ becomes negative.

Combining the two implications proves that $\mathcal{P}_{\mathrm{ND}}(\Delta)$ is negative if and only if MRps is violated.

5.A.4 NSIT and operational non-invasiveness

Finally, NSIT follows from the projector identities used in the derivation of Eq. (5.40). Marginalizing over all but one time index collapses the corresponding projectors to the identity and yields the Born-rule single-time probabilities, confirming that the ND protocol is non-invasive in the operational NSIT sense.

Chapter 6

Quantum simulation of macrorealism violation via the QNDM protocol

6.1 Introduction and relation to the previous chapter

Chapter 5 developed the conceptual and theoretical background required for temporal tests of macrorealism, with particular emphasis on (i) the logical status and limitations of Leggett–Garg inequalities (LGIs), (ii) operational notions of non-invasiveness via no-signaling-in-time (NSIT), and (iii) the Solinas–Gherardini non-demolition (ND/QNDM) framework in which macrorealism violation is characterized through the negativity of a temporal quasi-probability distribution (see in particular Secs. 4.3–4.5 and Appendix 4.A of this thesis).

The present chapter builds directly on that foundation and shifts the focus from conceptual structure to explicit implementation. The core objective is to assess, in a realistic finite-sampling scenario, how efficiently macrorealism violation can be detected by (a) inequality-based tests (LGIs) and (b) the QNDM protocol based on phase imprinting and quasi-probability reconstruction. In particular, we quantify how statistical uncertainty (finite number of circuit executions) and hardware-level noise affect the practical detectability of macrorealism violation, and we compare the resource requirements of the two approaches in a concrete, experimentally motivated setting.

The analysis is performed through detailed quantum simulations implemented in IBM's `Qiskit` framework [44]. We consider both noiseless simulations (where only finite-shot statistical noise is present) and realistic noisy simulations obtained by adopting IBM noise models, thus emulating near-term hardware behaviour. Beyond providing a necessary-and-sufficient witness of macrorealism violation (as established in Chapter 4 and Ref. [78]), the QNDM protocol turns out to be remarkably robust to statistical and environmental noise. As will be discussed, this robustness is intimately connected to the Fourier reconstruction step used to obtain the quasi-probability distribution from the measured quasi-characteristic function.

The chapter is structured as follows. Section 6.2 introduces the concrete measurement scenario analysed here and summarizes how LGIs and QNDM provide

diagnostics of macrorealism violation in that setting. In Sec. 6.3, we present noiseless numerical simulations for both protocols and compare their performance and resource consumption. In Sec. 6.4, we extend the analysis to a realistic noise model. Finally, Sec. 6.5 summarizes the main conclusions.

6.2 Violation of macrorealism: Leggett–Garg inequalities and non-demolition protocols

We begin by introducing the notation relevant to the case under investigation. We consider a two-level quantum system S evolving unitarily in a time interval $0 \leq t \leq T$. At three times $t_0 \leq t_1 \leq t_2 = T$, we probe a dichotomic observable $\hat{Q}$ with eigenvalues $q_i = \pm 1$ and corresponding eigenstates $|i\rangle$, i.e.

$$\hat{Q}\,|i\rangle = q_i\,|i\rangle\,. \tag{6.1}$$

Between successive probing times the system evolves under unitary operators $\hat{U}_1$ and $\hat{U}_2$. In general $[\hat{Q}, \hat{U}_i] \neq 0$, so that the interplay between evolution and measurement is nontrivial. The same formal scheme also covers sequences of non-commuting observables $\hat{Q}_a$, $\hat{Q}_b$, $\hat{Q}_c$ in the absence of intermediate dynamics.

Within this set-up, we aim to diagnose quantum behaviour through experimentally implementable protocols, and to compare their statistical and resource performance under finite sampling.

6.2.1 Leggett–Garg inequalities

In this subsection, we briefly recall some definitions introduced in the previous chapter, both for clarity and in order to examine a specific application of the general framework developed above. As a first approach, we consider LGIs constructed from two-time correlation functions C_{ij} between the outcomes of projective measurements performed at times t_i and t_j. In the Heisenberg picture we define

$$\hat{Q}(t_i) = \hat{U}_i^\dagger\,\hat{Q}\,\hat{U}_i, \tag{6.2}$$

so that the symmetrized correlator can be written as

$$C_{ij} = \frac{1}{2}\mathrm{Tr}\Big[(\hat{Q}(t_i)\hat{Q}(t_j) + \hat{Q}(t_j)\hat{Q}(t_i))\hat{\rho}\Big] = \sum_{i,j} q_i q_j\, p(q_i, q_j), \tag{6.3}$$

where $p(q_i, q_j)$ denotes the joint probability of observing outcome q_i at time t_i and q_j at time t_j.

With the three correlators, we form one of the standard Leggett–Garg parameters, which were defined in Chap. 5 Eq. (5.1):

$$K_3 = C_{12} + C_{23} - C_{13}. \tag{6.4}$$

For a macrorealistic theory one has the bound $-3 \leq K_3 \leq 1$ [32]; a violation therefore signals incompatibility with the conjunction of macrorealism and non-invasive measurability.

Two further equivalent combinations, likewise bounded in $[-3, 1]$, are

$$\begin{aligned} K_1 &= \quad C_{23} - C_{12} + C_{13}, \\ K_2 &= -C_{23} - C_{12} - C_{13}. \end{aligned} \tag{6.5}$$

6.2.2 QNDM protocol

We then proceed to implement the QNDM protocol described in the previous chapter. Let $\hat{p}$ be an operator acting on the detector Hilbert space, with eigenvalues p and eigenstates $|p\rangle$, $\hat{p}\,|p\rangle = p\,|p\rangle$. In the QNDM framework, probing at three times can be implemented as a sequence of impulsive system–detector interactions

$$\hat{u}(\lambda) = \exp\left\{ i\frac{\lambda}{2}\,\hat{Q}\otimes\hat{p} \right\}, \tag{6.6}$$

interspersed with unitary evolutions $\hat{U}_1$ and $\hat{U}_2$. The overall unitary acting on the joint system+detector reads

$$\hat{U}_{\rm tot} = \hat{u}\,\hat{U}_2\,\hat{u}\,\hat{U}_1\,\hat{u} = e^{i\frac{\lambda}{2}\hat{Q}\otimes\hat{p}}\,\hat{U}_2\,e^{i\frac{\lambda}{2}\hat{Q}\otimes\hat{p}}\,\hat{U}_1\,e^{i\frac{\lambda}{2}\hat{Q}\otimes\hat{p}}. \tag{6.7}$$

Let $|\psi_0\rangle_S = \sum_i \psi_i^0\,|i\rangle$ be the initial system state and $|\psi_0\rangle_D$ the initial detector state. For the general theoretical expression below, we assume $|\psi_0\rangle_D$ to be an equal superposition of N eigenstates of $\hat{p}$, and we take the initial joint state to be the product state $|\Psi_0\rangle = |\psi_0\rangle_S \otimes |\psi_0\rangle_D$. Under the evolution in Eq. (6.7), the final joint state reads [78]

$$|\Psi\rangle = \frac{1}{\sqrt{N}} \sum_p \sum_{ijk} e^{i\frac{\lambda p}{2}(q_i+q_j+q_k)}\,U_{kj}U_{ji}\psi_i^0\;|i\rangle\,|p\rangle\,. \tag{6.8}$$

The detector phase information is encoded in the quantity G_λ defined as

$$G_\lambda = \frac{\mathrm{Tr}\Big[(\mathbb{I}\otimes\langle p|)\hat{R}(\mathbb{I}\otimes|-p\rangle)\Big]}{\langle p|\hat{r}_0|-p\rangle}, \tag{6.9}$$

where $\hat{R} = |\Psi\rangle\langle\Psi|$ is the final density operator of the joint system and $\hat{r}_0 = |\psi_0\rangle\,\langle\psi_0|_D$ is the detector initial density operator. The function G_λ plays the role of a quasi-characteristic function for the temporal measurement statistics of $\hat{Q}$ [73, 74, 75, 78]. The inverse Fourier transform of G_λ yields the QNDM quasi-probability distribution

$$\begin{aligned} \mathcal{P}_{\rm ND}(\Delta) &= \frac{1}{2\pi}\int d\lambda\, e^{-i\lambda\Delta}\,G_\lambda \\ &= \sum_{ijklm} P_{\rm ND}(i,j,k,l,m)\,\delta(\Delta-\Delta_{ijklm}), \end{aligned} \tag{6.10}$$

with

$$P_{\rm ND}(i,j,k,l,m) = U_{2,ij}\,U_{1,jl}\,\rho^0_{lm}\,U^*_{1,mk}\,U^*_{2,ki}, \tag{6.11}$$

$\rho^0_{ij} = \psi^0_i(\psi^0_j)^*$, and $\Delta_{ijklm} = q_i + (q_j + q_k + q_l + q_m)/2$.

The distribution $\mathcal{P}_{\mathrm{ND}}(\Delta)$ is a quasi-probability density: it is real and normalized, but it may take negative values. As for the Wigner function, negativity is a direct signature of quantum interference. In the Solinas–Gherardini framework, negativity of $\mathcal{P}_{\mathrm{ND}}$ is directly linked to the presence of coherent superpositions during the dynamics [73, 74, 78] and, crucially, provides a necessary and sufficient condition for the violation of MRps [78]. Moreover, by construction $\mathcal{P}_{\mathrm{ND}}$ satisfies NSIT; therefore any violation of MRps detected through negativity entails the violation of macrorealism in the broader sense.

6.3 Numerical study

To compare the practical efficiency of LGIs and QNDM in detecting macrorealism violation, we consider a simple benchmark model already discussed in Refs. [40, 78, 68].

Let $\hat{\sigma}_i$ $(i = x, y, z)$ denote Pauli operators. We take the monitored observable on the system qubit to be

$$\hat{Q} = \hat{\sigma}_z^S, \tag{6.12}$$

while the dynamics is generated by the Hamiltonian

$$\hat{H} = \frac{\omega}{2}\,\hat{\sigma}_x^S \qquad (\hbar = 1). \tag{6.13}$$

Measurements (or QNDM couplings) occur at $t_0 = 0$, $t_1 = \tau$, and $t_2 = 2\tau$. The initial system state is chosen as

$$|\psi_0\rangle_S = \frac{|0\rangle_S + i\,|1\rangle_S}{\sqrt{2}}, \tag{6.14}$$

where $|0\rangle_S$ and $|1\rangle_S$ are eigenstates of $\hat{\sigma}_z$.

6.3.1 Leggett–Garg numerical implementation

For this model, the correlations C_{ij} take the analytic form [41, 78, 68]

$$C_{ij} = \cos\big(\omega(t_i - t_j)\big). \tag{6.15}$$

Consequently, the LG parameter K_3 becomes

$$K_3 = C_{12} + C_{23} - C_{13} = 2\cos(\omega\tau) - \cos(2\omega\tau). \tag{6.16}$$

We study K_3 as a function of $\omega\tau$. Values outside $-3 \le K_3 \le 1$ imply LGI violation.

To investigate this numerically we perform quantum simulations using IBM's `Qiskit` framework [44]. Implementation details are provided in Appendix 6.A. The simulation results are shown in Fig. 6.1.

To obtain the simulated curves, for each value of $\omega\tau$ we perform $N = 10^2$ independent runs and compute the average of the resulting K_3 values (solid blue line). The dashed red curve shows the theoretical prediction of Eq. (6.16). In the absence of environmental noise, the two curves overlap within statistical fluctuations.

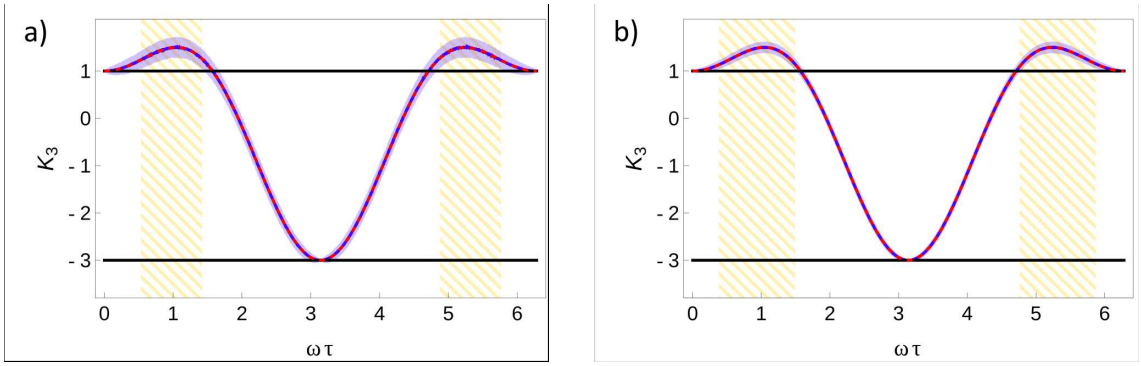

(a) $\delta\lambda = 0.1$, $N_{\text{shots}}^{\text{LG}} = 10^3$ (b) $\delta\lambda = 1$, $N_{\text{shots}}^{\text{LG}} = 10^4$

Figure 6.1: Simulation results for the LG parameter K_3 in a noiseless scenario, using $N_{\text{shots}}^{\text{LG}} = 10^3$ (a) and $N_{\text{shots}}^{\text{LG}} = 10^4$ (b). The solid blue line represents the average simulated curve obtained over $N = 10^2$ repetitions, while the dashed red line corresponds to the theortical prediction from Eq. (6.16). The blue-shaded region indicates statistical uncertainty, while the yellow-shaded region highlights the range of $\omega\tau$ where, considering statistical errors, a violation of the LGIs is confidently detected.

A key practical question is whether LGI violation can be confidently detected within a single run consisting of $N_{\text{shots}}^{\text{LG}}$ circuit executions. The impact of finite-shot noise is visualized by the blue-shaded regions in Fig. 6.1. Figure 6.1a corresponds to $N_{\text{shots}}^{\text{LG}} = 10^3$, while Fig. 6.1b uses $N_{\text{shots}}^{\text{LG}} = 10^4$. The yellow-shaded region highlights those $\omega\tau$ values for which the LGI violation remains distinguishable even in the presence of statistical errors. As expected, increasing $N_{\text{shots}}^{\text{LG}}$ reduces statistical fluctuations and enlarges the confidently detectable violation region.

In the ideal limit of vanishing statistical noise, violations occur for $0 \leq \omega\tau \leq \pi/2$ and $3\pi/2 \leq \omega\tau \leq 2\pi$, covering 50% of the range. For finite sampling, the detectable interval shrinks: for $N_{\text{shots}}^{\text{LG}} = 10^3$, the violation region covers approximately 32% of the range, while for $N_{\text{shots}}^{\text{LG}} = 10^4$ it extends to 38%.

6.3.2 QNDM numerical implementation

For the numerical implementation of the QNDM protocol we use a two-level quantum detector. We take

$$\hat{p} = \hat{\sigma}_z^D, \qquad |\psi_0^D\rangle = \frac{|0^D\rangle + |1^D\rangle}{\sqrt{2}}, \tag{6.17}$$

and we choose the interaction operator

$$\hat{u}(\lambda) = \exp\left\{ i\frac{\lambda}{2}\, \hat{\sigma}_z^S \otimes \hat{\sigma}_z^D \right\}. \tag{6.18}$$

Its `Qiskit` implementation is provided in Appendix 6.A.

A central advantage of the QNDM protocol is that the mere presence of negative regions in $\mathcal{P}_{\text{ND}}(\Delta)$—independently of their precise amplitude or detailed shape—is sufficient to identify macrorealism violation. This confers an intrinsic robustness to finite-shot imprecision, as illustrated in Fig. 6.2.

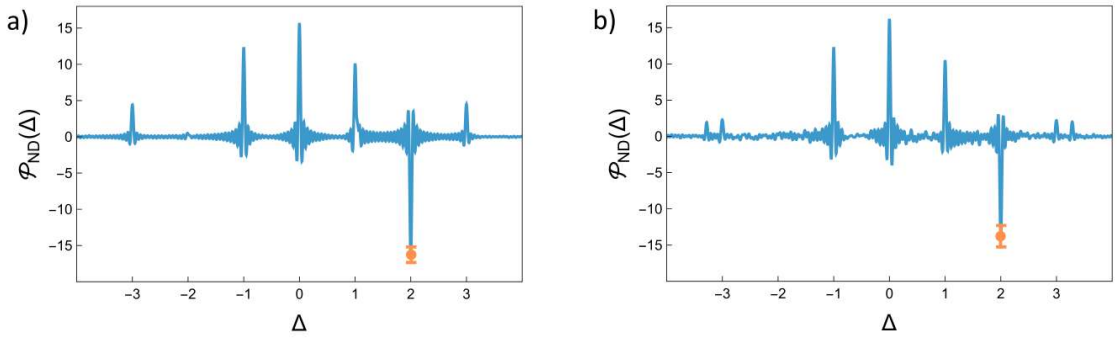

(a) $\delta\lambda = 0.1$, $N_{\mathrm{shots}}^{\mathrm{QNDM}} = 10^3$ (b) $\delta\lambda = 1$, $N_{\mathrm{shots}}^{\mathrm{QNDM}} = 10^2$

Figure 6.2: Quasi-probability $\mathcal{P}_{\mathrm{ND}}(\Delta)$ for $\omega\tau = 1.5$. Statistical uncertainty is shown with orange bars and is computed over 10^2 repetitions. As discussed in the main text, the plots represent a quasi-probability distribution. Probabilities are obtained by integrating over intervals of width 0.1 around each peak. For example, the central peak at $\Delta = 0$ is associated to a probability of 0.52 in (a) and 0.53 in (b), with the other peaks scaling accordingly.

To obtain these results we fix $\omega\tau = 1.5$, the number of shots $N_{\mathrm{shots}}^{\mathrm{QNDM}}$ (which determines the precision of the measured detector phase), and the discretization step $\delta\lambda$ (which affects the numerical Fourier reconstruction accuracy). The `Qiskit` implementation used to extract $\Re(G_\lambda)$ and $\mathrm{Im}(G_\lambda)$ is provided in Appendix 6.A.

We choose $0 \leq \lambda \leq 100$ with discretization $\delta\lambda = 0.1$ and $N_{\mathrm{shots}}^{\mathrm{QNDM}} = 10^3$. The resulting quasi-probability distribution is shown in Fig. 6.2a. A clearly negative peak appears at $\Delta = 2$, indicating the presence of quantum interference and hence macrorealism violation. Quantitatively, the minimum at $\Delta = 2$ is

$$\mathcal{P}_{\mathrm{ND}}^{\mathrm{min}} = -16.7 \pm 0.6. \tag{6.19}$$

The statistical error is computed as the standard error of the mean of the negative peak, obtained by repeating the full reconstruction $N = 10^2$ times.

The robustness of $\mathcal{P}_{\mathrm{ND}}$ against variations in both $\delta\lambda$ and $N_{\mathrm{shots}}^{\mathrm{QNDM}}$ is illustrated in Fig. 6.2b. For $\delta\lambda = 1$ and $N_{\mathrm{shots}}^{\mathrm{QNDM}} = 10^2$, the negative region remains clearly identifiable and the minimum becomes

$$\mathcal{P}_{\mathrm{ND}}^{\mathrm{min}} = -14.9 \pm 1.7. \tag{6.20}$$

This resilience to discretization stems from the fact that the theoretical QPD in Eq. (6.10) is a sum of delta functions. As a consequence, the variance of the reconstructed distribution arises solely from statistical noise, which can be assumed to have approximately uniform variance across frequencies. By Parseval's identity for the discrete inverse Fourier transform [18], the QPD variance scales linearly with $\delta\lambda$ according to

$$\sigma_{\mathcal{P}_{\mathrm{ND}}} = \delta\lambda\, \sigma_{G_\lambda}, \tag{6.21}$$

where $\sigma_{\mathcal{P}_{\mathrm{ND}}}$ and σ_{G_λ} denote the variances associated with the QPD and with the quasi-characteristic function, respectively.

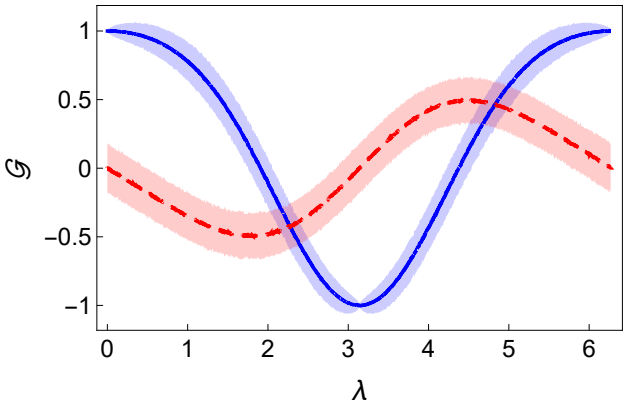

Figure 6.3: $\Re(G_\lambda)$ (solid blue) and $\mathrm{Im}(G_\lambda)$ (dashed red) for $N_{\text{shots}}^{\text{QNDM}} = 10^3$ and $\delta\lambda = 0.1$. The solid lines are mean values, while shaded regions indicate statistical errors.

In Fig. 6.2b, the parameters are chosen to minimize the resources needed to estimate G_λ, i.e. $\delta\lambda = 1$ and $N_{\text{shots}}^{\text{QNDM}} = 10^2$. The increase in $\delta\lambda$ leads to a spread of the peaks (finite Fourier resolution) and introduces small spurious features around ± 3. However, the only feature relevant for macrorealism violation—negativity—remains clearly visible.

To estimate the maximum admissible $\delta\lambda$ before aliasing effects corrupt the reconstruction, we note that the highest-frequency contribution in Eqs. (6.9) and (6.10) is set by the oscillatory factor $\exp\{\pm i\lambda\Delta_{\max}\}$. In the present model the maximal relevant value is $\Delta_{\max} = \pm 3$. By Nyquist's theorem, the largest spacing avoiding undersampling is therefore

$$\delta\lambda_{\max} = \frac{2\pi}{2\Delta_{\max}} \approx 1. \tag{6.22}$$

Thus, $\delta\lambda \approx 1$ is sufficient to capture the relevant oscillatory behaviour while avoiding loss of information due to undersampling.

The stability of negative regions even for low $N_{\text{shots}}^{\text{QNDM}}$ can be understood by inspecting the behaviour of G_λ. Figure 6.3 shows $\Re(G_\lambda)$ (solid) and $\mathrm{Im}(G_\lambda)$ (dashed) for $N_{\text{shots}}^{\text{QNDM}} = 10^3$ and $\delta\lambda = 0.1$. For each value of λ, we repeat the estimation $N = 10^2$ times and compute the mean and statistical error. Finite-shot noise in G_λ effectively introduces high-frequency fluctuations. These contributions are typically small in amplitude compared to the physically relevant oscillations and, importantly, they are largely filtered out in the inverse Fourier reconstruction when restricting attention to the interval $-\Delta_{\max} \leq \Delta \leq \Delta_{\max}$. These features allow one to reduce both $\delta\lambda$ and $N_{\text{shots}}^{\text{QNDM}}$ while still reliably detecting negativity.

To confirm the broad applicability of the approach, we performed analogous simulations for $\omega\tau$ in the interval $[0.1, 6]$. In almost all cases with the above parameters, the QNDM protocol successfully identifies negative regions and thus reveals macrorealism violation. The only failures occur for $\omega\tau = 0, \pi, 2\pi$, corresponding to sequences of commuting observables (cf. the discussion at the beginning of Sec. 6.2), which are not of interest in the original Leggett–Garg setting [52].

6.3.3 Resource estimation

We now estimate the computational resources required by the two approaches.

For LG simulations, the total number of circuit evaluations is

$$N_{\mathrm{LG}} = N_{\mathrm{meas}}^{\mathrm{LG}} \cdot N_{\mathrm{shots}}^{\mathrm{LG}}, \tag{6.23}$$

where $N_{\mathrm{meas}}^{\mathrm{LG}} = 3$ is the number of distinct circuits needed to compute the correlators entering K_3 and $N_{\mathrm{shots}}^{\mathrm{LG}}$ is the number of shots per circuit.

For QNDM, one needs to estimate both $\Re(G_\lambda)$ and $\mathrm{Im}(G_\lambda)$ for each λ, hence

$$N_{\mathrm{QNDM}} = N_{\mathrm{meas}}^{\mathrm{QNDM}} \cdot N_{\mathrm{steps}}^{\lambda} \cdot N_{\mathrm{shots}}^{\mathrm{QNDM}}, \tag{6.24}$$

with $N_{\mathrm{meas}}^{\mathrm{QNDM}} = 2$ and $N_{\mathrm{steps}}^{\lambda} = 100/\delta\lambda$ for the range $0 \leq \lambda \leq 100$.

In Fig. 6.1, the LG simulations correspond to $N_{\mathrm{LG}} = 3 \cdot 10^3$ and $3 \cdot 10^4$ circuit evaluations, respectively. For QNDM, the parameter choice of Fig. 6.2a ($N_{\mathrm{shots}}^{\mathrm{QNDM}} = 10^3$, $\delta\lambda = 0.1$) yields $N_{\mathrm{QNDM}} = 2 \cdot 10^6$. In contrast, the optimized parameters of Fig. 6.2b ($N_{\mathrm{shots}}^{\mathrm{QNDM}} = 10^2$, $\delta\lambda = 1$) give $N_{\mathrm{QNDM}} = 2 \cdot 10^4$.

Thus, with an appropriate choice of $(\delta\lambda, N_{\mathrm{shots}}^{\mathrm{QNDM}})$ enabled by the intrinsic robustness of the reconstruction, QNDM resources can be made comparable to (and in some regimes smaller than) those required by LG simulations, while providing a strictly stronger diagnostic criterion: QNDM negativity identifies macrorealism violation whenever it is present, whereas LGIs may fail to do so.

6.4 Realistic simulations with environmental noise

The previous section accounted only for finite-shot statistical uncertainty. For near-term hardware (noisy intermediate-scale quantum, NISQ) devices, environmental noise and gate imperfections must also be included. This consideration is particularly relevant for QNDM, since the protocol relies on phase accumulation in the detector, which is generally sensitive to decoherence and dephasing.

We therefore extend the analysis by incorporating a noise model using IBM's `Qiskit` simulators [44], which emulate the behaviour of specific quantum processing units. In particular, we employ the `FakeBogotaV2` simulator, representative of a 5-qubit IBM device [44].

The noisy LG simulations are shown in Fig. 6.4. As before, we consider $N_{\mathrm{shots}}^{\mathrm{LG}} = 10^3$ [Fig. 6.4a] and $N_{\mathrm{shots}}^{\mathrm{LG}} = 10^4$ [Fig. 6.4b]. In the presence of noise, the average simulated curve (solid blue) deviates from the noiseless theoretical prediction (dashed red), and—more importantly—the regions where LGI violation can be asserted with confidence are drastically reduced. Quantitatively, the confidently detectable violation interval covers about 15% of the $\omega\tau$ range for $N_{\mathrm{shots}}^{\mathrm{LG}} = 10^3$ and about 24% for $N_{\mathrm{shots}}^{\mathrm{LG}} = 10^4$. Indeed, $N_{\mathrm{shots}}^{\mathrm{LG}} = 10^3$ is close to the limiting regime, and further reduction eliminates the detectable violation interval.

In contrast, QNDM remains robust to hardware noise, as shown in Fig. 6.5. We choose parameters minimizing resources, namely $\delta\lambda = 1$ and $N_{\mathrm{shots}}^{\mathrm{QNDM}} = 10^2$. Despite the presence of environmental noise, the negative region at $\Delta = 2$ remains clearly visible, with

$$\mathcal{P}_{\mathrm{ND}}^{\mathrm{min}} = -13.5 \pm 1.8, \tag{6.25}$$

where the statistical error is computed as in Sec. 6.3.2.

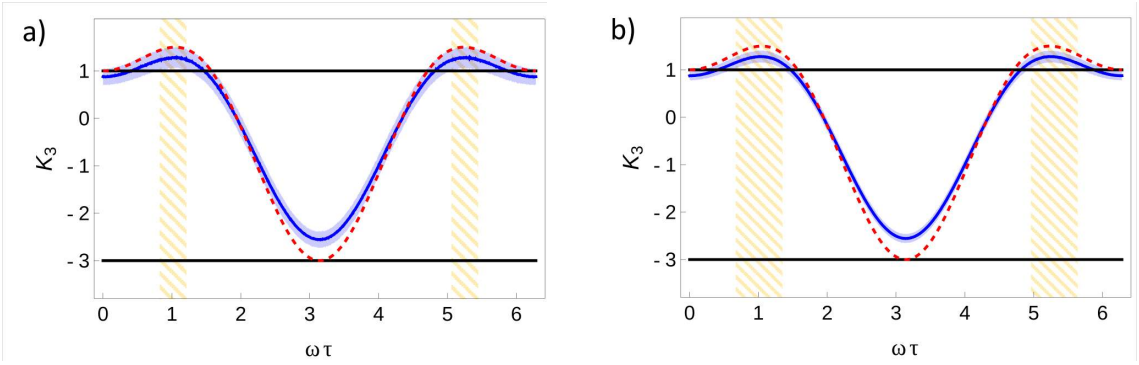

(a) (b)

Figure 6.4: LG noisy simulations for K_3 with $N_{\text{shots}}^{\text{LG}} = 10^3$ (a) and $N_{\text{shots}}^{\text{LG}} = 10^4$ (b). The solid blue line is the simulated average curve, while the dashed red line is the noiseless theoretical prediction. Blue-shaded regions indicate statistical uncertainty; yellow-shaded regions indicate $\omega\tau$ values for which LGI violation can be asserted within statistical errors.

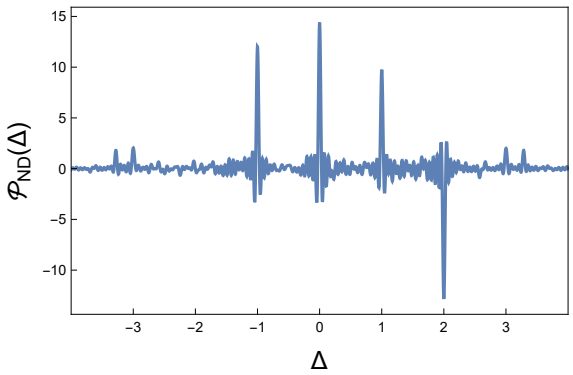

Figure 6.5: Quasi-probability $\mathcal{P}_{\text{ND}}(\Delta)$ for $\delta\lambda = 1$ and $N_{\text{shots}}^{\text{QNDM}} = 10^2$, including both finite-shot statistical uncertainty and the IBM noise model. The simulation is performed at $\omega\tau = 1.5$.

Resource estimation proceeds as in Sec. 6.3.3. For Fig. 6.5 we have $N_{\text{QNDM}} = 2{\cdot}10^4$ circuit evaluations. In comparison, identifying LGI violations under noise typically requires at least $N_{\text{shots}}^{\text{LG}} \gtrsim 10^4$, corresponding to $N_{\text{LG}} \sim 3 \cdot 10^4$. Hence QNDM is slightly more efficient (or at least comparable) in the noisy regime, while providing a strictly stronger diagnostic of macrorealism violation.

6.5 Conclusions

This chapter has presented a detailed numerical comparison between two experimentally motivated approaches for detecting macrorealism violation: (i) Leggett–Garg inequality tests based on sequential correlators, and (ii) the QNDM protocol, where sequential information is stored in a detector phase and macrorealism violation is witnessed by negativity of a reconstructed quasi-probability distribution.

By implementing both approaches in IBM's `Qiskit` framework, we explicitly accounted for the finite number of circuit executions and the resulting statistical uncertainty. In the noiseless setting, we found that the total number of circuit runs required by the two approaches can be of comparable order of magnitude, with a slight advantage for QNDM in optimized regimes. Importantly, once one accounts for the logical content of the diagnostics, QNDM is strictly more reliable: the presence or absence of negativity provides a necessary-and-sufficient criterion for MRps violation [78], whereas LGIs provide only sufficient conditions and may fail to detect violations present in the full temporal statistics.

These conclusions are strengthened in the presence of realistic environmental noise modelled through IBM's built-in noise simulators. Even though QNDM relies on phase accumulation—typically sensitive to decoherence—the negativity of the reconstructed quasi-probability remains robust, and the protocol continues to reveal macrorealism violation at resource levels comparable to (or lower than) those required for confident LGI violation detection.

The underlying reason for this robustness is the Fourier reconstruction step: both statistical and environmental noise primarily introduce high-frequency fluctuations in the estimated quasi-characteristic function. Such contributions are largely suppressed or filtered out in the inverse Fourier transform and do not substantially affect the coarse feature that matters for macrorealism violation, namely the presence of negative regions in $\mathcal{P}_{\mathrm{ND}}$.

Overall, the results indicate that QNDM-based negativity tests provide a practical and resource-efficient alternative to LGI tests, particularly in realistic noisy conditions, while also delivering a logically complete (necessary-and-sufficient) witness of macrorealism violation.

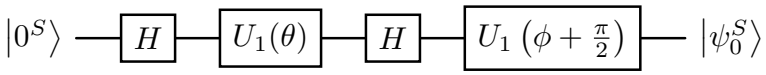

Figure 6.6: Initial state implementation.

6.A Qiskit implementation

This appendix summarizes the Qiskit implementation of the gates and circuits used in the simulations. We first present the preparation of the initial state, then the unitary evolution operator and the interaction operator. Finally, we outline the circuits implementing the QNDM readout of $\Re(G_\lambda)$ and $\mathrm{Im}(G_\lambda)$.

A generic one-qubit state can be parametrized by angles θ and ϕ as

$$|\psi_0^S\rangle = \cos\frac{\theta}{2}|0\rangle + e^{i\phi}\sin\frac{\theta}{2}|1\rangle\,. \tag{6.26}$$

The gate sequence implementing

$$|0\rangle \longrightarrow \cos\frac{\theta}{2}|0\rangle + e^{i\phi}\sin\frac{\theta}{2}|1\rangle \tag{6.27}$$

is

$$U_{\mathrm{init}}(\theta,\phi) = U_1\!\left(\phi+\frac{\pi}{2}\right) H\, U_1(\theta)\, H, \tag{6.28}$$

where

$$U_1(\alpha) = \begin{pmatrix} 1 & 0 \\ 0 & e^{i\alpha} \end{pmatrix}. \tag{6.29}$$

Figure 6.6 shows the circuit implementation. The initial state used in this chapter, $|\psi_0^S\rangle = (|0\rangle + i\,|1\rangle)/\sqrt{2}$, corresponds to $\theta = \pi/2$ and $\phi = \pi/2$ in Eq. (6.28).

The unitary evolution corresponding to rotation generated by $\hat{\sigma}_x$ is

$$U(\alpha) = e^{-i\alpha\hat{\sigma}_x} = \begin{pmatrix} \cos\alpha & -i\sin\alpha \\ -i\sin\alpha & \cos\alpha \end{pmatrix}. \tag{6.30}$$

This can be decomposed into elementary gates as

$$e^{-i\alpha\hat{\sigma}_x} = H\cdot R_z(2\alpha)\cdot H, \tag{6.31}$$

with H the Hadamard gate and

$$R_z(\theta) = e^{-i\frac{\theta}{2}\hat{\sigma}_z} = \begin{pmatrix} e^{-i\frac{\theta}{2}} & 0 \\ 0 & e^{i\frac{\theta}{2}} \end{pmatrix}. \tag{6.32}$$

The system–detector interaction operator is

$$\hat{u}(\lambda) = \exp\!\left\{ i\frac{\lambda}{2}\,\hat{\sigma}_z^S \otimes \hat{\sigma}_z^D \right\}. \tag{6.33}$$

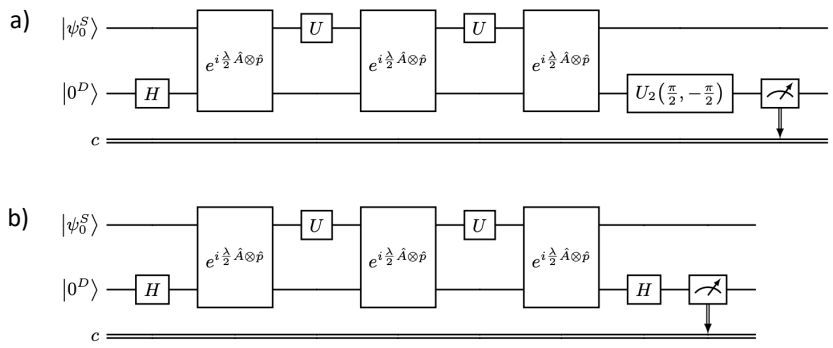

Figure 6.7: QNDM circuit to extract $\mathrm{Im}(G_\lambda)$ (a) and $\Re(G_\lambda)$ (b). Here, $|\psi_0^S\rangle$ is the initial system state as in Fig. 6.6, and c is the classical register storing measurement outcomes. The gates U_2 and H implement standard interferometric readout of the imaginary and real parts of the accumulated detector phase.

In the basis $\{|0_S0_D\rangle, |0_S1_D\rangle, |1_S0_D\rangle, |1_S1_D\rangle\}$, its matrix form is

$$\hat{u}(\lambda) = \begin{pmatrix} e^{i\lambda/2} & 0 & 0 & 0 \\ 0 & e^{-i\lambda/2} & 0 & 0 \\ 0 & 0 & e^{-i\lambda/2} & 0 \\ 0 & 0 & 0 & e^{i\lambda/2} \end{pmatrix}. \tag{6.34}$$

Up to a global phase $e^{i\lambda}$, a convenient `Qiskit` decomposition is

$$\hat{u}(\lambda/2) = CX_{1,2}\,[\mathbb{I}\otimes U_1(-\lambda)]\,CX_{1,2}, \tag{6.35}$$

where qubit 1 is the system and qubit 2 the detector.

In the QNDM protocol, for each value of λ two circuits are required to extract G_λ: one for $\mathrm{Im}(G_\lambda)$ and one for $\Re(G_\lambda)$, shown in Fig. 6.7a) and Fig. 6.7b), respectively. The measurement outcomes yield the probabilities of the detector states $|0^D\rangle$ and $|1^D\rangle$ as functions of λ.

The real and imaginary parts of G_λ can be measured with interferometric techniques [72, 76]. In particular, to extract $\Re(G_\lambda)$ we apply a Hadamard gate H, while for $\mathrm{Im}(G_\lambda)$ we apply the U_2 gate defined as

$$U_2(\alpha,\beta) = \frac{1}{\sqrt{2}}\begin{pmatrix} 1 & -e^{i\beta} \\ e^{i\alpha} & e^{i(\alpha+\beta)} \end{pmatrix}. \tag{6.36}$$

In our case $\alpha = \pi/2$ and $\beta = -\pi/2$, hence

$$U_2\left(\frac{\pi}{2},-\frac{\pi}{2}\right) = \frac{1}{\sqrt{2}}\begin{pmatrix} 1 & i \\ i & 1 \end{pmatrix}. \tag{6.37}$$

6.B Note on the complementarity of LGIs

In the simulations presented in this chapter, we choose the standard set-up in which the monitored observable and the Hamiltonian generator are orthogonal. In this

regime, the three-time LGIs display a form of complementarity: for every $\omega\tau \in [0, 2\pi)$ there exists at least one K_i that violates the classical bounds. Specifically, K_3 in Eq. (6.4) is violated for $0 \leq \omega\tau \leq \pi/2$ and $3\pi/2 \leq \omega\tau \leq 2\pi$, while it is satisfied in $\pi/2 \leq \omega\tau \leq 3\pi/2$. Conversely, the LGI associated with K_2 is violated for $\pi/2 \leq \omega\tau \leq 3\pi/2$ and satisfied elsewhere. Lastly, K_1 is always satisfied.

This complementarity is not guaranteed in general [56, 43]. In practice, one often needs to consider higher-order LGIs [32], i.e. n-measurement Leggett–Garg strings

$$K_n = C_{21} + C_{32} + C_{43} + \cdots + C_{n(n-1)} - C_{n1}. \tag{6.38}$$

This increases resource requirements because more correlators and circuits must be estimated. By contrast, the QNDM protocol detects macrorealism violation with a fixed number of detector interactions, independent of the specific system being studied.

Conclusions and Outlook

This thesis has pursued a unified operational perspective on two domains that are often treated separately: the response of quantum probes in non-inertial motion and the extent to which such responses warrant thermodynamic language, and the characterization of non-classical temporal correlations together with the operational limits of macrorealistic descriptions. In both contexts, detector-based protocols provide a concrete framework in which structural properties can be translated into measurable quantities and analysed under controlled and realistic conditions.

Within non-inertial quantum field theory, a central conceptual point is that proper acceleration alone is not sufficient to guarantee thermality. Uniform linear acceleration remains exceptional in that it supports an exact equilibrium structure, while more general motions, even when stationary, do not necessarily admit a thermal interpretation.

In this setting, one of the main results of this thesis concerns the role of the detector as a finite physical system. The analysis developed shows explicitly how these features can generate an ambiguity in associating a single Unruh temperature to an extended thermometer, and how that ambiguity is resolved—or persists—depending on dynamical conditions. In particular, when the internal readout degree of freedom effectively couples to a restricted set of spatial modes, one can obtain a reduced state that is accurately approximated by a thermal form and thereby assign an effective temperature with clear operational meaning. In that regime, the temperature should be interpreted as a nonlocal quantity induced by the probe's spatial profile and coupling structure, rather than as a pointwise property of the trajectory.

A second original contribution concerns the analysis of the Unruh effect in circular motion within a realistic magnetic setting. Building on the general result that circular trajectories do not exhibit exact thermality, the thesis develops a magnetic circular detector model in which both the motion and the detector's internal splitting are controlled by laboratory parameters. The numerical analysis shows that the detector response is governed, to a very good approximation, by a single dimensionless parameter $k = |q|BR/(mc)$, leading to a universal scaling behaviour across different configurations.

In the ultrarelativistic regime, the excitation probability is found to approach a saturation plateau, in agreement with the asymptotic analysis. This result provides a clear operational characterization of non-thermal steady states and identifies the parameter regimes in which such effects could become experimentally accessible. The analysis also clarifies the physical origin of this saturation: the same external parameters that increase the non-inertiality of the motion simultaneously increase the detector gap, preventing the ratio E/T_U from diverging and leading to a finite

asymptotic excitation probability.

The second part of the thesis adopts the same operational viewpoint in the context of temporal non-classicality. It emphasizes that Leggett–Garg inequalities provide only partial information about the underlying temporal statistics, motivating the use of protocols that access the probability structure more directly. In particular, the quantum non-demolition measurement framework allows for the reconstruction of temporal quasi-probability distributions whose negativity provides a complete criterion for the violation of macrorealism.

Within this framework, the contribution of this thesis is to analyse the practical performance of such protocols. Through explicit numerical simulations, it is shown that quasi-probability reconstruction based on QNDM remains robust under realistic noise and finite sampling, and can be competitive with, or even outperform, inequality-based approaches in relevant regimes. In particular, the Fourier-based reconstruction inherent in the protocol provides a mechanism for mitigating statistical fluctuations, improving the reliability of the extracted signatures of non-classicality.

Taken together, these results support a unified operational perspective in which detector-based methods provide a bridge between abstract theoretical structures and experimentally accessible quantities. On the one hand, they clarify the conditions under which thermodynamic language can be meaningfully applied to non-inertial motion. On the other hand, they provide concrete tools for diagnosing temporal non-classicality beyond the limitations of correlator-based approaches.

Several directions follow naturally from this work. On the non-inertial side, it would be of interest to extend the analysis of extended detectors and effective temperatures to broader classes of stationary trajectories and more realistic detector models, such as extended thermometers in circular motion. The magnetic circular model suggests further developments toward experimentally relevant scenarios, including the role of environmental effects and decoherence.

On the temporal side, further work could focus on optimizing the implementation of QNDM protocols on near-term quantum devices, as well as exploring connections with other frameworks for temporal correlations.

In summary, this thesis shows that quantum detectors provide a versatile operational tool for probing both thermality and temporal non-classicality, and that in both contexts the structure of the measurement process plays a central role in determining when equilibrium and classicality are meaningful concepts.

Bibliography

[1] B. Abi et al. "Measurement of the Positive Muon Anomalous Magnetic Moment to 0.46 ppm". In: *Phys. Rev. Lett.* 126 (14 Apr. 2021), p. 141801. DOI: 10.1103/PhysRevLett.126.141801. URL: https://link.aps.org/doi/10.1103/PhysRevLett.126.141801.

[2] D. P. Aguillard et al. "Detailed report on the measurement of the positive muon anomalous magnetic moment to 0.20 ppm". In: *Phys. Rev. D* 110 (3 Aug. 2024), p. 032009. DOI: 10.1103/PhysRevD.110.032009. URL: https://link.aps.org/doi/10.1103/PhysRevD.110.032009.

[3] D. P. Aguillard et al. "Measurement of the Positive Muon Anomalous Magnetic Moment to 0.20 ppm". In: *Phys. Rev. Lett.* 131 (16 Oct. 2023), p. 161802. DOI: 10.1103/PhysRevLett.131.161802. URL: https://link.aps.org/doi/10.1103/PhysRevLett.131.161802.

[4] T. Albahri et al. "Beam dynamics corrections to the Run-1 measurement of the muon anomalous magnetic moment at Fermilab". In: *Phys. Rev. Accel. Beams* 24 (4 Apr. 2021), p. 044002. DOI: 10.1103/PhysRevAccelBeams.24.044002. URL: https://link.aps.org/doi/10.1103/PhysRevAccelBeams.24.044002.

[5] T. Albahri et al. "Magnetic-field measurement and analysis for the Muon $g-2$ Experiment at Fermilab". In: *Phys. Rev. A* 103 (4 Apr. 2021), p. 042208. DOI: 10.1103/PhysRevA.103.042208. URL: https://link.aps.org/doi/10.1103/PhysRevA.103.042208.

[6] Adam Bednorz and Wolfgang Belzig. "Quasiprobabilistic Interpretation of Weak Measurements in Mesoscopic Junctions". In: *Phys. Rev. Lett.* 105 (10 Sept. 2010), p. 106803. DOI: 10.1103/PhysRevLett.105.106803. URL: http://link.aps.org/doi/10.1103/PhysRevLett.105.106803.

[7] Adam Bednorz, Wolfgang Belzig, and Abraham Nitzan. "Nonclassical time correlation functions in continuous quantum measurement". In: *New Journal of Physics* 14.1 (Jan. 2012), p. 013009. DOI: 10.1088/1367-2630/14/1/013009. URL: https://doi.org/10.1088/1367-2630/14/1/013009.

[8] J. S. Bell. "On the Einstein Podolsky Rosen paradox". In: *Physics Physique Fizika* 1 (3 Nov. 1964), pp. 195–200. DOI: 10.1103/PhysicsPhysiqueFizika.1.195. URL: https://link.aps.org/doi/10.1103/PhysicsPhysiqueFizika.1.195.

[9] J. S. Bell, Richard J. Hughes, and J. M. Leinaas. "The Unruh effect in extended thermometers". In: *Zeitschrift für Physik C Particles and Fields* 28.1 (Mar. 1, 1985), pp. 75–80. DOI: 10.1007/BF01550251. URL: https://doi.org/10.1007/BF01550251.

[10] J.S. Bell and J.M. Leinaas. "The Unruh effect and quantum fluctuations of electrons in storage rings". In: *Nuclear Physics B* 284 (1987), pp. 488–508. ISSN: 0550-3213. DOI: https://doi.org/10.1016/0550-3213(87)90047-2. URL: https://www.sciencedirect.com/science/article/pii/0550321387900472.

[11] F. Benatti, G.C. Ghirardi, and R. Geassi. "Testing macroscopic quantum coherence". In: *Nuov Cimento B* 110 (May 1995), pp. 593–610. DOI: 10.1007/BF02741468.

[12] Steffen Biermann et al. "Unruh and analogue Unruh temperatures for circular motionin 3+1 and 2+1 dimensions". In: *Physical Review D* 102.8 (Oct. 2020). ISSN: 2470-0029. DOI: 10.1103/physrevd.102.085006. URL: http://dx.doi.org/10.1103/PhysRevD.102.085006.

[13] N. D. Birrell and P. C. W. Davies. *Quantum Fields in Curved Space*. Cambridge University Press, 1982.

[14] J. J Bisognano and E. H. Wichmann. "On the Duality Condition for a Hermitian Scalar Field". In: *J. Math. Phys.* 16 (1975), pp. 985–1007. DOI: 10.1063/1.522605.

[15] J. J Bisognano and E. H. Wichmann. "On the Duality Condition for Quantum Fields". In: *J. Math. Phys.* 17 (1976), pp. 303–321. DOI: 10.1063/1.522898.

[16] J.D. Bjorken and S.D. Drell. *Relativistic Quantum Fields*. International series in pure and applied physics. McGraw-Hill, 1965. ISBN: 9780700549405. URL: https://books.google.it/books?id=ZczvAAAAMAAJ.

[17] Karl Blum. *Density matrix theory and applications*. Springer series on atomic, optical, and plasma physics. Berlin: Springer, 2012. DOI: 10.1007/978-3-642-20561-3. URL: https://cds.cern.ch/record/1433745.

[18] R.N. Bracewell. *The Fourier Transform and its Applications*. Second. Tokyo: McGraw-Hill Kogakusha, Ltd., 1978.

[19] Vladimir B. Braginsky, Farid Ya Khalili, and Kip S. Thorne. *Quantum Measurement*. Cambridge University Press, 1992.

[20] O. Bratteli and D.W. Robinson. *Operator Algebras and Quantum Statistical Mechanics 1: C*- and W*-Algebras. Symmetry Groups. Decomposition of States*. Operator Algebras and Quantum Statistical Mechanics. Springer, 1987. ISBN: 9783540170938. URL: https://books.google.it/books?id=YuR4VQOQQUIC.

[21] H. P. Breuer and F. Petruccione. *The theory of open quantum systems*. Great Clarendon Street: Oxford University Press, 2002.

[22] Detlev Buchholz and Rainer Verch. "Macroscopic aspects of the Unruh effect". In: *Classical and Quantum Gravity* 32.24 (Dec. 2015), p. 245004. DOI: 10.1088/0264-9381/32/24/245004. URL: https://dx.doi.org/10.1088/0264-9381/32/24/245004.

[23] Detlev Buchholz and Rainer Verch. "Unruh versus Tolman: on the heat of acceleration: Dedicated to the memory of Rudolf Haag". In: *General Relativity and Gravitation* 48.3 (Feb. 2016). ISSN: 1572-9532. DOI: 10.1007/s10714-016-2029-2. URL: http://dx.doi.org/10.1007/s10714-016-2029-2.

[24] Cameron R. D. Bunney. "Stationary trajectories in Minkowski spacetimes". In: *Journal of Mathematical Physics* 65.5 (May 2024), p. 052501. ISSN: 0022-2488. DOI: 10.1063/5.0205471. eprint: https://pubs.aip.org/aip/jmp/article-pdf/doi/10.1063/5.0205471/19923852/052501_1_5.0205471.pdf. URL: https://doi.org/10.1063/5.0205471.

[25] M. Cardi, P. Solinas, and N. Zanghì. "Measurement of the Unruh effect through extended quantum thermometers". In: *Phys. Rev. D* 111 (3 Feb. 2025), p. 036031. DOI: 10.1103/PhysRevD.111.036031. URL: https://link.aps.org/doi/10.1103/PhysRevD.111.036031.

[26] Lucas Clemente and Johannes Kofler. "Necessary and sufficient conditions for macroscopic realism from quantum mechanics". In: *Phys. Rev. A* 91 (6 June 2015), p. 062103. DOI: 10.1103/PhysRevA.91.062103. URL: https://link.aps.org/doi/10.1103/PhysRevA.91.062103.

[27] Lucas Clemente and Johannes Kofler. "No Fine Theorem for Macrorealism: Limitations of the Leggett-Garg Inequality". In: *Phys. Rev. Lett.* 116 (15 Apr. 2016), p. 150401. DOI: 10.1103/PhysRevLett.116.150401. URL: https://link.aps.org/doi/10.1103/PhysRevLett.116.150401.

[28] Cameron R D Bunney and Jorma Louko. "Circular motion analogue Unruh effect in a 2+1 thermal bath: robbing from the rich and giving to the poor". In: *Classical and Quantum Gravity* 40.15 (June 2023), p. 155001. DOI: 10.1088/1361-6382/acde3b. URL: https://doi.org/10.1088/1361-6382/acde3b.

[29] P C W Davies. "Scalar production in Schwarzschild and Rindler metrics". In: *Journal of Physics A: Mathematical and General* 8.4 (Apr. 1, 1975), p. 609. DOI: 10.1088/0305-4470/8/4/022. URL: https://dx.doi.org/10.1088/0305-4470/8/4/022.

[30] B. S. DeWitt. *General relativity : an Einstein centenary survey / edited by S. W. Hawking, W. Israel*. eng. Cambridge (GB): Cambridge University Press, 1979. ISBN: 0-521-22285-0.

[31] RH Dicke. "Interaction-free quantum measurements: A paradox?" In: *American Journal of Physics* 49.10 (1981), pp. 925–930.

[32] Clive Emary, Neill Lambert, and Franco Nori. "Leggett–Garg inequalities". In: *Reports on Progress in Physics* 77.1 (Dec. 2013), p. 016001. DOI: 10.1088/0034-4885/77/1/016001. URL: https://doi.org/10.1088/0034-4885/77/1/016001.

[33] Paul Embrechts and Giovanni Puccetti. "Bounds for the sum of dependent risks having overlapping marginals". In: *Journal of Multivariate Analysis* 101.1 (2010), pp. 177–190. ISSN: 0047-259X. DOI: https://doi.org/10.1016/j.jmva.2009.07.004. URL: https://www.sciencedirect.com/science/article/pii/S0047259X09001304.

[34] F. Frenet. "Sur les courbes à double courbure". fr. In: *Journal de Mathématiques Pures et Appliquées* 1e série, 17 (1852), pp. 437–447. URL: https://www.numdam.org/item/JMPA_1852_1_17__437_0/.

[35] Tobias Fritz and Rafael Chaves. "Entropic Inequalities and Marginal Problems". In: *IEEE Transactions on Information Theory* 59.2 (Feb. 2013), pp. 803–817. ISSN: 1557-9654. DOI: 10.1109/tit.2012.2222863. URL: http://dx.doi.org/10.1109/TIT.2012.2222863.

[36] Stephen A. Fulling. "Nonuniqueness of Canonical Field Quantization in Riemannian Space-Time". In: *Phys. Rev. D* 7 (10 May 1973), pp. 2850–2862. DOI: 10.1103/PhysRevD.7.2850. URL: https://link.aps.org/doi/10.1103/PhysRevD.7.2850.

[37] Sheldon Goldstein et al. "Approach to thermal equilibrium of macroscopic quantum systems". In: *Phys. Rev. E* 81 (1 Jan. 2010), p. 011109. DOI: 10.1103/PhysRevE.81.011109. URL: https://link.aps.org/doi/10.1103/PhysRevE.81.011109.

[38] Michael Good et al. "Unruh-like effects: effective temperatures along stationary worldlines". In: *Journal of High Energy Physics* 2020.6 (June 2020). ISSN: 1029-8479. DOI: 10.1007/jhep06(2020)059. URL: http://dx.doi.org/10.1007/JHEP06(2020)059.

[39] R. Haag. *Local quantum physics: Fields, particles, algebras*. 1992.

[40] J J Halliwell. "Necessary and sufficient conditions for macrorealism using two- and three-time Leggett-Garg inequalities". In: *Journal of Physics: Conference Series* 1275.1 (Sept. 2019), p. 012008. DOI: 10.1088/1742-6596/1275/1/012008. URL: https://doi.org/10.1088/1742-6596/1275/1/012008.

[41] J. J. Halliwell. "Leggett-Garg inequalities and no-signaling in time: A quasiprobability approach". In: *Phys. Rev. A* 93 (2 Feb. 2016), p. 022123. DOI: 10.1103/PhysRevA.93.022123. URL: https://link.aps.org/doi/10.1103/PhysRevA.93.022123.

[42] S. W. Hawking. "Particle creation by black holes". In: *Communications in Mathematical Physics* 43.3 (1975), pp. 199–220.

[43] S. F. Huelga, T. W. Marshall, and E. Santos. "Proposed test for realist theories using Rydberg atoms coupled to a high-Q resonator". In: *Phys. Rev. A* 52 (4 Oct. 1995), R2497–R2500. DOI: 10.1103/PhysRevA.52.R2497. URL: https://link.aps.org/doi/10.1103/PhysRevA.52.R2497.

[44] IBM. *IBM documentation*.

[45] Johannes Kofler and Časlav Brukner. "Condition for macroscopic realism beyond the Leggett-Garg inequalities". In: *Phys. Rev. A* 87 (5 May 2013), p. 052115. DOI: 10.1103/PhysRevA.87.052115. URL: https://link.aps.org/doi/10.1103/PhysRevA.87.052115.

[46] Jan Ivar Korsbakken and Jon Magne Leinaas. "Fulling-Unruh effect in general stationary accelerated frames". In: *Phys. Rev. D* 70 (8 Oct. 2004), p. 084016. DOI: 10.1103/PhysRevD.70.084016. URL: https://link.aps.org/doi/10.1103/PhysRevD.70.084016.

[47] Friedrich Kottler. "Relativitätsprinzip und beschleunigte Bewegung". In: *Annalen der Physik* 349.13 (1914), pp. 701–748. DOI: https://doi.org/10.1002/andp.19143491303. eprint: https://onlinelibrary.wiley.com/doi/pdf/10.1002/andp.19143491303. URL: https://onlinelibrary.wiley.com/doi/abs/10.1002/andp.19143491303.

[48] Ryogo Kubo. "Statistical-Mechanical Theory of Irreversible Processes. I. General Theory and Simple Applications to Magnetic and Conduction Problems". In: *Journal of the Physical Society of Japan* 12.6 (1957), pp. 570–586. DOI: 10.1143/JPSJ.12.570. eprint: https://doi.org/10.1143/JPSJ.12.570. URL: https://doi.org/10.1143/JPSJ.12.570.

[49] Lev Davidovich Landau and E. M. Lifshits. *Quantum Mechanics: Non-Relativistic Theory*. Vol. v.3. Course of Theoretical Physics. Oxford: Butterworth-Heinemann, 1991. ISBN: 978-0-7506-3539-4.

[50] A J Leggett. "Realism and the physical world". In: *Reports on Progress in Physics* 71.2 (Jan. 2008), p. 022001. DOI: 10.1088/0034-4885/71/2/022001. URL: https://doi.org/10.1088/0034-4885/71/2/022001.

[51] A J Leggett. "Testing the limits of quantum mechanics: motivation, state of play, prospects". In: *Journal of Physics: Condensed Matter* 14.15 (Apr. 2002), R415. DOI: 10.1088/0953-8984/14/15/201. URL: https://doi.org/10.1088/0953-8984/14/15/201.

[52] A. J. Leggett and Anupam Garg. "Quantum mechanics versus macroscopic realism: Is the flux there when nobody looks?" In: *Phys. Rev. Lett.* 54 (9 Mar. 1985), pp. 857–860. DOI: 10.1103/PhysRevLett.54.857.

[53] Jon Magne Leinaas. *Quantum Aspects of Beam Physics*. WORLD SCIENTIFIC, 2002. DOI: 10.1142/4961. eprint: https://www.worldscientific.com/doi/pdf/10.1142/4961. URL: https://www.worldscientific.com/doi/abs/10.1142/4961.

[54] John R. Letaw. "Stationary world lines and the vacuum excitation of noninertial detectors". In: *Phys. Rev. D* 23 (8 Apr. 1981), pp. 1709–1714. DOI: 10.1103/PhysRevD.23.1709. URL: https://link.aps.org/doi/10.1103/PhysRevD.23.1709.

[55] John R. Letaw and Jonathan D. Pfautsch. "Quantized scalar field in rotating coordinates". In: *Phys. Rev. D* 22 (6 Sept. 1980), pp. 1345–1351. DOI: 10.1103/PhysRevD.22.1345. URL: https://link.aps.org/doi/10.1103/PhysRevD.22.1345.

[56] Shayan Majidy, Jonathan J. Halliwell, and Raymond Laflamme. "Detecting violations of macrorealism when the original Leggett-Garg inequalities are satisfied". In: *Phys. Rev. A* 103 (6 June 2021), p. 062212. DOI: 10.1103/PhysRevA.103.062212. URL: https://link.aps.org/doi/10.1103/PhysRevA.103.062212.

[57] Yuanyuan Mao et al. "Structure of dimension-bounded temporal correlations". In: *Phys. Rev. A* 105 (2022), p. L020201. DOI: 10.1103/PhysRevA.105.L020201. arXiv: 2005.13964 [quant-ph].

[58] O.J.E. Maroney. "Measurements, disturbances and the quantum three box paradox". In: *Studies in History and Philosophy of Science Part B: Studies in History and Philosophy of Modern Physics* 58 (May 2017), pp. 41–53. ISSN: 1355-2198. DOI: 10.1016/j.shpsb.2016.12.003. URL: http://dx.doi.org/10.1016/j.shpsb.2016.12.003.

[59] Paul C. Martin and Julian Schwinger. "Theory of Many-Particle Systems. I". In: *Phys. Rev.* 115 (6 Sept. 1959), pp. 1342–1373. DOI: 10.1103/PhysRev.115.1342. URL: https://link.aps.org/doi/10.1103/PhysRev.115.1342.

[60] D. Melegari, M. Cardi, and P. Solinas. "Quantum simulations of macrorealism violation via the quantum nondemolition measurement protocol". In: *Phys. Rev. A* 111 (5 May 2025), p. 052435. DOI: 10.1103/PhysRevA.111.052435. URL: https://link.aps.org/doi/10.1103/PhysRevA.111.052435.

[61] Christian Møller. *The Theory of Relativity*. Oxford, Clarendon Press, 1972.

[62] Leo J A Parry et al. "Waiting around for Unruh". In: *Classical and Quantum Gravity* 42.24 (Dec. 2025), p. 245012. ISSN: 1361-6382. DOI: 10.1088/1361-6382/ae2377. URL: http://dx.doi.org/10.1088/1361-6382/ae2377.

[63] Juan Pablo Paz and Günter Mahler. "Proposed test for temporal Bell inequalities". In: *Phys. Rev. Lett.* 71 (20 Nov. 1993), pp. 3235–3239. DOI: 10.1103/PhysRevLett.71.3235. URL: https://link.aps.org/doi/10.1103/PhysRevLett.71.3235.

[64] Asher Peres. "How to differentiate between non-orthogonal states". In: *Physics Letters A* 128.1 (1988), p. 19. ISSN: 0375-9601. DOI: https://doi.org/10.1016/0375-9601(88)91034-1. URL: https://www.sciencedirect.com/science/article/pii/0375960188910341.

[65] M. E. Peskin and D. V. Schroeder. *An Introduction to Quantum Field Theory*. Addison-Wesley, 1995.

[66] Max Planck. "On the Law of Distribution of Energy in the Normal Spectrum". In: *Annalen Phys.* 4 (1901), p. 553.

[67] W. Rindler. "Kruskal Space and the Uniformly Accelerated Frame". In: *American Journal of Physics* 34.12 (Dec. 1966), pp. 1174–1178. ISSN: 0002-9505. DOI: 10.1119/1.1972547. eprint: https://pubs.aip.org/aapt/ajp/article-pdf/34/12/1174/11370636/1174_1_online.pdf. URL: https://doi.org/10.1119/1.1972547.

[68] Alessandro Santini and Vittorio Vitale. "Experimental violations of Leggett-Garg inequalities on a quantum computer". In: *Phys. Rev. A* 105 (3 Mar. 2022), p. 032610. DOI: 10.1103/PhysRevA.105.032610. URL: https://link.aps.org/doi/10.1103/PhysRevA.105.032610.

[69] E. Schrödinger. "Die gegenwärtige Situation in der Quantenmechanik". In: *Naturwissenschaften* 23 (Nov. 1935), pp. 807–812. DOI: 10.1007/BF01491891. URL: https://link.aps.org/doi/10.1103/PhysRevD.110.032009.

[70] J.-A. Serret. “Sur quelques formules relatives à la théorie des courbes à double courbure”. fr. In: *Journal de Mathématiques Pures et Appliquées* 1e série, 16 (1851), pp. 193–207. URL: https://www.numdam.org/item/JMPA_1851_1_16__193_0/.

[71] A. Sirois, M. Olson, and B. Pabla. “The use of spectral analysis to examine model and observed O3 data”. In: *Atmospheric Environment* 29.3 (1995), pp. 411–422. ISSN: 1352-2310. DOI: https://doi.org/10.1016/1352-2310(94)00268-P. URL: https://www.sciencedirect.com/science/article/pii/135223109400268P.

[72] P. Solinas, M. Amico, and N. Zanghì. “Measurement of work and heat in the classical and quantum regimes”. In: *Phys. Rev. A* 103 (6 June 2021), p. L060202. DOI: 10.1103/PhysRevA.103.L060202. URL: https://link.aps.org/doi/10.1103/PhysRevA.103.L060202.

[73] P. Solinas and S. Gasparinetti. “Full distribution of work done on a quantum system for arbitrary initial states”. In: *Phys. Rev. E* 92 (4 Oct. 2015), p. 042150. DOI: 10.1103/PhysRevE.92.042150. URL: http://link.aps.org/doi/10.1103/PhysRevE.92.042150.

[74] P. Solinas and S. Gasparinetti. “Probing quantum interference effects in the work distribution”. In: *Phys. Rev. A* 94 (5 Nov. 2016), p. 052103. DOI: 10.1103/PhysRevA.94.052103. URL: https://link.aps.org/doi/10.1103/PhysRevA.94.052103.

[75] Paolo Solinas, Dmitri V. Averin, and Jukka P. Pekola. “Work and its fluctuations in a driven quantum system”. In: *Phys. Rev. B* 87 (6 Feb. 2013), p. 060508. DOI: 10.1103/PhysRevB.87.060508. URL: http://link.aps.org/doi/10.1103/PhysRevB.87.060508.

[76] Paolo Solinas, Simone Caletti, and Giovanni Minuto. “Quantum gradient evaluation through quantum non-demolition measurements”. In: *The European Physical Journal D* 77.5 (May 2023). ISSN: 1434-6079. DOI: 10.1140/epjd/s10053-023-00648-y. URL: http://dx.doi.org/10.1140/epjd/s10053-023-00648-y.

[77] Paolo Solinas and Stefano Gherardini. “Negativity of nondemolition quasiprobability distribution as a necessary and sufficient condition for macrorealism violation”. In: *Phys. Rev. A* 111 (5 May 2025), p. 052217. DOI: 10.1103/PhysRevA.111.052217. URL: https://link.aps.org/doi/10.1103/PhysRevA.111.052217.

[78] Paolo Solinas and Stefano Gherardini. “Quantum Non-Demolition Measurements and Leggett-Garg inequality”. In: (2024). arXiv: 2408.00088 [quant-ph]. URL: https://arxiv.org/abs/2408.00088.

[79] Mark Srednicki. “Chaos and quantum thermalization”. In: *Phys. Rev. E* 50 (2 Aug. 1994), pp. 888–901. DOI: 10.1103/PhysRevE.50.888. URL: https://link.aps.org/doi/10.1103/PhysRevE.50.888.

[80] Shin Takagi. "Vacuum Noise and Stress Induced by Uniform Acceleration: Hawking-Unruh Effect in Rindler Manifold of Arbitrary Dimension". In: *Progress of Theoretical Physics Supplement* 88 (Mar. 1986), pp. 1–142. DOI: 10.1143/PTP.88.1. URL: https://doi.org/10.1143/PTP.88.1.

[81] M. Takesaki. *Tomita's Theory of Modular Hilbert Algebras and its Applications*. Lecture Notes in Mathematics. Springer-Verlag, 1970. DOI: 10.1007/bfb0065832.

[82] B. Thaller. *The Dirac equation*. 1992.

[83] R. C. Tolman. *Relativity Thermodynamics and Cosmology*. Oxford: Claredon Press, 1934, p. 319. DOI: 10.2307/3605486.

[84] W. G. Unruh. "Notes on black-hole evaporation". In: *Phys. Rev. D* 14 (4 Aug. 1976), pp. 870–892. DOI: 10.1103/PhysRevD.14.870. URL: https://link.aps.org/doi/10.1103/PhysRevD.14.870.

[85] Giuseppe Vitagliano and Costantino Budroni. "Leggett-Garg macrorealism and temporal correlations". In: *Phys. Rev. A* 107 (4 Apr. 2023), p. 040101. DOI: 10.1103/PhysRevA.107.040101. URL: https://link.aps.org/doi/10.1103/PhysRevA.107.040101.

[86] R. M. Wald. *Quantum Field Theory in Curved Spacetime and Black Hole Thermodynamics*. University of Chicago Press, 1994.

[87] Steven Weinberg. *The Quantum Theory of Fields, Volume 1: Foundations*. Cambridge University Press, 2005. ISBN: 0521670535.

[88] A S Wightman and L Garding. "FIELDS AS OPERATOR-VALUED DISTRIBUTIONS IN RELATIVISTIC QUANTUM THEORY". In: *Arkiv Fys.* Vol: 28 (Jan. 1965). URL: https://www.osti.gov/biblio/4606723.